PRODUCTION DATA ANALYSIS OF SHALE GAS RESERVOIRS

A Thesis

Submitted to the Graduate Faculty in the
Louisiana State University and
Agricultural and Mechanical College
in partial fulfillment of the
requirements for the degree of
Master of Science in Petroleum Engineering

in

The Department of Petroleum Engineering

by
Adam Michael Lewis
B.S., Louisiana State University, 2005
December, 2007

ACKNOWLEDGEMENTS

I would like to thank Louisiana State University for providing me the opportunity to conduct this research. I would especially like to thank my mentor and advisor Dr. Richard G. Hughes for guiding me in this research and sharing his knowledge and experience with me. It has been a wonderful learning opportunity.

I would also like to thank the other members of my committee Dr. Christopher White and Dr. Julius Langlinais for their guidance and support in completing this work. Finally, I would like to thank Devon Energy Corporation who were the providers of the data used in this research. I greatly appreciate all those people who have helped me along the way; this research and this experience would have been worse off without your support. Thank you.

TABLE OF CONTENTS

LIST OF TABLES

LIST OF FIGURES

ABSTRACT

Hydrocarbon resources from unconventional shale gas reservoirs are becoming very important in the United States in recent years. Understanding the effects of adsorption on production data analysis will increase the effectiveness of reservoir management in these challenging environments.

The use of an adjusted system compressibility proposed by Bumb and McKee (1988) is critical in this process. It allows for dimensional and dimensionless type curves to be corrected at a reasonably fundamental level, and it breaks the effects of adsorption into something that is relatively simple to understand. This coupled with a new form of material balance time that was originally put forth by Palacio and Blasingame (1993), allows the effects of adsorption to be handled in production data analysis.

The first step in this process was to show the effects of adsorption on various systems: single porosity, dual porosity, hydraulically fractured, and dual porosity with a hydraulic fracture. These systems were first viewed as constant terminal rate systems then as constant terminal pressure systems. Constant pressure systems require a correction to be made to material balance time in order to apply the correction for adsorption in the form of an adjusted total system compressibility.

Next, various analysis methods were examined to test their robustness in analyzing systems that contain adsorbed gas. Continuously, Gas Production Analysis (GPA) (Cox, et al. 2002) showed itself to be more accurate and more insightful. In combination with the techniques put forth in this work, it was used to analyze two field cases provided by Devon Energy Corporation from the Barnett Shale.

The effects of adsorption are reasonably consistent across the reservoir systems examined in this work. It was confirmed that adsorption can be managed and accounted for using the method put forth in this work. Also, GPA appears to be the best and most insightful analysis method tested in this work.

1. INTRODUCTION

1.1 Shale Gas Reservoirs in the US

The vast majority of gas production in the United States comes from what are known as conventional hydrocarbon reservoirs. However, these conventional reservoirs are becoming increasingly difficult to find and exploit. In an era of rising prices for crude oil and natural gas, the ability to produce these commodities from unconventional reservoirs becomes very important. To date, there has been less research done in the area of unconventional gas production compared to what has been done for conventional gas production.

The term unconventional reservoir requires further explanation. The United States Geological Survey (USGS) offers a complex definition of which a portion will be presented here. Among other things, an unconventional reservoir must have: regional extent, very large hydrocarbon reserves in place, a low expected ultimate recovery, a low matrix permeability, and typically has a lack of a traditional trapping mechanism (Schenk, 2002).

In particular, shale gas reservoirs present a unique problem to the petroleum industry. They contain natural gas in both the pore spaces of the reservoir rock and on the surface of the rock grains themselves that is referred to as adsorbed gas (Montgomery, et al., 2005). This is a complicated problem in that desorption time, desorption pressure, and volume of the adsorbed gas all play a role in how this gas affects the production of the total system. Adsorption can allow for significantly larger quantities of gas to be produced.

Historically, the first commercially successful gas production in the U.S. came from what would now be considered an unconventional reservoir in the Appalachian Basin in 1821. Currently, some of the largest gas fields in North America are unconventional, shale gas reservoirs such as the Lewis Shale of the San Juan Basin, the Barnett Shale of the Fort Worth Basin, and the Antrim Shale of the Michigan Basin. In addition, gas production from unconventional reservoirs accounts for roughly 2% of total U.S. dry gas production. (Hill, et al., 2007)

With the world's, and particularly the U.S.'s, increasing appetite for hydrocarbon based energy sources, the demand for gas will likely increase. Most experts agree that the days of easy, conventional gas production are nearly gone. This paves the way for an increase in the gas production from unconventional reservoirs. As far as the oil industry is concerned, nothing fuels the desire for more knowledge of a subject quite like an increase in production.

1.2 Production Data Analysis in the Petroleum Industry

For almost as long as oil and gas wells have been produced, there has been some sort of analysis done on the production data. The main effort has always been, and will continue to be, to forecast long-term production. Many wells put on production exhibit some sort of decrease in production over time. Excluding reservoirs with very strong aquifer support, this is due to a decrease in reservoir pressure. In all cases that will be considered here, this is caused by the removal of mass (oil or gas) from the reservoir. This decrease in production rate resulted in this field of petroleum engineering being called decline curve analysis (DCA).

Arguably, the first scientific approach to production forecasting was made by Arps (1945). He developed a set of empirical type curves for oil reservoirs. Little advancement beyond this empirical method was made until the early 1980's. Fetkovich (1980) took Arps' curves and developed a mathematical derivation by tying them to the pseudosteady state inflow equation. In doing so, he revolutionized this field of petroleum engineering because the technique presented showed that there were physical reasons for certain declines which removed much of the empirical stigma that surrounded DCA. For the first time, an analyst could determine reservoir properties such as permeability and net pay from an analytical model while having the confidence that the match to the production data was somewhat unique.

Next, the work of researchers such as Fraim and Wattenbarger (1987) and Palacio and Blasingame (1993) furthered that of Fetkovich. Fraim and Wattenbarger's pseudofunctions for time and pressure accounted for changes gas properties over time; this allowed decline curve analysis to be rigorously applied to gas reservoirs for the first time. In addition, Palacio and Blasingame's development of material balance time allowed for a much more rigorous match to the production data. Material balance time also allows for constant pressure data to be treated as constant rate data. This is important because the field of pressure transient analysis (PTA) emphasizes analytic models for constant rate data. These models are solutions for various scenarios that are governed by the diffusivity equation. These solutions are much more effective at identifying flow regimes and reservoir properties than traditional decline curve analysis.

1.3 Project Objectives

Shale gas reservoirs present a unique problem for production data analysis. The effects of the adsorbed gas are not clearly understood except that it tends to increase production and ultimate recovery. Lane et al. (1989) presented a methodology based on empirically calculated adsorption parameters. However, there is no rigorous analytic approach to infer the presence of adsorbed gas from production data analysis.

That said, this work will outline the effects of adsorbed gas on the common methods of production data analysis. This will focus on the effect of adsorbed gas on the type curves used for constant rate and constant pressure production schedules. In addition, the extent to which the presence of adsorbed gas can be identified with standard production data analysis techniques will be ascertained.

Lastly, the methods put forth in the work will be applied to a simulated dataset and two datasets from producing wells in the Barnett Shale. The effects and effectiveness of the methods presented will be evaluated using these datasets. In addition, what benefit does analyzing production data as an equivalent well test yield when compared to other analysis methods?

1.4 Overview of Thesis

This first chapter describes the problem that adsorbed gas presents to production data analysis and why it is necessary to better understand and solve this problem. It also outlines the objectives of this work.

Chapter 2 is a literature review of production data analysis techniques that are in common use today. It is intended to serve as refresher of the roots of production data analysis.

Chapter 3 is a literature review of shale gas reservoir analysis techniques.

Chapter 4 presents the results of a simulation study that shows the constant rate and constant pressure type curves for common systems without any effects of adsorbed gas.

Chapter 5 presents the results of a simulation study that shows the effects of adsorbed gas on the same systems presented in Chapter 4.

Chapter 6 presents 3 example cases, a simulated case and two field cases from the Barnett Shale, using systems with adsorbed gas. It presents a method for analyzing these systems and the effects of not treating these systems as adsorbed systems.

Chapter 7 details the conclusions of this work and outlines possible future work in this area.

2. PRODUCTION DATA ANALYSIS LITERATURE REVIEW

This literature review is intended to present three overarching concepts. First, there has been a lot of work done in this area, and most readers will recognize that this review is only a cursory summary at best. Only the major topics have been covered in an attempt to keep the discussion flowing. Second, all areas of production data analysis and pressure transient analysis are connected and very closely related. In reality, these two disciplines of petroleum engineering are merely working with two different boundary conditions of the same equation. Lastly, there is room for work to be done regarding the methodology of production data analysis of shale gas reservoirs.

2.1 The Diffusivity Equation

The roots of production data analysis lie in the diffusivity equation. All production data analysis makes the assumption that all or part of the production data occurs in boundary-dominated flow. If this is true, then certain assumptions can be made as to which boundary conditions can be used to solve the diffusivity equation. To start from the beginning, the diffusivity equation is a combination of the continuity equation, a flux equation, and an equation of state. The flux equation used here is Darcy's Law. For the purposes of this work, the real gas law is used as an equation of state. This allows for the handling of compressible fluids (i.e. dry gas). Typically, an exponential relationship between pressure and density is used for cases with small and constant compressibility, like liquids. The continuity equation and Darcy's Law are (Lee and Wattenbarger, 1996)

$$-\frac{1}{r}\left(\frac{\partial(r\rho v_r)}{\partial r}\right)=\frac{\partial(\phi\rho)}{\partial t} \qquad \text{Eq 1}$$

$$v_r=-\frac{k\rho}{\mu}\frac{\partial\Phi}{\partial r} \qquad \text{Eq 2}$$

Assuming that gravity effects are negligible (applicable for an approximately horizontal reservoir), Darcy's Law can be re-written as

$$v_r=-\frac{k}{\mu}\frac{\partial p}{\partial r} \qquad \text{Eq 3}$$

The density term from the real gas law is

$$\rho=\frac{M}{RT}\frac{p}{z} \qquad \text{Eq 4}$$

Combining the continuity equation, Darcy's Law, and the real gas law and assuming a homogeneous medium with constant gas composition and temperature yields (Lee and Wattenbarger, 1996)

$$\frac{1}{r}\frac{\partial}{\partial r}\left(r\frac{M}{RT}\frac{p}{z}\frac{k}{\mu}\frac{\partial p}{\partial r}\right)=\frac{\partial}{\partial t}\left(\phi\frac{M}{RT}\frac{p}{z}\right) \qquad \text{Eq 5}$$

Assuming permeability and viscosity changes are small and isothermal flow, the equation can be rearranged and have like terms canceled

$$\frac{1}{r}\frac{k}{\mu}\frac{\partial}{\partial r}\left(r\frac{p}{z}\frac{\partial p}{\partial r}\right)=\frac{\partial}{\partial t}\left(\phi\frac{p}{z}\right) \qquad \text{Eq 6}$$

The right hand side of the above equation can be expanded to (Lee and Wattenbarger, 1996)

$$\frac{\partial}{\partial t}\left(\phi\frac{p}{z}\right)=\frac{p}{z}\frac{\partial\phi}{\partial t}+\phi\frac{\partial}{\partial t}\left(\frac{p}{z}\right)=\phi\frac{p}{z}\frac{\partial p}{\partial t}\left(\frac{1}{\phi}\frac{\partial\phi}{\partial p}+\frac{z}{p}\frac{\partial}{\partial p}\left(\frac{p}{z}\right)\right) \qquad \text{Eq 7}$$

Recalling the definitions of isothermal formation and gas compressibility

$$c_f=\left(\frac{1}{\phi}\frac{\partial\phi}{\partial p}\right) \qquad \text{Eq 8}$$

$$c_g=\frac{z}{p}\frac{\partial(p/z)}{\partial p} \qquad \text{Eq 9}$$

Substituting using the above equations for compressibility

$$\frac{\partial}{\partial t}\left(\phi\frac{p}{z}\right)=\phi\frac{p}{z}\frac{\partial p}{\partial t}\left(c_f+c_g\right) \qquad \text{Eq 10}$$

Now, substituting back into the diffusivity equation

$$\frac{1}{r}\frac{\partial}{\partial r}\left(r\frac{p}{\mu z}\frac{\partial p}{\partial r}\right)=\frac{\phi\mu(c_f+c_g)}{k}\frac{p}{\mu z}\frac{\partial p}{\partial t}=\frac{\phi\mu c_t}{k}\frac{p}{\mu z}\frac{\partial p}{\partial t} \qquad \text{Eq 11}$$

This is the radial diffusivity equation for a single-phase compressible real gas in a homogeneous, horizontal medium. In order to solve this equation, it is necessary to treat it like a slightly compressible fluid. To do this, and retain its applicability to gas reservoirs, the changes in gas viscosity and compressibility must be taken into account. This is done with the two new variables called the pseudopressure (m(p)) and the pseudotime (t_a) (Lee and Wattenbarger, 1996).

$$m(p) = 2\int_{p_b}^{p} \frac{p}{\mu z} dp \qquad \text{Eq 12}$$

$$t_a = (\mu c_t)_i \int_0^t \frac{dt}{\mu c_t} \qquad \text{Eq 13}$$

Substituting these equations into the diffusivity equation yields

$$\frac{1}{r}\frac{\partial}{\partial r}\left(r\frac{\partial m(p)}{\partial r}\right) = \frac{\phi}{k}\frac{\partial m(p)}{\partial t_a} \qquad \text{Eq 14}$$

In field units (t in days)

$$\frac{1}{r}\frac{\partial}{\partial r}\left(r\frac{\partial m(p)}{\partial r}\right) = \frac{\phi}{0.00634k}\frac{\partial m(p)}{\partial t_a} \qquad \text{Eq 15}$$

Now, the above equation is ready to be solved by choosing a set of initial and boundary conditions. There are many methods and sets of initial/boundary conditions; only a select number of these solutions will be discussed here. Production data analysis assumes boundary-dominated flow at a constant bottomhole pressure. This will be discussed later; constant pressure solutions can also be transformed into constant rate solutions. For this discussion, the constant rate solution for a well in the center of a cylindrical reservoir will be used. The initial and boundary conditions are then (in field units) (Lee and Wattenbarger, 1996)

$$m(p)(r, t = 0) = m(p_i) \qquad \text{Eq 16}$$

$$\left(r\frac{\partial m(p)}{\partial r}\right)_{r=r_w} = \frac{50300\, p_{sc} T q}{khT_{sc}} \qquad \text{Eq 17}$$

$$\left(\frac{\partial m(p)}{\partial r}\right)_{r=r_e} = 0 \qquad \text{Eq 18}$$

The approximate, dimensional-space solution to the diffusivity equation with the above assumptions is (Lee and Wattenbarger, 1996)

$$m(p_i) - m(p_{wf}) = \Delta p_p = \frac{2q_g p_i}{(\mu_g c_t z)_i G} t_a + \frac{1.417E^{-6}Tq_g}{kh}\left(\ln\frac{r_e}{r_w} - \frac{3}{4}\right) \qquad \text{Eq 19}$$

This is a very important solution because it is so similar to some of the solutions used in production data analysis.

2.2 Dimensionless Variables and the Laplace Transform

The solution to the diffusivity equation presented earlier is a perfectly valid dimensional space solutions. To solve more complicated systems, certain steps must be taken. To start, the diffusivity equation for a single-phase compressible fluid in a homogeneous, horizontal medium is

$$\frac{1}{r}\frac{\partial}{\partial r}\left(r\frac{\partial p}{\partial r}\right) = \frac{\phi\mu c_t}{k}\frac{\partial p}{\partial t} \qquad \text{Eq 20}$$

A solution to the above equation can be seen in Eq 19. However, a more simple solution exists if certain variables are created that allow for the simplification of the expressions involved. For instance, the following equation for pressure has no units, but it encompasses all of the variables that have an effect on pressure.

$$p_d = \frac{kh(p_i - p_{wf})}{q\mu B} \qquad \text{Eq 21}$$

Dimensionless time and dimensionless radius can also be presented in the same manner.

$$t_d = \frac{kt}{\phi\mu c_t r_w^2} \qquad \text{Eq 22}$$

$$r_d = \frac{r}{r_w} \qquad \text{Eq 23}$$

The definition of dimensionless variables can mainly be a matter of recognizing the important groups that govern the equation that is being solved and knowing how to simplify algebraic expressions. Also, they may be developed from the boundary conditions used for the equations with the aim of simplifying the resulting solution. In particular, the diffusivity equation sets the definition of r_d and t_d, while the boundary conditions determine the scaling for p_d. Now, using Eq 23-25, the diffusivity equation can be re-written in dimensionless form as

$$\frac{1}{r_d}\frac{\partial}{\partial r_d}\left(r_d\frac{\partial p_d}{\partial r_d}\right)=\frac{\partial p_d}{\partial t_d} \qquad \text{Eq 24}$$

with initial condition as

$$p_d(r_d)_{t_d=0}=0 \qquad \text{Eq 25}$$

and inner boundary condition (constant-rate production) and outer boundary condition (closed outer boundary) as

$$\left(\frac{\partial p_d}{\partial r_d}\right)_{r_d=1}=-1 \qquad \text{Eq 26}$$

$$\left(\frac{\partial p_d}{\partial r_d}\right)_{r_d=r_{ed}}=0 \qquad \text{Eq 27}$$

Since, by definition, the dimensionless variables incorporate all of the terms that affect that variable, most pressure transient plots and production data analysis plots are done using dimensionless pressure and time variables.

There are many different methods employed to arrive at a solution to the diffusivity equation with the above boundary conditions. However, a very useful method for solving this dimensionless equation is by utilizing the Laplace transform. The Laplace transform for dimensionless pressure is given as (Van Everdingen and Hurst, 1949)

$$\overline{P_d}(r_d,s)=\int_0^\infty p_d(r_d,t_d)e^{-st_d}\,dt \qquad \text{Eq 28}$$

where *s* is the Laplace variable. The diffusivity equation and boundary conditions in Laplace space are given as

$$\frac{d^2\overline{P_d}}{dr_d^2}+\frac{1}{r_d}\frac{d\overline{P_d}}{dr_d}=s\overline{P_d} \qquad \text{Eq 29}$$

$$\left(\frac{\partial\overline{P_d}}{\partial r_d}\right)_{r_d=1}=-\frac{1}{s} \qquad \text{Eq 30}$$

$$\left(\frac{\partial\overline{P_d}}{\partial r_d}\right)_{r_d=r_{ed}}=0 \qquad \text{Eq 31}$$

The solution to Eq 29 with the given boundary conditions in Laplace space is

$$\overline{P_d}=\frac{K_1(r_{ed}\sqrt{s})I_0(r_d\sqrt{s})+I_1(r_{ed}\sqrt{s})K_0(r_d\sqrt{s})}{s^{3/2}\left[I_1(r_{ed}\sqrt{s})K_1(\sqrt{s})-K_1(r_{ed}\sqrt{s})I_1(\sqrt{s})\right]} \qquad \text{Eq 32}$$

with I_0 , I_1, K_0, and K_1 being modified Bessel functions of the first and second kind of order 0 and 1. This is the complete form of the analytic solution for a single porosity, homogeneous, bounded system produced at constant rate. There are many more systems that will be discussed in this work and their solutions were arrived at in a similar manner as this one. However, one extremely useful attribute of solutions in Laplace space is the manner in which solutions with terminal constant pressure boundaries (instead of constant rate) are obtained. In Laplace space, the relationship between pressure and rate is given as (Van Everdingen and Hurst, 1949)

$$\overline{P}=\frac{1}{s^2\overline{Q}} \qquad \text{Eq 33}$$

In Eq 33, $\overline{P}$ is the cumulative pressure drop (i.e. the change in reservoir pressure) in Laplace space while $\overline{Q}$ is the cumulative production due to a constant rate in Laplace space. Constant rate solutions to the diffusivity equation are almost ubiquitous in the petroleum industry. The definition in Eq 33 implies that the constant pressure solution for any system with a constant rate solution can be obtained by mere algebra thanks to the Laplace transform.

These solutions are relatively useless if left in Laplace space. The most common method in use within the petroleum industry is to numerically invert the Laplace space solution using the Stehfest algorithm one version of which is (Stefhest, 1970)

$$V_i = (-1)^{\frac{N}{2}+i} \sum_{F=\frac{i+1}{2}}^{\max\left(\frac{N}{2},\, i\right)} \frac{F^{\frac{N}{2}+1}(2F)!}{\left(\frac{N}{2}-F\right)!(F!)^2(i-F)!(2F-i)!} \qquad \text{Eq 34}$$

where V_i is the Stehfest coefficient and N is the Stehfest number. For the solutions considered in this work, Stehfest numbers between 8 and 12 yield the most stable results.

2.3 Type Curves for Single Porosity Systems

Now, let us examine a specific case that is commonly analyzed in both pressure transient analysis and production data analysis. It becomes clear why so much effort was spent in describing the origins of the diffusivity equation in detail, since the analysis of the various commonly encountered reservoirs almost entirely relies upon type curves. A type curve can be created for any situation for which an all encompassing, or general solution can be obtained. These solutions all come from the diffusivity equation and differ only in the assumptions they make as to the system structure, boundary conditions, and the dimensionless groups chosen.

For instance, a very common solution is the single porosity, slightly compressible liquid type curves (Eq 32). They use the same p_d and t_d given in Eq 21 and Eq 22, and they include a dimensionless wellbore storage term given as (Lee and Wattenbarger, 1996)

$$C_d = \frac{C}{\phi c_t h r_w^2} \qquad \text{Eq 35}$$

where, for wellbores containing only a single fluid

$$C = V_{well} * c_{well} \qquad \text{Eq 36}$$

and c_{well} is the compressibility of fluid in the wellbore. In pressure transient analysis, type curves are typically displayed two ways. First, the dimensionless pressure is plotted against dimensionless time. Second, a diagnostic plot (i.e. derivative plot) is made. For this case, the y-axis will be $t_d/C_d\,(d\ln(p_d)/d(t_d/C_d))$ and the x-axis will be t_d/C_d. The derivative plot allows for flow regimes to be identified more easily. The type curves can be seen in Figure 1. The early time "hump" is the characteristic effect of wellbore storage in which fluid production comes from the expansion of both the fluid already inside the well and the fluid in the reservoir. The plotting functions for the plot shown below are p_d, as given in Eq 21, and t_d/C_d.

There have been numerous pressure transient (constant rate) solutions developed over the years. As has been shown (Eq 33), it is fairly easy to get a solution for a constant pressure system if the constant rate solution in Laplace space is available. In reality, data is never collected at truly

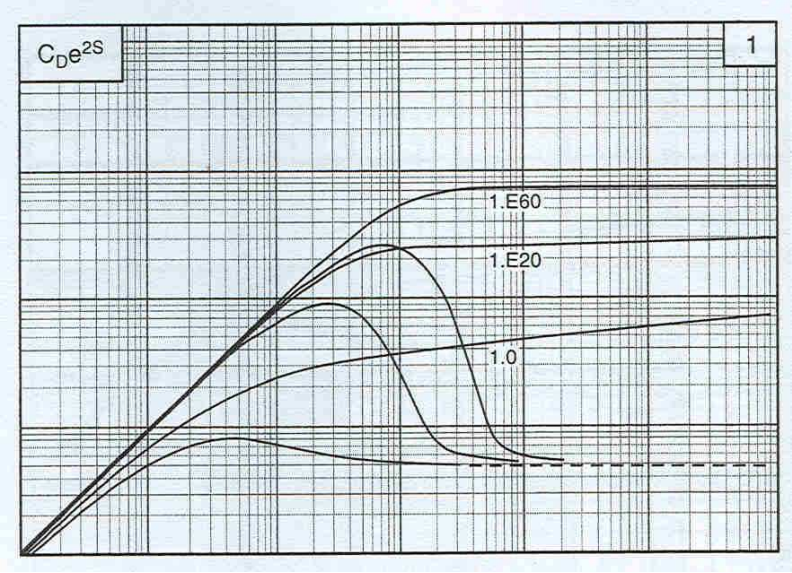

Figure 1 – Type Curves for a Single Porosity Homogeneous Reservoir from Schlumberger (1994)

constant rate or constant pressure. There are always variations. The data, whether constant rate or pressure, must be re-initialized at each change. With constant rate data, this is done only with the time function and is known as superposition. With constant pressure data, re-initialization must be done in both rate and time and the superposition calculations are more difficult.

Until recently, production data analysis has relied on more empirical methods/solutions because of the difficulty of analytic solutions. In the last decade, the more rigorous constant pressure solutions have begun to make a comeback. Building on the success of Fetkovich's decline curves, much of the credit for this goes to research groups at Texas A&M University and Fekete Associates in Canada. Fekete has developed numerous software tools that allow users to access the analytical constant pressure solutions in the same way pressure transient analysts have done for years. This combined with high-resolution production data that has historically been available only for pressure transient testing has breathed new life into production data analysis.

2.4 Arps and Fetkovich

Fetkovich's main advancement to the area of DCA was to place it on firm mathematical/theoretical ground. All DCA is in some way based on Arp's original set of type curves. These curves were completely empirical and had been regarded as non-scientific. Arps' decline equation is (Arps, 1945)

$$q(t) = \frac{q_i}{(1 + bD_i t)^{\frac{1}{b}}} \qquad \text{Eq 37}$$

where the empirical relationship for D_i is

$$D_i = \frac{q_i}{N_{pi}} \qquad \text{Eq 38}$$

N_{pi} is the cumulative oil production to a hypothetical reservoir pressure of 0 psi. The Arps equation yields an exponential decline when b = 0 (b = 1 is hyperbolic decline) with an exponent of $-D_i*t$. The value of b can be indicative of the reservoir type and drive mechanism. Anything over 0.5 is usually considered multi-layered or heterogeneous. It should be noted that surface facilities can affect the b value as well. Backpressure on a well will result in a higher b value than would otherwise be obtained. (Fetkovich et al., 1987)

Hurst (1943) proposed solutions for steady-state water influx. Using modified versions of these solutions for finite water influx, Fetkovich (1980) proposed that

$$q(t) = \frac{J(p_i - p_{wf})}{e^{\frac{(q_i * t)}{N_{pi}}}} \qquad \text{Eq 39}$$

where

$$J = q_i / p_i \qquad \text{Eq 40}$$

and

$$N_{pi} = \frac{\pi(r_e^2 - r_w^2)\phi c_t h p_i}{5.615B} \qquad \text{Eq 41}$$

Assuming that $p_{wf} = 0$ (wide open decline), one arrives at Arps' (1945) equation which is

$$\frac{q(t)}{q_i} = e^{-\frac{q_i}{N_{pi}}t} \qquad \text{Eq 42}$$

So, Fetkovich rederived Arp's equation and then merged that with pseudosteady-state inflow equations. So $D_i = q_i / N_{pi}$ and $t_{Dd} = (q_i / N_{pi}) * t$. Assuming a circular reservoir and pseudosteady inflow, Fetkovich (1980) proposed that

$$q_i = \frac{kh(p_i - p_{wf})}{141.2\mu B\left[\ln\left(\frac{r_e}{r_w}\right) - 0.5\right]} \qquad \text{Eq 43}$$

$$t_{Dd} = \frac{\dfrac{.00634kt}{\phi\mu c_t r_w^{\,2}}}{0.5\left[\left(\dfrac{r_e}{r_w}\right)^2 - 1\right]\left[\ln\left(\dfrac{r_e}{r_w}\right) - 0.5\right]} \qquad \text{Eq 44}$$

with $q_{Dd} = q(t) / q_i$

$$q_{Dd} = \frac{\dfrac{q(t)}{kh(p_i - p_{wf})}}{141.2\mu B\left[\ln\left(\dfrac{r_e}{r_w}\right) - 0.5\right]} = q_d\left[\ln\left(\frac{r_e}{r_w}\right) - 0.5\right] \qquad \text{Eq 45}$$

where q_d is the dimensionless flowrate given by

$$q_d = \frac{141.2quB}{kh(p_i - p_{wf})}$$

Plotting q_{Dd} vs. t_{Dd} yields the classic Fetkovich decline curve plot which can be seen in Figure 2.

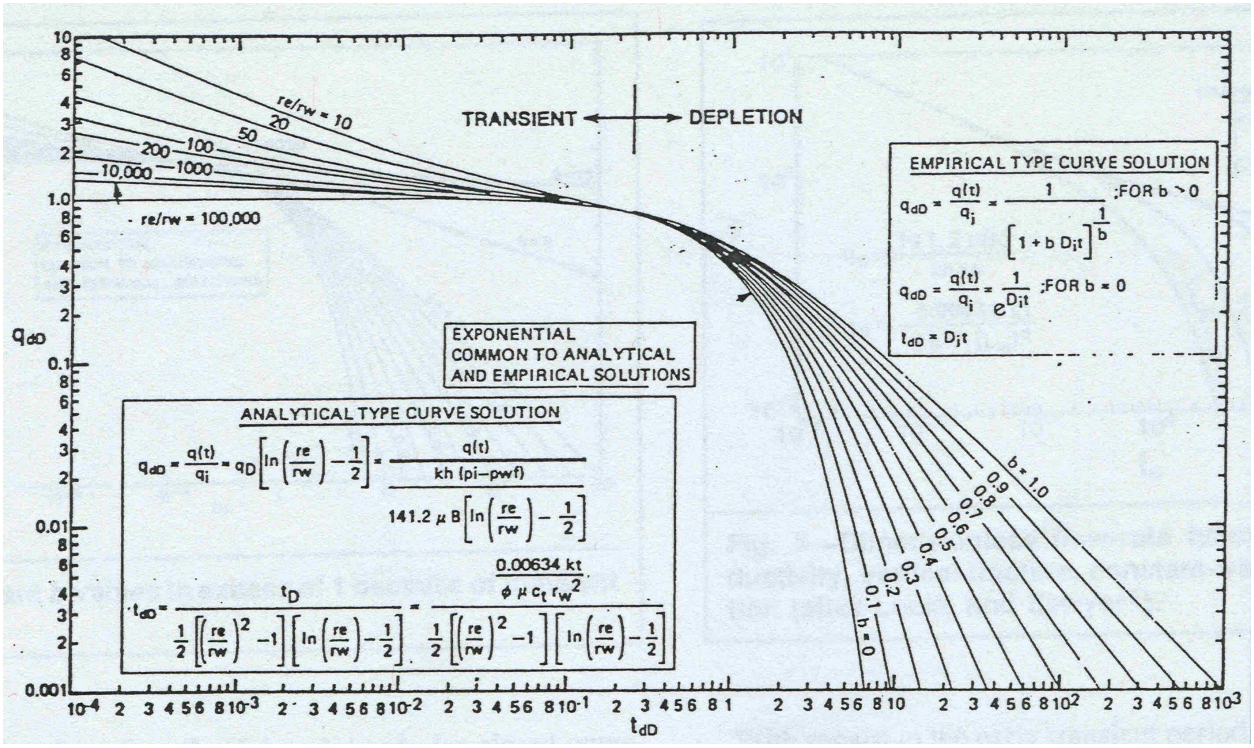

Figure 2 – Fetkovich Type Curves from Fetkovich, et al. (1987)

Fetkovich combined the constant pressure solution to the diffusivity equation with the Arps equation in a consistent manner which allows a relatively simple, single type curve to be developed.

Fetkovich never shows the full derivation of his solution. Ehlig-Economides and Joseph (1987) presented the full derivation of the solution. They also showed that the 0.5 term in Eq 45-47 should be 0.75 considering that this is a pseudosteady-state solution. They also stated that 0.5 appeared to be a better fit to field data even though it is not theoretically correct.

Another important concept introduced to DCA by Fetkovich was re-initialization. Any time the flow regime changes (for instance, if the well is shut-in, cut back, or stimulated), the production data must be re-initialized in time and rate. This is done by changing the reference p_i and q_i and resetting the time to 0.

2.5 Use of Pseudofunctions by Carter and Wattenbarger

Fetkovich's decline curves were developed for liquid systems. Carter (1981) recognized that the assumption of small and constant compressibility was very inaccurate for gas reservoirs produced at a high drawdown pressure. He developed a variable (γ_g) that qualified the magnitude of the error being made when analyzing a gas system using the decline curves for a liquid system. Carter (1981) defined γ_g as

$$\lambda_{cart} = \frac{\mu_{gi} c_{gi}}{2} \frac{m(p_i) - m(p_{wf})}{(p/z)_i - (p/z)_{wf}} \qquad \text{Eq 46}$$

Where μ_{gi} and c_{gi} are the gas viscosity and compressibility at the initial pressure and $\bar{\mu}_g$ and $\bar{c}_g$ are evaluated at average reservoir pressure. Each value of λ_{cart} had its own set of decline curve stems. This is a rather empirical approach that allowed gas systems to plot on liquid system decline curves. An example of Carter's decline curves can be seen in Figure 3.

The next significant advancement in DCA came from Fraim and Wattenbarger (1987). Drawing on concepts from pressure transient analysis and earlier work done by Fetkovich (1980) and Carter (1981), they introduced the concept of pseudotime for analyzing gas well production data. Fraim and Wattenbarger (1987) derived the following equation for bounded, radial, gas reservoirs:

$$\ln\left(\frac{q}{q_i}\right) = \frac{-2J_g (p/z)_i}{G(\mu_g c_g)_i} \int_0^t \frac{(\mu_g c_g)_i}{\bar{\mu}_g \bar{c}_g} dt \qquad \text{Eq 47}$$

where

$$J_g = \frac{1.9875E^{-5} k_g h}{0.5 \ln\left(\frac{2.2458A}{C_A r_w^{\,2}}\right)} \frac{T_{sc}}{p_{sc} T} \qquad \text{Eq 48}$$

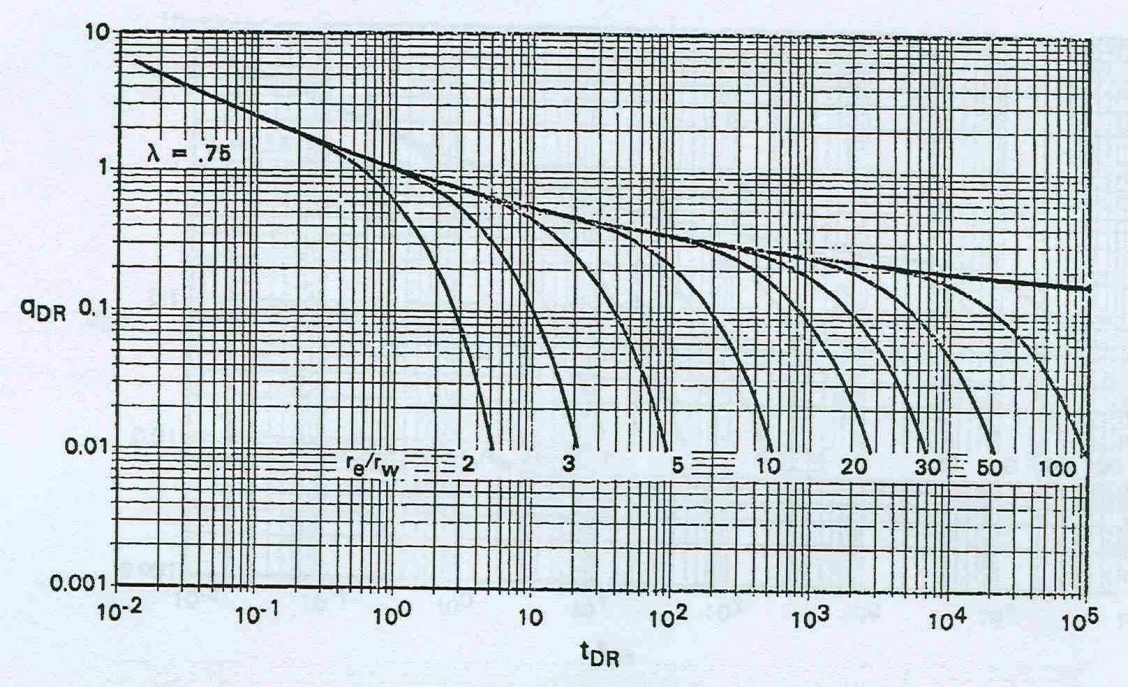

Figure 3 – Type Curves for Gas Systems from Carter (1981)

The shape factor (C_A) used in the equation for J_g is 19.1785 rather than the 31.62 for a circular reservoir. This is done in order to conform to Fetkovich's type curves. The need for a pseudotime function is evident after examining Eq 47. Fraim and Wattenbarger (1987) define it as:

$$t_a = (\mu c_t)_i \int_0^t \frac{dt}{\mu c_t} \qquad \text{Eq 49}$$

The difference between pseudotime and actual time can be seen in Figure 4 from Fraim and Wattenbarger (1987). Now, any homogeneous, closed, gas reservoir will exhibit exponential decline when plotted with the pseudotime function.

2.6 Material Balance Time by Palacio and Blasingame

Palacio and Blasingame (1993) presented the use of material balance time functions to minimize the effects of variable rate/pressure production histories on the accuracy of DCA forecasts. All previous methods of DCA required that the well being analyzed be in pseudosteady state (constant pressure/rate production) in order to isolate the correct transient and decline stems. Their equation for liquid decline was:

$$\frac{q_o}{p_i - p_{wf}} \frac{141.2\mu B}{kh}\left[0.5\ln\left(\frac{4A}{e^{\gamma} C_A r_w{}^2}\right)\right] = \frac{1}{1+\bar{t}_{Dd}} \qquad \text{Eq 50}$$

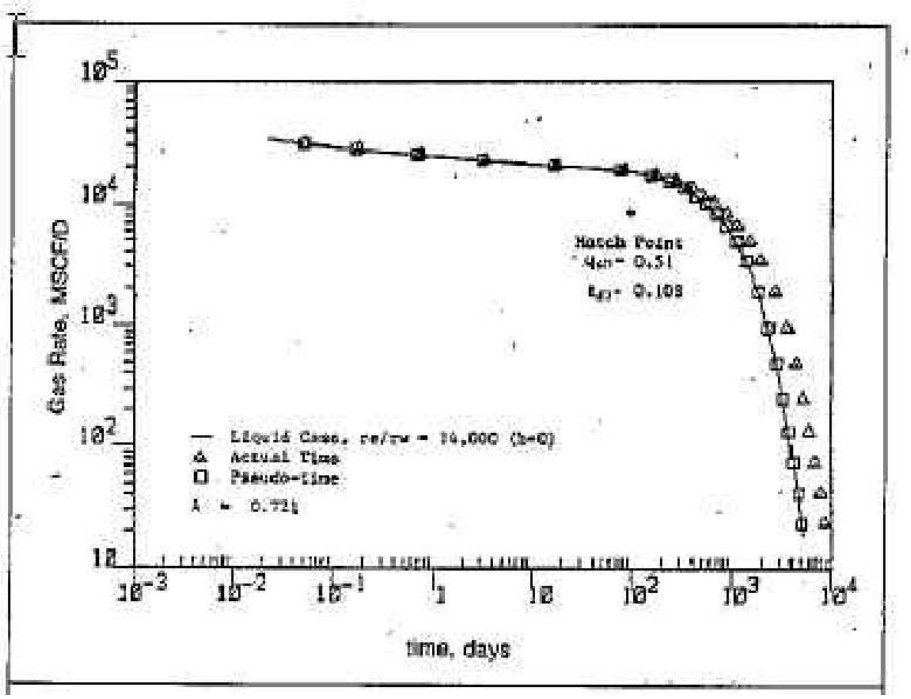

Figure 4 – The effect of gas compressibility and gas viscosity on a rate-time decline curve from Fraim and Wattenbarger (1987)

where

$$\bar{t}_{Dd} = \frac{2\pi\left(\frac{.00634k}{\phi\mu c_t A}\right)\bar{t}}{0.5\ln\left(\frac{4A}{e^{\gamma}C_A r_w^{\,2}}\right)} \qquad \text{Eq 51}$$

with

$$\bar{t} = \frac{N_p}{q_o} \text{ (material balance time)} \qquad \text{Eq 52}$$

The only two differences between this and Fetkovich's equations are the use of material balance time, and the right hand side of Eq 50 is a harmonic instead of a hyperbolic.

Palacio and Blasingame's (1993 proposed the use of material balance pseudotime which is based on the real gas pseudopressure. Their decline equation for gas was:

$$\frac{\Delta p_p}{q_g} = m_a t_a \qquad \text{Eq 53}$$

where

$$m_a = \frac{1}{Gc_{ti}} \qquad \text{Eq 54}$$

The pseudosteady-state inflow equation is as follows

$$\frac{m(p_i) - m(\overline{p})}{q_g} = 141.2 \frac{\mu_{gi} B_{gi}}{k_g h} \left[\frac{1}{2} \ln\left(\frac{4}{e^{\gamma}} \frac{A}{C_A r_w^2} \right) \right] \qquad \text{Eq 55}$$

Adding Eq 54 and Eq 55 gives Palacio and Blasingame's (1993) coupled decline equation as

$$\frac{m(p_i) - m(\overline{p})}{q_g b_{a,pss}} = 1 + \frac{m_a}{b_{a,pss}} t_a \qquad \text{Eq 56}$$

where

$$b_{a,pss} = 141.2 \frac{\mu_{gi} B_{gi}}{k_g h} \left[\frac{1}{2} \ln\left(\frac{4}{e^{\gamma}} \frac{A}{C_a r_w^2} \right) \right] \qquad \text{Eq 57}$$

$$B_g = \frac{zTp_{sc}}{z_{sc} T_{sc} p} \qquad \text{Eq 58}$$

Now, Palacio and Blasingame's (1993) equation can be re-written as

$$\Delta m(p) = q_g 141.2 \frac{\mu_{gi} B_{gi}}{k_g h} \left[\frac{1}{2} \ln\left(\frac{4}{e^{\gamma}} \frac{A}{C_A r_w^2} \right) \right] + \frac{q_g}{Gc_{ti}} t_a \qquad \text{Eq 59}$$

While it does not look exactly the same as the solution to the diffusivity equation that was presented earlier, it is equivalent if you consider that the natural log term in Palacio and Blasingame's equation is the more shape factor. The approximation for a well in the middle of a cylindrical reservoir is $\ln(r_e/r_w - 3/4)$.

Now, it is necessary to examine the decline portion of Eq 59 to elaborate on Palacio and Blasingame's approach and their derivation of material balance pseudotime. As was previously mentioned, the decline equation for gas as presented by Palacio and Blasingame (1993) is

$$\frac{\Delta m(p)}{q_g} = \frac{1}{Gc_t} t_a \qquad \text{Eq 60}$$

For gas reservoirs, this equation is valid when the pseudotime (t_a) includes a material balance component given as

$$t_a = \bar{t}_a = \frac{\mu_{gi} c_{ti}}{q_g} \int_0^t \frac{q_g}{\bar{\mu}_g \bar{c}_t} dt \qquad \text{Eq 61}$$

(material balance incorporated into t_a). Pseudopressure is taken as

$$m(p) = 2\int_0^p \frac{p}{\mu_g z} dp \qquad \text{Eq 62}$$

Explaining the derivation of material balance pseudotime requires the use of the gas material balance equation. This is a well known and widely used relationship between gas production, corrected reservoir pressure, and original gas in place. The equation for gas material balance assumes that the reservoir has a closed outer boundary (i.e. is volumetric with no water influx). Also, the only energy from the reservoir that drives gas production comes from the expansion of the gas itself. Rock and connate water expansion/compressibility are assumed negligible. The gas material balance equation under these assumptions is

$$G_p = G\left(1 - \frac{\bar{p}}{\bar{z}} \frac{z_i}{p_i}\right) \qquad \text{Eq 63}$$

Where G_p = cumulative gas production, and the original gas in place, G, is given by

$$G = \frac{V_b \phi (1 - S_w)}{B_g} \qquad \text{Eq 64}$$

For the purposes of this development, gas production rate is more important than cumulative production. So, the derivative of the gas material balance equation will yield the flowrate. This expression is then

$$q_g = \frac{dG_p}{dt} = -G\frac{z_i}{p_i}\frac{d}{dt}\left(\frac{\bar{p}}{\bar{z}}\right) \qquad \text{Eq 65}$$

Rewriting the gas material balance equation

$$q_g = -G\frac{z_i}{p_i}\frac{d\left(\bar{p}/\bar{z}\right)}{d\bar{p}}\frac{\partial\bar{p}}{\partial t} \qquad \text{Eq 66}$$

Substituting the definition of gas compressibility (Eq 9) into the material balance equation

$$q_g = -G\frac{z_i}{p_i}\frac{\bar{p}}{\bar{z}}c_g\frac{d\bar{p}}{dt} \qquad \text{Eq 67}$$

Now, this definition of q_g can be substituted into the expression for $\bar{t}_a$ (Eq 63). The result is

$$\bar{t}_a = \frac{\mu_{gi}c_{ti}}{q_g}\left(-\frac{Gz_i}{p_i}\right)\int_0^t \frac{\bar{p}}{\bar{z}}\frac{c_g}{\bar{\mu}_g\bar{c}_t}\frac{dp}{dt}dt \qquad \text{Eq 68}$$

To make this integral easier to solve, Palacio and Blasingame (1993) suggested that, consistent with the assumptions in gas material balance, the compressibility could be removed by assuming that gas compressibility (c_g) is roughly equal to total system compressibility (c_t). This is can be seen in the equation for system compressibility of a dry gas reservoir below.

$$c_t = (1-S_w)c_g + S_w c_w + c_f \qquad \text{Eq 69}$$

Water compressibility is typically around $1\text{x}10^{-6}$ and formation compressibility is typically around $4 \text{ x } 10^{-6}$ in consolidated formations. Both of these are 2 to 3 orders of magnitude smaller than typical values of gas compressibility, even at high pressure. Thus, under these conditions $c_t \approx c_g$ and the equation for material balance time can be re-written as

$$\bar{t}_a = \frac{\mu_{gi}c_{ti}}{q_g}\left(-\frac{Gz_i}{p_i}\right)\int_{p_i}^{\bar{p}} \frac{p}{z\mu_g}dp \qquad \text{Eq 70}$$

The integral term in this equation is an expression for the real gas pseudopressure difference. So, the final equation for gas material balance pseudotime is

$$\bar{t}_a = \frac{\mu_{gi} c_{ti}}{q_g} \left(\frac{G z_i}{2 p_i} \right) \left[m(p_i) - m(\bar{p}) \right] \qquad \text{Eq 71}$$

The use of pseudopressure is extremely important when dealing with gas reservoirs because it accounts for changes in gas viscosity and compressibility, especially if there is a significant change in reservoir pressure over time. This is the most accurate means of accounting for these changes in gas properties (Wattenbarger and Lee, 1996).

2.7 Agarwal

The most significant contribution of Agarwal et al. (1999) was their verification of the Palacio and Blasingame (1993) development of material balance time. Agarwal et al. (1999) used a single-phase reservoir simulator to compare constant rate and constant pressure systems. They verified that any system produced at constant pressure could be converted to an equivalent constant rate system using the material balance time transformation. This is a very important finding because now the vast library of well known analytical solutions for constant rate systems can be utilized in production data analysis. In addition, the concept of re-initialization of production data is much more simple in a constant rate system than in a constant pressure system.

Agarwal et al. (1999) also made a significant contribution with the use of derivatives in type curve analysis to greatly aid in the identification of the transition between the transient and pseudosteady state flow regimes. They used the Palacio and Blasingame (1993) method of calculating dimensionless adjusted time (t_{aD}), which is identical to that of Palacio and Blasingame (1993) (Eq 69). They also developed their own function of dimensionless time based on area (t_{DA}).

$$t_{DA} = t_{aD} \left(\frac{r_w^2}{A} \right) \qquad \text{Eq 72}$$

Agarwal et al. (1999) modified three varieties of type curves: rate-time, rate-cumulative production, and cumulative production-time. Their plot of rate-time is made with $1/p_{wd}$ vs. t_{DA}. They also plot p_{wd}' vs. t_{DA} and $1/d\ln(p_{wd}')$ vs. t_{DA}. As is seen in Figure 5, p_{wd}' has a slope of 2 in the transient period and a slope of 0 during pseudosteady state. This makes it fairly easy to identify flow regimes when analyzing production data. The Agarwal et al. (1999) equation for p_{wd} and dimensionless cumulative production ($Q_D A$) are

$$\frac{1}{p_{wd}} = \frac{1422 T q(t)}{kh * [m(p_i) - m(p_{wf})]} \qquad \text{Eq 73}$$

$$Q_{AD} = \frac{200 T z_i G_i}{\phi h r_{wa}^2 p_i} \frac{m(p_i) - m(\bar{p})}{m(p_i) - m(p_{BHP})} \qquad \text{Eq 74}$$

$$Q_{DA} = Q_{AD} \frac{r_{wa}^2}{A} \qquad \text{Eq 75}$$

2.8 Well Performance Analysis by Cox et al.

Cox et al. (2002) used Palacio and Blasingame's material balance time approach coupled with standard dimensionless variables (p_{wd} and t_d). Since Palacio and Blasingame's t_a approach "converts" constant pressure data to constant rate data, Cox, et al. (2002) showed that production data could be analyzed as an equivalent, constant rate well test. While these authors brought no theory forward, their work is an excellent example of combining constant-pressure decline curves with constant-rate, pressure transient type curves.

This kind of paired analysis makes for very good, relatively speaking, reservoir characterization and production forecasting. Constant rate analysis allows for easy recognition of flow regimes. For example, the radial flow regime is always a horizontal line on the derivative plot of a constant rate solution. Boundary dominated flow (i.e. depletion) is always a unit-slope on both the dimensionless pressure and pressure derivative plots. Recognizing these flow regimes is critical to the accuracy of forecasting cumulative production.

In summary, production data analysis no longer requires that q_d vs. t_d be plotted and re-initialized. Now, there is a tool, material balance time, that allows all of the production data to be used without re-initialization assuming that the rate and pressure values are correct.

Agarwal et al. (1999) showed that constant rate and constant pressure solutions are equivalent with material balance time. This, combined with the analytical solutions in Laplace space allows all of the pressure transient solutions to be utilized in production data analysis. Cox et al. (2002) showed that production data could be plotted as an equivalent well test and that the flow regimes were preserved in their entirety. The hypothesis of this work is that if the parameters of shale gas reservoirs were well quantified and the effects of adsorbed gas were understood, production data from these complex reservoirs should be able to be analyzed in a similar manner to what has been discussed so far.

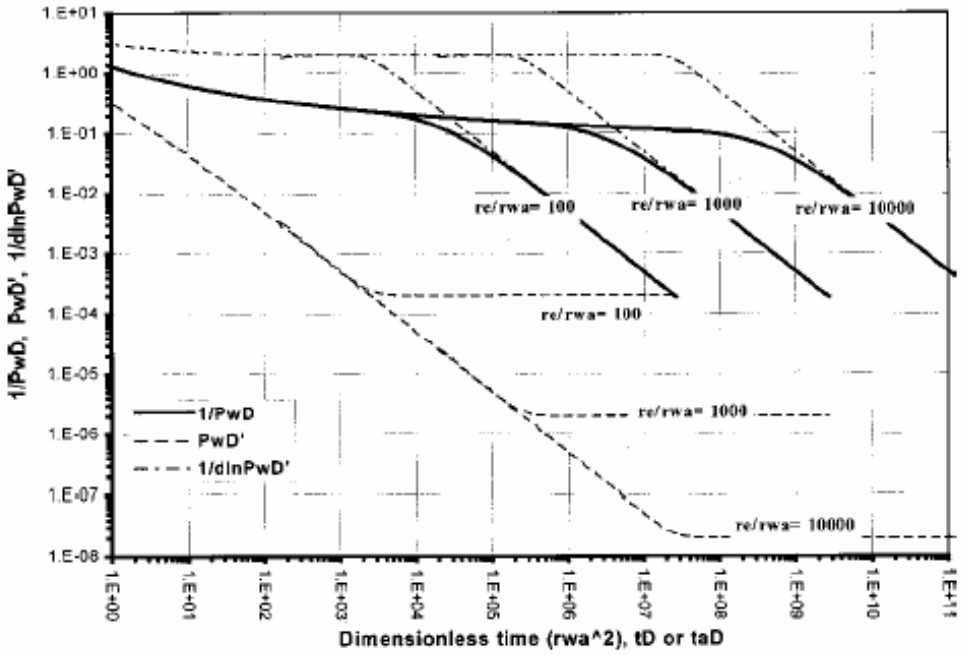

Figure 5 – Dimensionless Type Curves from Agarwal (1999)

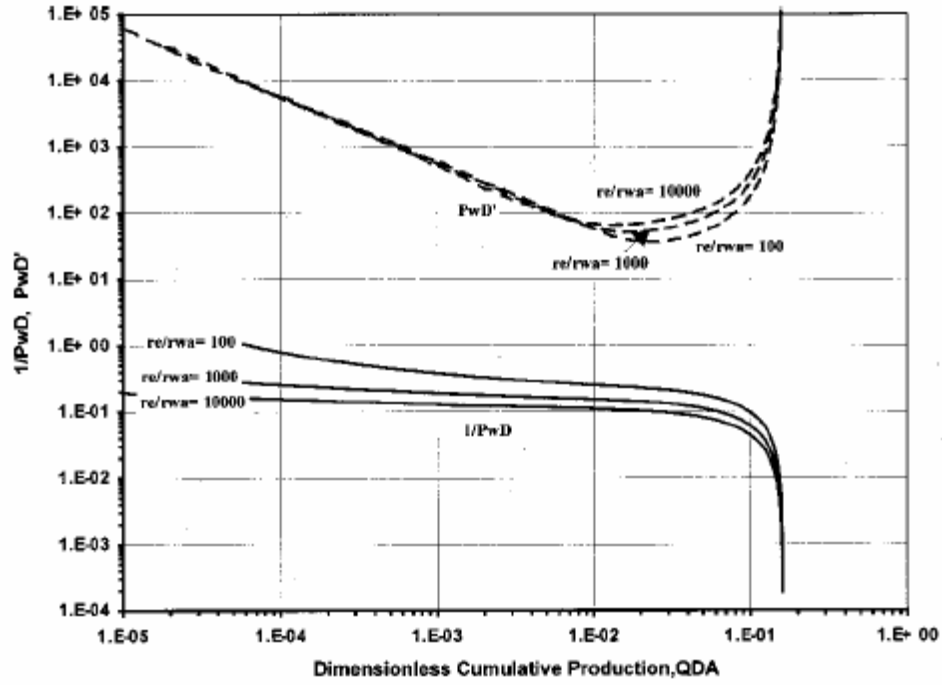

Figure 6 – Cumulative Production plot from Agarwal (1999)

3. SHALE GAS ANALYSIS TECHIQUES LITERATURE REVIEW

As was mentioned earlier, unconventional reservoirs are playing a larger and larger role in supplying the demand for hydrocarbons in the United States. In particular, the Barnett shale formations of the Fort Worth Basin have shown increasing promise in recent years. It is estimated that the Barnett Shale could contain as much as 250 TCF of gas originally in place. Ultimate recoveries range from 10 to 20 percent. (Montgomery et al., 2005)

3.1 Description of Shale Gas Reservoirs

Shale gas reservoirs present numerous challenges to analysis that conventional reservoirs simply do not provide. The first of these challenges to be discussed is the dual porosity nature of these reservoirs. Similar to carbonate reservoirs, shale gas reservoirs almost always have two different storage volumes for hydrocarbons, the rock matrix and the natural fractures (Gale et al., 2007). Because of the plastic nature of shale formations, these natural fractures are generally closed due to the pressure of the overburden rock (Gale et al., 2007). Consequently, their very low, matrix permeability, usually on the order of hundreds of nanodarcies (nd), makes un-stimulated, conventional production impossible. Therefore, almost every well in a shale gas reservoir must be hydraulically stimulated (fractured) to achieve economical production. These hydraulic fracture treatments are believed to re-activate and re-connect the natural fracture matrix (Gale et al., 2007).

Another key difference between conventional gas reservoirs and shale gas reservoirs is adsorbed gas. Adsorbed gas is gas molecules that are attached to the surface of the rock grains (Montgomery et al., 2005). The nature of the solid sorbent, temperature, and the rate of gas diffusion all affect the adsorption (Montgomery et al., 2005). Currently, the only method for accurately determining the adsorbed gas in a formation is through core sampling and analysis. The amount of adsorbed gas is usually reported in SCF/ton of rock or SCF/ft^3 of rock. Depending on the situation, adsorbed gas can represent a large percentage of the gas in place and can have a dramatic impact on production.

3.2 Empirical Methods

Previous efforts of production data analysis of shale reservoirs have focused on identifying the presence of adsorption/desorption and determining the correct plotting parameters necessary to accurately estimate reservoir parameters. Lane and Watson (1989) used various types of numerical simulation models (single porosity with and without adsorption, and dual porosity with and without adsorption) to attempt to identify adsorption parameters. In addition, they attempted to determine which type of model gave the best results. They performed a history match to production data for each type of model. Based on which model yielded the best statistical match to the production data, they were able to determine whether or not the desorption mechanism was present.

However, they noted that the shape of the Langmuir isotherm greatly affected their ability to identify desorption. A linear isotherm indicates very little gas is adsorbed onto the surface of the shale grains; a non-linear, highly curved, isotherm indicates that large quantities of gas are adsorbed. In the case of a linear isotherm, the models without desorption were not significantly different from those with desorption.

Lane and Watson (1989) noted that estimating the values of the desorption parameters (and the Langmuir isotherm) accurately from production data was not possible, but they were able to accurately determine permeability. However, they stated that if certain reservoir parameters were independently known, the error in estimating desorption parameters would be greatly reduced.

Hazlett and Lee (1986) focused on finding an appropriate correlating parameter (plotting function) for shale gas reservoirs. They correctly noted that the early and intermediate time flow in dual porosity systems is dominated by the fracture system. Thus, λ, the interporosity flow coefficient, plays no role. During late time, λ plays a major role while ω, the storativity ratio, plays only a minor role. So, the approximate solutions to the dual porosity analytical model are:

Early time:

$$q_d = \left(\frac{\omega}{\pi t_d}\right)^{\frac{1}{2}} \qquad \text{Eq 76}$$

Intermediate time:

$$q_d = \frac{1}{\ln r_{eD} - 0.75} \exp\left(\frac{2t_d}{r_{eD}^2(\ln r_{eD} - 0.75)}\right) \qquad \text{Eq 77}$$

Late time:

$$q_d = \frac{(r_{eD}^2 - 1)\lambda}{2} \exp\left(\frac{(-\lambda)t_d}{(1-\omega)}\right) \qquad \text{Eq 78}$$

They also developed new versions of the plotting variables q_d and t_d. Their versions include the parameter λr_{eD}^2, q is replaced with N_p/t, and r_w is replaced with r_e. This yields:

$$Q_{Dre} = \frac{0.894 N_p B_g (1-\omega)}{\phi c_t h r_e^2 (p_i - p_{wf})} \qquad \text{Eq 79}$$

and

$$t_{Dre} = \frac{0.00634 kt(1-\omega)}{\phi \mu_g c_t r_e^2} \qquad \text{Eq 80}$$

When, Q_{Dre}/t_{Dre} is plotted against t_{Dre}, an average rate versus time is seen instead of an instantaneous rate versus time. Hazlett and Lee (1986) noted that accurate values can be

determined for the product k x h. However, they showed that the match generated by their method was not unique for any value of λ, ω, or r_e.

The methods mentioned do not attempt to characterize the system with any of the known reservoir models that have analytical solutions. As was stated earlier, the early attempts were mostly empirical. However, the character of shale gas reservoirs is believed to be known; they are naturally fractured reservoirs that generally have wells that have been hydraulically fractured to increase production rate. They have very low matrix permeability and generally contain adsorbed gas. This forthcoming discussion will outline what analytical models are available that are similar to shale gas systems. These models can potentially be used in production data analysis of shale gas reservoirs.

3.3 Dual/Double Porosity Systems

Earlier, analytical type curves for single porosity systems were discussed. Now, a more complicated solution, the dual porosity reservoir will be examined as it applies better to shale gas systems. Unless it is otherwise stated, dimensionless time and pressure are those defined in Eq 21 and Eq 22. Here it is necessary to assume several more variables that describe the more intricate interactions between the naturally occurring fractures in the reservoir and the matrix rock. Essentially, these reservoirs are treated as two reservoirs, the fractures and the matrix.

The first of these variables is the interporosity flow coefficient (λ) (Gringarten, 1984). This describes how well the natural fractures are connected to one another and to the matrix rock itself.

$$\lambda = \frac{\alpha k_m r_w^{\ 2}}{\overline{k_f}} \qquad \text{Eq 81}$$

where

$$\alpha = \frac{4n(n+2)}{L_m^2} \qquad \text{Eq 82}$$

where n is the number of normal (90° to one another) fracture planes in the reservoir. For horizontal fractures or multilayered reservoirs, this number is 1. The maximum value for n is 3 (x, y, and z directions). L_m is the commonly referred to as the characteristic fracture spacing. A visual depiction is given in Figure 7. (Gringarten, 1984)

The next variable important to dual porosity reservoirs is the storativity coefficient (ω) (Gringarten, 1984). In essence, it compares how large the fracture storativity is in relation to the total storativity of the reservoir.

$$\omega = \frac{(\phi c_t)_f}{(\phi c_t)_f + (\phi c_t)_m} \qquad \text{Eq 83}$$

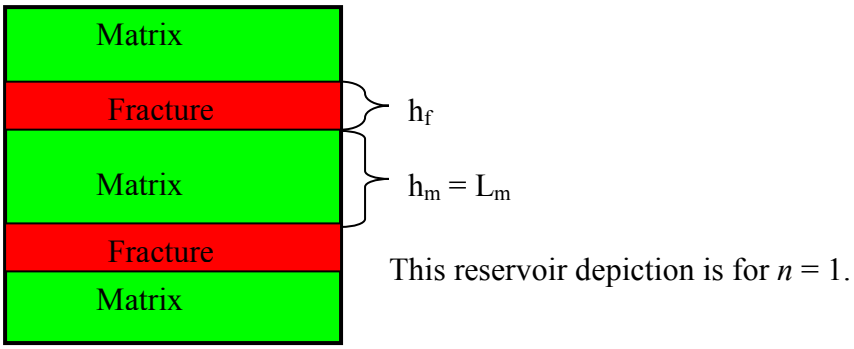

Figure 7 – Depiction of dual porosity reservoir (after Serra, et al. 1983)

Both λ and ω are dimensionless. The dimensionless plotting functions are slightly different for dual porosity systems when compared to those of single porosity systems. Permeability is now taken as fracture permeability since that number is usually significantly higher and has more impact on production performance. Also, total system compressibility and total system porosity must now incorporate the fractures.

$$c_t = c_{tf} + c_{tm} \qquad \text{Eq 84}$$

$$\phi_t = \phi_f + \phi_m \qquad \text{Eq 85}$$

The effects of ω and λ on pressure transient type curves with the new plotting functions can clearly be seen in Figure 8 and Figure 9.

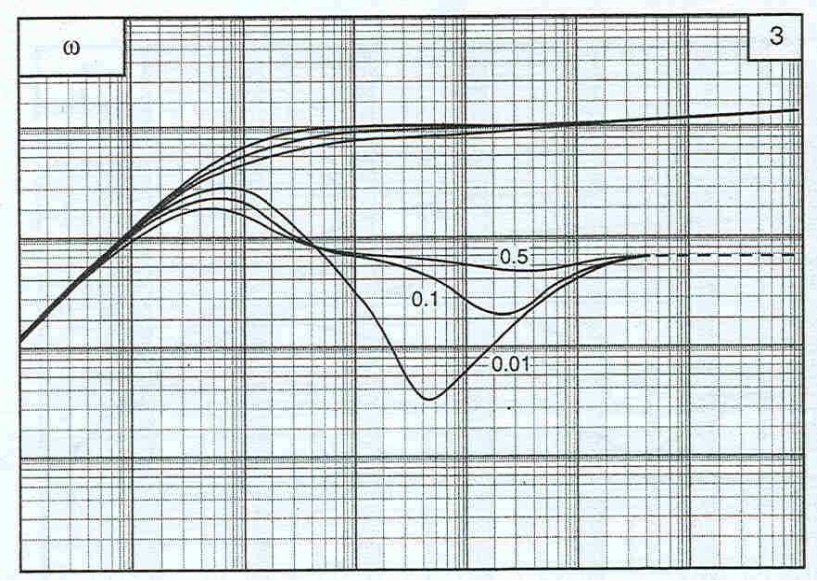

Figure 8 – Type Curves for a Dual Porosity Reservoir showing varying ω from Schlumberger (1994)

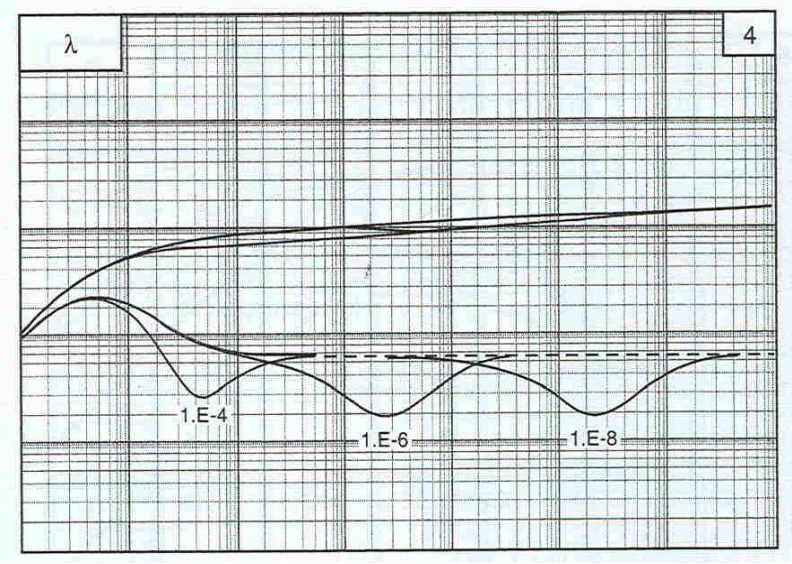

Figure 9 – Type Curves for a Dual Porosity Reservoir showing varying λ from Schlumberger (1994)

Figure 8 and Figure 9 clearly show that early time is dominated by the flow from the fractures themselves. This can be seen in the effects of changing the value of ω. The larger the dips seen in Figure 8 represent decreasing fracture storativity. Intermediate time is dominated by flow from the matrix into the fractures. This is controlled by the interporosity flow coefficient λ. Figure 9 shows that decreasing fracture-matrix connectivity delays the onset of the effects of ω. In late time, the system behaves like a single porosity system and would exhibit either boundary-dominated flow (unit-slope) or infinite-acting flow.

3.4 Hydraulically Fractured Systems

Man-made hydraulic fractures are often used in reservoirs that have low permeability that is not capable of economic production rates. These are very different in character to the naturally fractured reservoirs that are classified as having a dual/double porosity. Hydraulic fractures are generally characterized by three variables: fracture half-length x_f, fracture width w, and fracture permeability k_{fh}. These three variables make up the dimensionless fracture conductivity which is given by (Lee and Wattenbarger, 1996)

$$C_{df} = \frac{k_{fh} w}{\pi k_m x_f} \qquad \text{Eq 86}$$

Unlike natural fractures, hydraulic fractures are almost entirely vertical in that they cut through the thickness of a reservoir, and they are typically small in length when they are compared to the drainage radius of the reservoir ($r_e/x_f >> 1$). Dimensionless plotting functions are also different for hydraulically fractured reservoirs. The time function is now t_{dxf}/C_{df} with fracture half-length in place of wellbore radius ($t_{dxf} = t_d * r_w^2 / x_f^2$). However, the pressure function still uses matrix permeability. This is counter-intuitive when compared to what was done with naturally fractured

reservoirs. Hydraulic fractures are thought of as point fractures in that they connect to only a single point in the reservoir. The new plotting functions in consistent units are

$$p_d = \frac{k_m h(p_i - p_{wf})}{q\mu B} \qquad \text{Eq 87}$$

$$\frac{t_{dxf}}{C_{df}} = \frac{k_{fh} t}{\phi \mu c_t x_f^2} \frac{\pi k_m x_f}{k_{fh} w} = \frac{\pi k_m t}{\phi \mu c_t x_f w} \qquad \text{Eq 88}$$

The type curves for hydraulically fractured, single porosity reservoirs with the plotting functions stated above can be seen in Figure 10 and Figure 11.

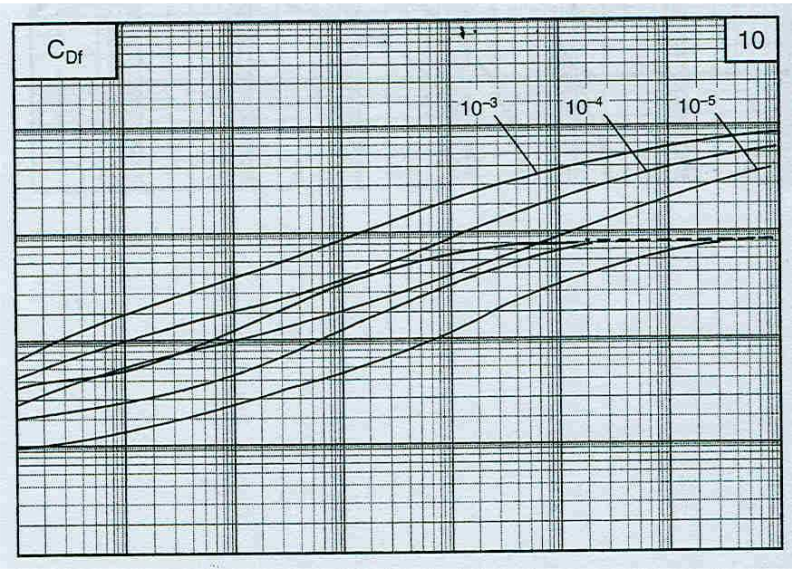

Figure 10 – Type Curves for a Reservoir with a Finite Conductivity Vertical Fracture from Schlumberger (1994)

3.5 Dual/Double Porosity Systems with Hydraulic Fractures

Finally, a particular area of interest to the results that will be presented later is dual porosity reservoirs that contain hydraulic fractures. These types of reservoirs are being discussed because it is usually standard practice to hydraulically fracture shale gas reservoirs in order to achieve economically sustainable flowrates. The real-world, field data cases that will be examined later are best described as dual porosity, hydraulically fractured reservoirs. It should be noted that little work in the area of type curves and production data analysis for this category of reservoirs has been done. However, certain authors have made efforts at describing the behavior of these systems.

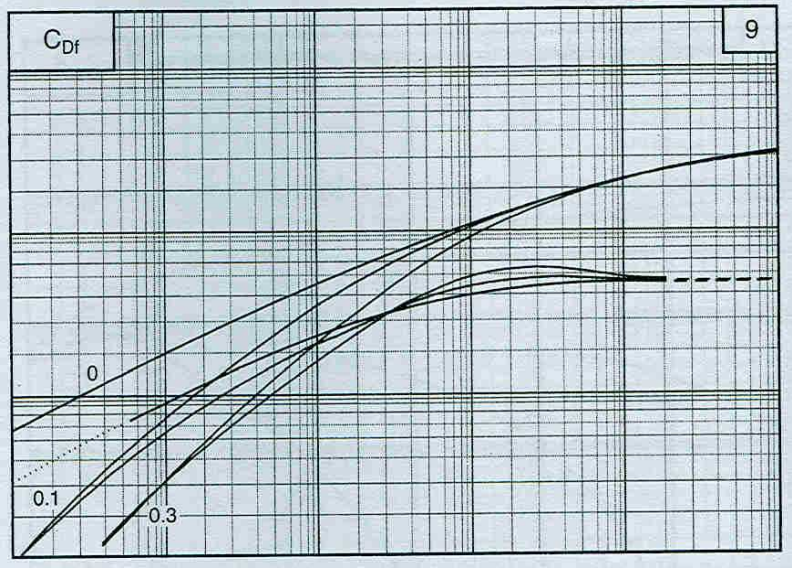

Figure 11 – Type Curves for a Reservoir with an Infinite Conductivity Vertical Fracture from Schlumberger (1994)

The characteristic dimensionless variables that govern this system and are used to solve it are very similar to those of standard dual porosity systems. The interporosity flow coefficient is now λ_{fh} rather than λ (Cinco-Ley and Meng, 1988). The equation for λ_{fh} is

$$\lambda_{fh} = \frac{\alpha k_m r_w^{\ 2}}{k_f}\frac{x_f^2}{r_w^2} = \lambda\frac{x_f^2}{r_w^2} \qquad \text{Eq 89}$$

In the above equation, k_f is the bulk permeability of the natural fractures. For a dual porosity system with hydraulic fractures, it is important to note that there are now 3 different systems with different permeability. There is the matrix permeability, k_m, the natural fracture permeability, k_f, and the hydraulic fracture permeability, k_{fh}. The hydraulic fracture permeability is not considered in the equation for λ_{fh} because hydraulic fractures are seen as being connected to only a single point in the reservoir rather than to the bulk reservoir properties (Aguilera, 1989). Thus, it is implied that only the extent to which the fracture penetrates the reservoir (x_f) will have an effect on production performance. This makes sense as long as $k_{fh} >= k_f$. This is usually a reasonable assumption for a typical hydraulic fracture.

These kinds of systems have the same ω as standard, dual porosity reservoirs. However, dimensionless time, t_d, uses x_f in the denominator in place of r_w. This is a similar t_d to a single porosity, hydraulically fractured system. Dimensionless fracture conductivity is also slightly different in this case. The equations for t_d, p_d, and C_{df} are

$$\frac{t_d}{C_{df}} = \frac{k_{fh}t}{(\phi c_t)_{f+m}\mu x_f^2}\frac{\pi k_f x_f}{k_{fh}w} = \frac{\pi k_f t}{\phi\mu c_t x_f w} \qquad \text{Eq 90}$$

and

$$p_d = \frac{k_f h \Delta p}{q \mu B} \qquad \text{Eq 91}$$

and

$$C_{df} = \frac{k_{fh} w}{\pi k_f x_f} \qquad \text{Eq 92}$$

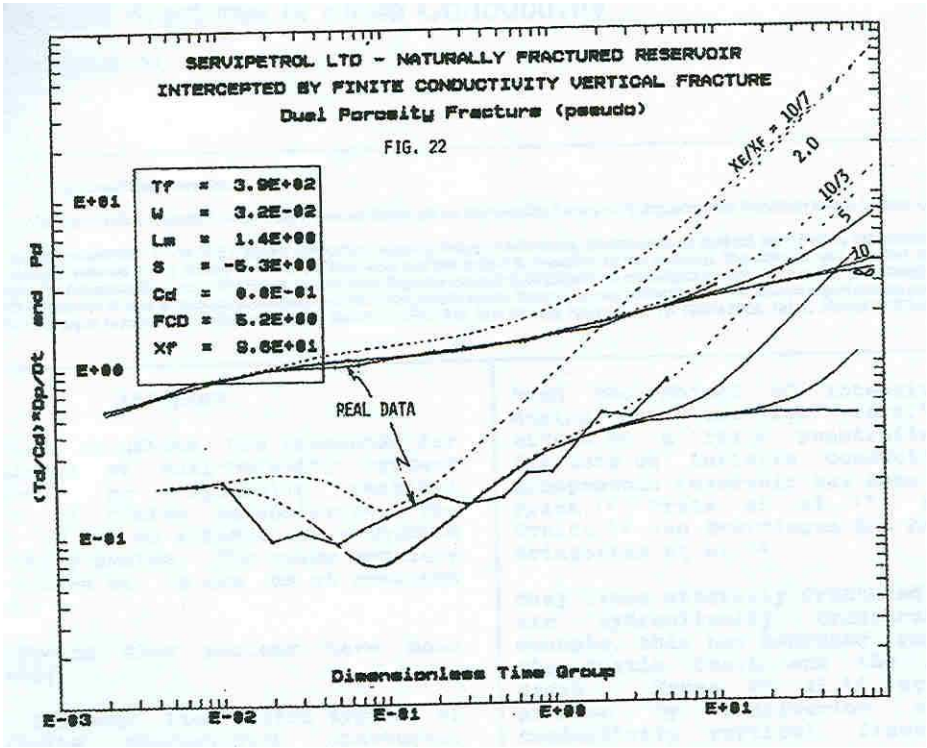

Figure 12 – Type Curves for a Dual Porosity Reservoir with a Finite Conductivity Vertical Fracture from Aguilera (1989)

All of these models have the potential to structurally represent shale gas systems in one form or another. However, all of these models do not account for a critical component in these systems, the presence of adsorbed gas. In this next discussion, it will be shown that a modified form of all of these solutions can be used in systems that contain adsorbed gas.

3.6 Bumb and McKee

Bumb and McKee (1988) derived a new solution to the diffusivity equation that takes gas desorption into account. This is such a significant breakthrough because they started from the beginning, with the original diffusivity equation. In the case of adsorbed gas, Bumb and McKee (1988) showed that the right hand side of Eq 1 must be treated very differently. Before, changes

in system density and porosity were only the result of gas and/or formation expansion. Now, desorption must be considered. Thus, assuming a Langmuir desorption isotherm the right side of Eq 1 is expanded to yield (Bumb and McKee, 1988)

$$\frac{\partial}{\partial t}(\phi\rho) = \left(\phi\frac{\partial\rho}{\partial t} + \rho\frac{\partial\phi}{\partial t} + \rho_{sc}\frac{\partial V_e}{\partial t}\right) \qquad \text{Eq 93}$$

where

$$V_e = \frac{v_L p}{p_L + p} \qquad \text{Eq 94}$$

and v_L is the adsorbed gas per cubic foot of rock and p_L is the Langmuir pressure.

The only difference between this equation and the original version of the diffusivity equation proposed earlier is the third term which accounts for adsorption. Substituting the expanded right hand side of the above equation, the Langmuir isotherm, and the real gas equation of state into the diffusivity equation yields

$$\frac{1}{r}\frac{k}{\mu}\frac{\partial}{\partial r}\left(r\frac{pM}{RTz}\frac{\partial p}{\partial r}\right) = \left(\phi\frac{\partial}{\partial t}\left(\frac{pM}{RTz}\right) + \frac{pM}{RTz}\frac{\partial\phi}{\partial t} + \rho_{sc}\frac{\partial}{\partial t}\left(\frac{v_L p}{p_L + p}\right)\right) \qquad \text{Eq 95}$$

Assuming that molecular gas composition and temperature are constant and rearranging

$$\frac{1}{r}\frac{k}{\mu}\frac{\partial}{\partial r}\left(r\frac{p}{z}\frac{\partial p}{\partial r}\right) = \left(\phi\frac{\partial}{\partial t}\left(\frac{p}{z}\right)\frac{\partial p}{\partial p} + \frac{p}{z}\frac{\partial\phi}{\partial t}\frac{\partial p}{\partial p} + \rho_{sc}\frac{\phi}{\phi}\frac{p}{z\rho}\frac{\partial}{\partial t}\left(\frac{v_L p}{p_L + p}\right)\frac{\partial p}{\partial p}\right) \qquad \text{Eq 96}$$

Differentiating and recognizing again the definitions of compressibility yields

$$\frac{1}{r}\frac{k}{\mu}\frac{\partial}{\partial r}\left(r\frac{p}{z}\frac{\partial p}{\partial r}\right) = \phi\frac{p}{z}\left(c_g + c_f + \frac{\rho_{sc} v_L p_L}{\phi\rho(p_L + p)^2}\right)\frac{\partial p}{\partial t} \qquad \text{Eq 97}$$

It is important to examine this current form of the diffusivity equation. The gas and formation compressibility are the same as they are in the original diffusivity equation. The difference is the third term again. It represents a correction to the total system compressibility to account for the adsorbed gas (Bumb and McKee, 1988). This compressibility is based on the Langmuir desorption isotherm. Now, this new total system compressibility is

$$c_t^* = c_g + c_f + c_{ads} \quad \text{Eq 98}$$

where

$$c_{ads} = \frac{\rho_{sc} v_L p_L}{\phi \rho (p_L + p)^2} \quad \text{Eq 99}$$

3.7 Spivey and Semmelbeck

The most recent efforts to accurately analyze production data analytically come from Spivey and Semmelbeck (1995) and Clarkson et al. (2007). Spivey and Semmelbeck (1995) used a numerical reservoir simulator to demonstrate the behavior of coalbed methane and shale gas reservoirs. Their model is simply a high porosity fracture sandwiched between two low ϕk "matrix" layers (i.e. a slab dual porosity model). They compared the simulator's results to a dual porosity analytical model and got accurate results when they used the modified version of the total system compressibility presented by Bumb and McKee (1988). They varied several parameters including dimensionless radius (r_d), interporosity flow coefficient (λ), storativity ratio (ω), flowing bottomhole pressure (p_{wf}), and Langmuir volume (v_L).

What is unique about their approach is that the effects of desorption are entirely accounted for by using the adjusted total compressibility. The Langmuir Volume (v_L) and the Langmuir pressure (p_L) are incorporated to account for adsorption. Spivey and Semmelbeck (1995) use standard equations for q_d and t_d, but substitute in Bumb and McKee's (1988) definition of compressibility.

$$c_t^* = S_w c_w + (1 - S_w) c_g + \frac{p_{sc} V_L p_L T z}{\phi T_{sc} z_{sc} (p_L + \bar{p})^2} + c_f \quad \text{Eq 100}$$

As expected, the effects of r_d and p_{wf} are large and can readily be identified. However, λ, ω, and v_L all work together to influence production rate. The Langmuir volume affects how much gas will actually be available to flow while interporosity flow coefficient and the storativity ratio affect it's ability to flow and how it flows. At high v_L, the effects of λ and ω are more pronounced, especially at late time. At small values of v_L and at early time, it is very difficult to discern the effects of changing λ and ω. This difficulty could be magnified when using actual production data as opposed to simulated data.

3.8 Summary of Literature Review

There have been significant advances in the field of production data analysis in the last ten years. Arguably, the methodology behind it is as mathematically grounded as that of pressure transient analysis. The advent of material balance time, the use of pseudofunctions, and the proliferation

of software to implement these things are the largest contributors to this new, more rigorous approach.

Shale gas reservoirs still present an enormous challenge due to their complexity. Generally speaking, a shale gas reservoir is probably best represented, analytically, by a dual porosity model with hydraulic fractures. It is expected that these reservoirs should behave similarly to their conventional reservoir counterparts. Specifically, all of the various flow regimes that one would expect should be visible on the derivative plots commonly used in pressure transient analysis. It has been shown that there is an analytical approach to account for adsorbed gas in the form of an adjusted compressibility. If this is all that is needed, there should be no reason for the appearance of the various flow regimes to be altered dramatically. However, the effect (s) of adsorption on dimensionless type curves is unknown except that it will most likely be very subtle as was seen when Spivey and Semmelbeck (1995) examined its effect on production data. In addition, it is not clear how the analysis approach impacts the outcome of an analysis when adsorption is present.

The Clarkson et al. (2007) work also used the Bumb and McKee (1988) transformation in a material balance time approach in coalbed methane systems. They also incorporated relative permeability effects. They showed that these adjustments were necessary and were applied to radial flow models.

For instance, does analyzing a shale gas reservoir as a single porosity system yield vastly different results than if one analyzes it as a dual porosity system with hydraulic fractures? If so, is this error due to the effect of adsorption or just a poor choice of an analytical model? In the coming chapters, the effects of adsorption on commonly used dimensional and dimensionless type curves will be shown. In addition, a methodology for analyzing production data from adsorbed reservoirs using analytical type curves that do not account for adsorption will be detailed. Finally, the effects applying this methodology to one simulated and two field cases and the effects of assuming different reservoir systems (single porosity, dual porosity, hydraulically fractured, and dual porosity with hydraulic fracture) will be shown and explained.

4. SIMULATION MODELING

This section shows that it is completely possible to correctly retrieve system parameters if one knows the system type. The analytic solutions for the various systems (single porosity, dual porosity, hydraulic fracture, and dual porosity with hydraulic fracture models) were compared to numerical simulation models. The analytic solutions would be used with real production data to estimate key reservoir parameters. The effects of all the parameters that influence these analytic solutions can be seen with clean simulated data. First, systems produced at constant rate and then constant pressure will be examined. Recall that one of the objectives of this work requires the analysis of production data as equivalent constant rate data. Adsorption will be discussed in the next chapter.

To aid in understanding the complexities of all the various systems involved, several finite-difference flow simulation models were constructed. Variations of these models show that the effects predicted by the fundamental models of pressure transient analysis (PTA) were visible. The finite-difference simulator used was GEM from the Computer Modeling Group.

PTA is best done with dimensionless variables. Previous researchers have shown that the use of dimensionless variables also improves analysis of production data. The main purpose of discussing pressure transient analysis techniques is to show that the visual indicators of flow regimes are consistent across all types of analysis. Boundary dominated flow is a unit-slope in both the pressure and pressure derivative curves in standard PTA; it can be any number of shapes in standard production data analysis in use today. To review concepts mentioned earlier, dimensionless time and dimensionless pressure are convenient arrangements of variables that allow the diffusivity equation to be solved more easily. For the purposes of this work, dimensionless pressure and dimensionless time will be generally defined by:

$$p_{wd} = \frac{kh[m(p_i) - m(p_{wf})]}{1422Tq_g} \qquad \text{Eq 101}$$

$$t_d = \frac{0.00634kt}{\mu_{gi}(\phi c_{ti})r_w^2} \qquad \text{Eq 102}$$

4.1 Systems Produced at Constant Terminal Rate

The first simulation model constructed (Model 1) was a single-layer, radial, single porosity (homogeneous) gas reservoir. There is one well in the center of the model. The model parameters are listed in Table 1. Note that this model is not representative of shale-gas systems; a separate model with parameters more realistic for shale gas systems was also constructed and will be discussed in Chapter 6. This model and its variations can be thought of as the base case.

Original gas in place for Model 1 is 188 BSCF. The grid system has 50 divisions along the radius arranged logarithmically increasing in size from the center. Model 1 was first run at a

constant surface gas rate of 3.5 MMSCF/day for 20 years. The wellbore pressure profile and the diagnostic plots can be seen in Figure 14, Figure 15, and Figure 16.

Table 1 – Model 1 Dataset

Height/Net Pay (ft)	200
Outer Radius, r_e (ft)	2500
Well Radius, r_w (ft)	0.25
Porosity, ϕ	0.48
Permeability, (md)	5
Initial Pressure, (psia)	1514
Water Saturation, S_w	0.05
Rock Density, (lb/ft^3)	152.95
Temperature, (^oF)	120
Gas Gravity	0.55
Gas Composition	100% CH_4

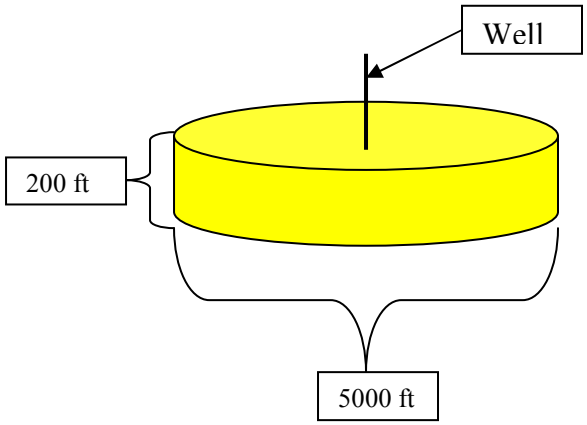

Figure 13 – Depiction of Model 1

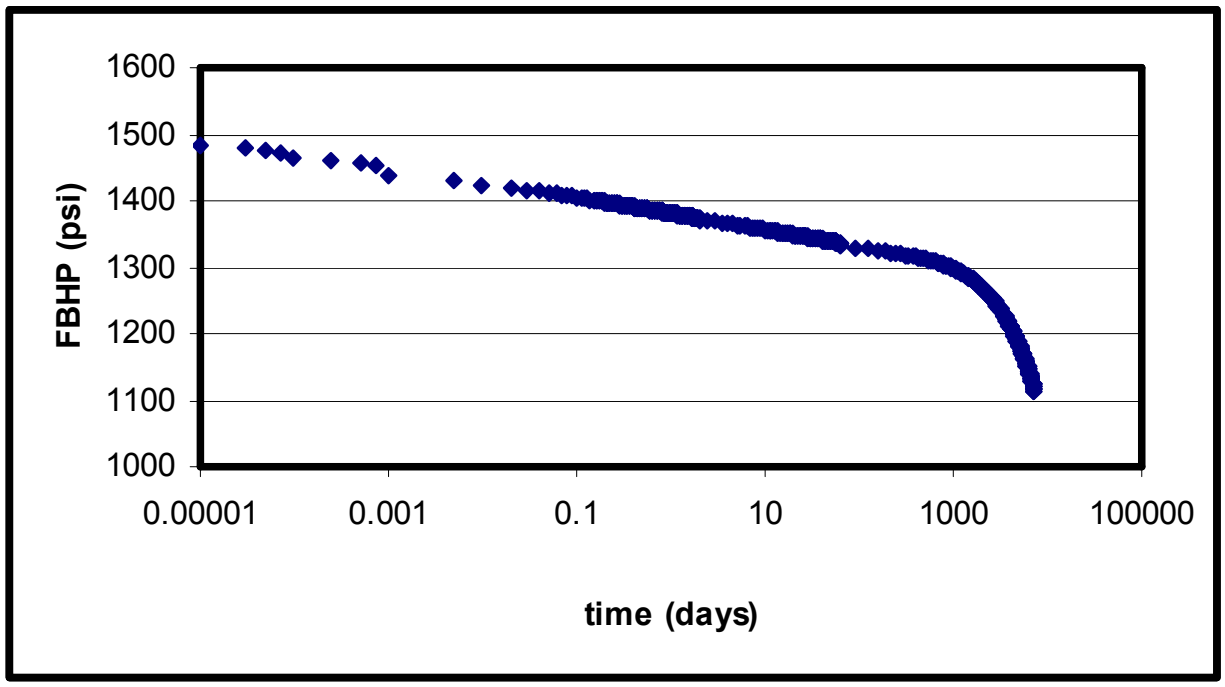

Figure 14 – Wellbore pressure profile for Model 1

In Figure 15 and Figure 16, it is clear that the dimensional and the dimensionless, constant-rate solutions have the same behavior. Thus, using dimensionless variables has no impact on the appearance of the solution, and it allows all variations of the solution to lie on the same curve (i.e. reservoir properties can be different and the solution will plot in the same place, if the values of t_d and p_{wd} remain the same)

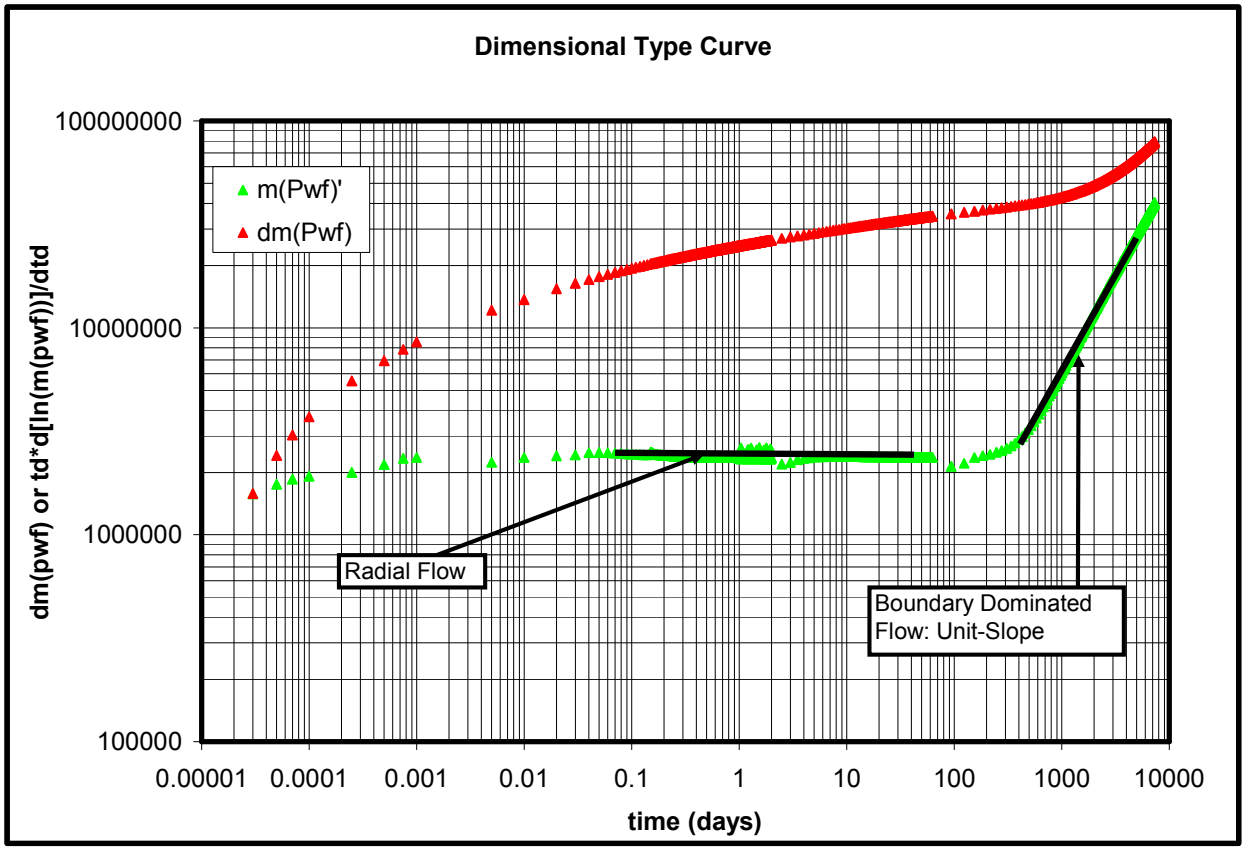

Figure 15 – Diagnostic plot for Model 1 using dimensional plotting functions

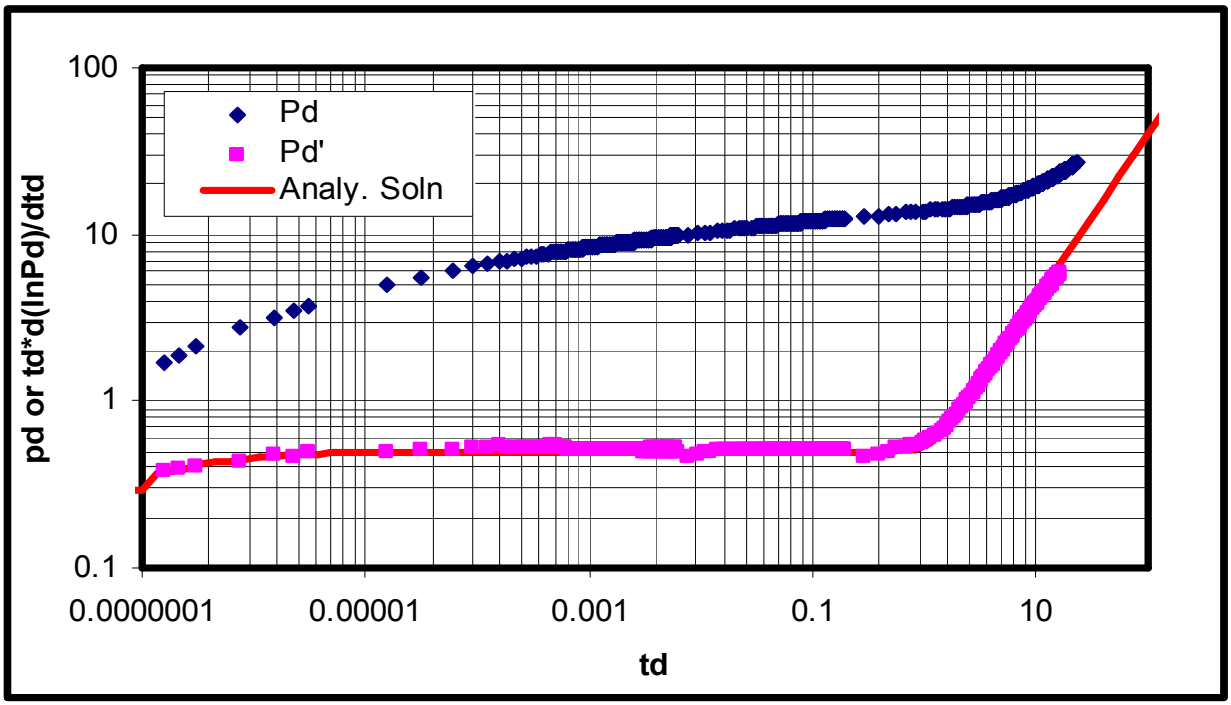

Figure 16 – Diagnostic plot for Model 1 using dimensionless plotting functions

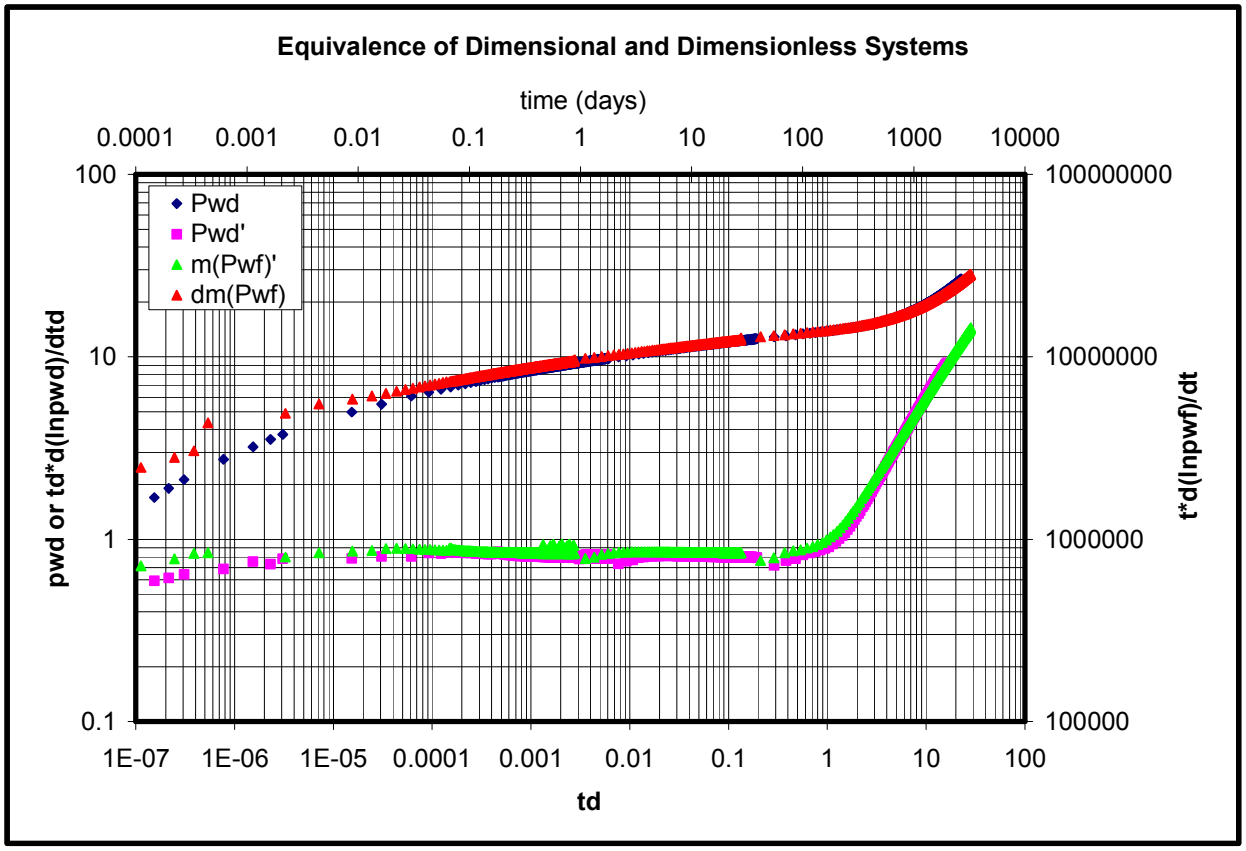

Figure 17 – Equivalence of dimensional and dimensionless systems

In Figure 17 above, the real time pressure derivative is overlaid on the dimensionless time pressure derivative to show the match. The zero slope of the radial flow regime can clearly be seen as can the unit slope of the boundary dominated flow regime (depletion). Their shapes are identical as are the lengths of the flow regimes.

Next, a dual porosity model (Kazemi and de Swaan slab model) was constructed using various values of λ and ω. The equations for λ and ω for this model can be seen in Eq 81 and Eq 83. In addition, the dimensionless plotting functions are slightly different than for single porosity systems. This was discussed earlier, but system permeability is now fracture permeability (natural fracture permeability) and system storativity (ϕc_t) must incorporate both fracture and matrix compressibilities. The new dimenionless plotting functions are then

$$p_{wd} = \frac{k_f h[m(p_i) - m(p_{wf})]}{1422 T q_g} \qquad \text{Eq 103}$$

$$t_d = \frac{0.00634 k_f t}{\mu_{gi} (\phi c_{ti})_{f+m} r_w^2} \qquad \text{Eq 104}$$

This first dual porosity model (Model 2) was created using $\lambda = 1x10^{-8}$ and $\omega = 0.1$. The model is a single-layer, radial, compositional, dual porosity reservoir. The values of the parameters of the flow model can be found in Table 2.

Table 2 – Dataset for Model 2

Height/Net Pay (ft)	200
Outer Radius, r_e (ft)	2500
Well Radius, r_w (ft)	0.25
Porosity, ϕ_m	0.05
Porosity, ϕ_f	0.00528 (from ω)
Permeability, k_m(md)	0.01
Permeability, k_f(md)	95 (from λ)
Initial Pressure, (psia)	1514
Water Saturation, S_w	0.05
Rock Density, (lb/ft^3)	152.95
Temperature, (^oF)	120
Gas Gravity	0.55
Gas Composition	100% CH_4

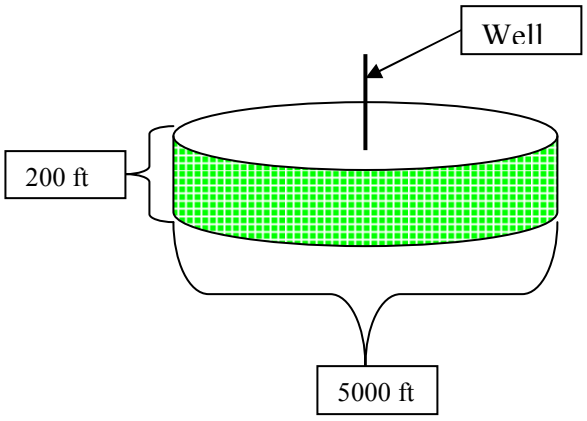

Figure 18 – Depiction of Model 2

Original gas in place for Model 2 is 34 BSCF. This model was produced from a single well located in the middle of the reservoir using the same grid system has Model 1. Model 2 was first run at a constant surface gas rate of 1 MMSCF/day for 20 years. In addition, the following values for λ and ω were changed to create separate flow models to record their effect. Table 3 shows the values for λ and ω that were used.

Table 3 – Values of λ and ω used in Model 2

λ	ω
$1x10^{-8}$	0.1
$1x10^{-7}$	0.01
$1x10^{-6}$	0.001

The wellbore pressure profiles and the diagnostic plots for the models described above can be seen in Figure 19 and Figure 20.

The dual porosity effects are clearly seen in Figure 19 but only in early time and for relatively small changes in wellbore pressure. The value of ω can be estimated using an analysis technique detailed by Gringarten (1984) where the number of log cycles between the 2 parallel lines drawn at early and late time is equivalent to ω. One log cycle would represent $\omega = 10^{-1}$. Gringarten (1984) acknowledges that this approximation is only accurate to one order of magnitude. $\omega = 1$ is not seen on this plot because it is a single porosity system and wellbore pressure drops too quickly to be seen at this scale.

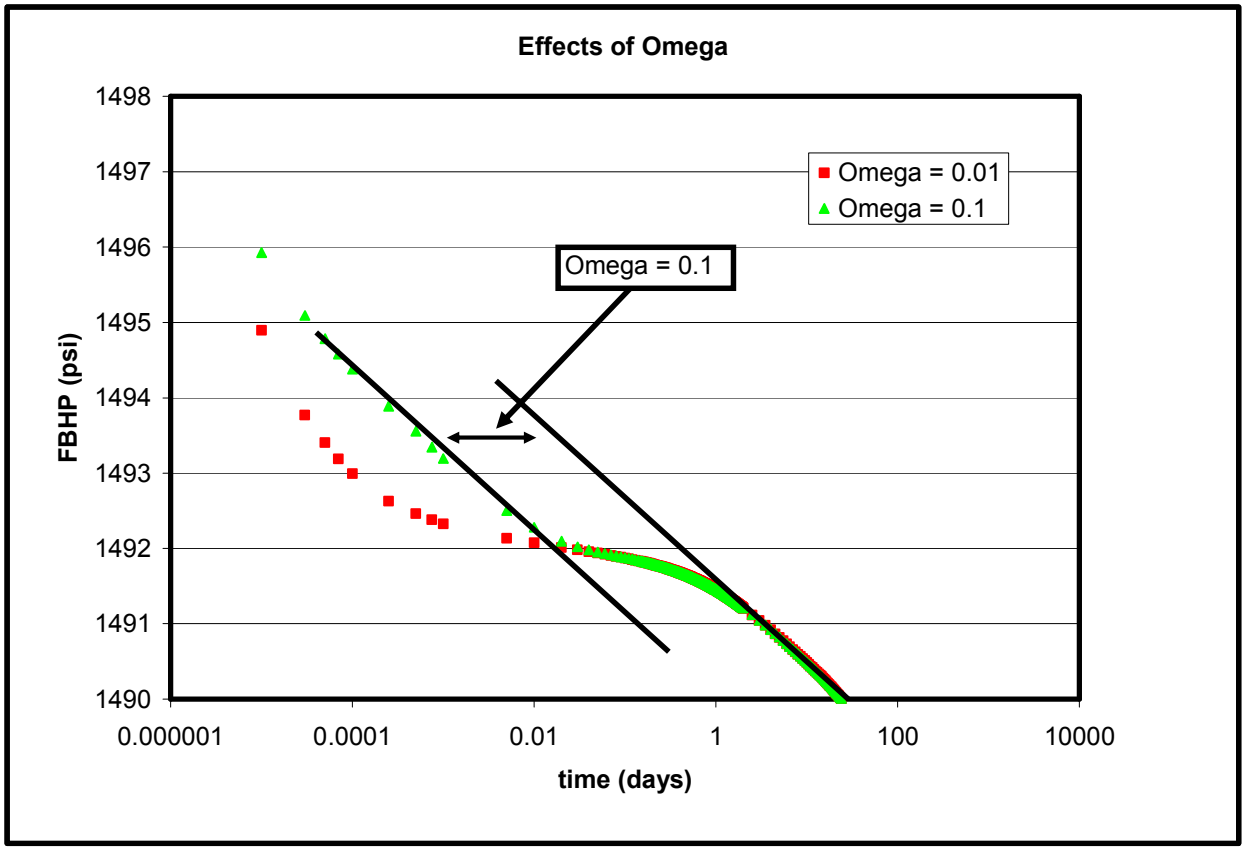

Figure 19 – Wellbore pressure profiles for Model 2 showing the effect of omega

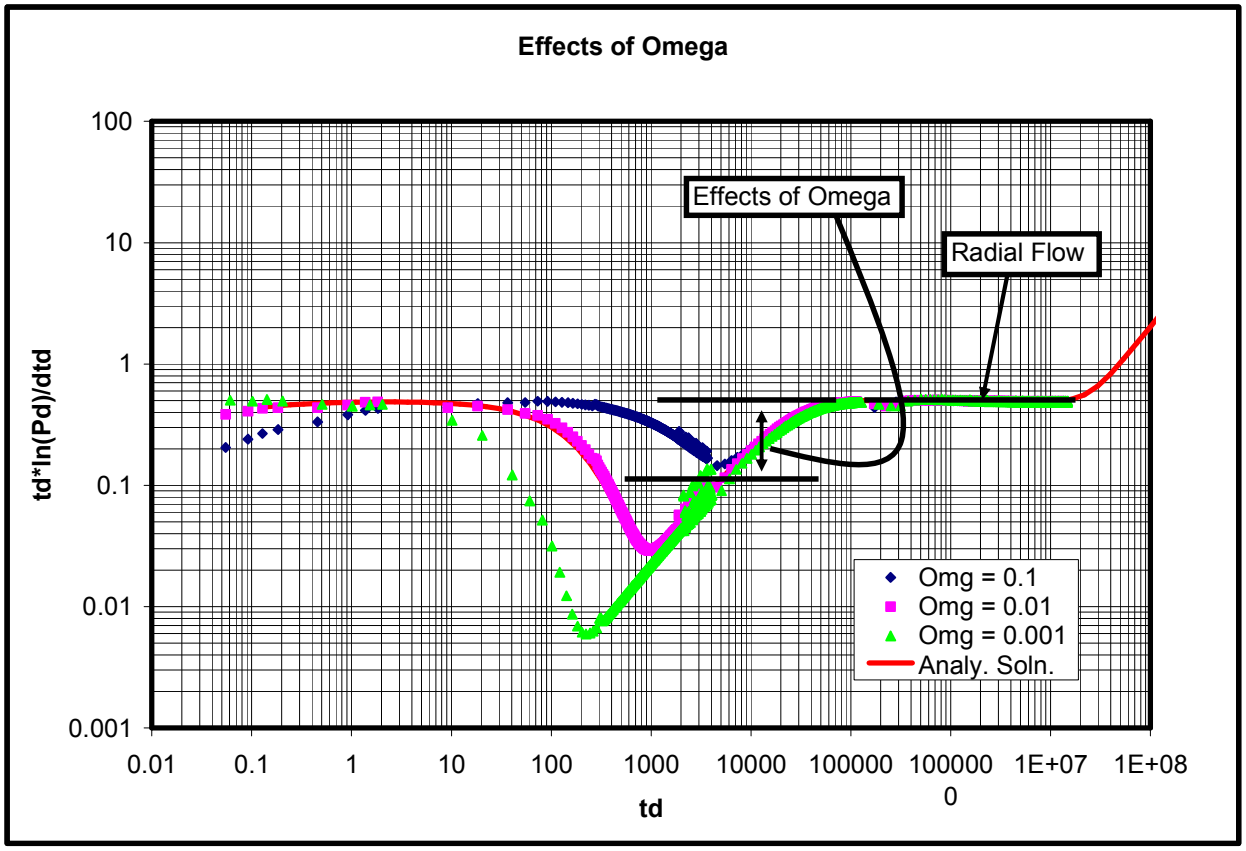

Figure 20 – Diagnostic plot of Model 2 showing the effects of lambda

Figure 20 shows the derivative plot for a dual porosity system. Note that all the systems merge together during late-time, radial flow. This is expected since all the models are the same physical size and are produced at the same constant rate. Boundary dominated flow was not reached here because the models were not allowed to run for a long enough period of time. The analytical solution shown here used input values from the simulator data file. It shows the "right" answer for $\omega = 0.01$. The other curves shown in Figure 20 are variations to the simulated data file to show the effects of ω.

Figure 21 and Figure 22 show the effects of changing the value of λ. It should be noted that these plots actually have some effects of ω as well (since the model has $\omega = 0.4$ which is the result of setting fracture porosity equal to formation porosity). ω is not 0.5 because matrix compressibility and fracture compressibility are not equal in this model. This also explains the very small "hump" that is characteristic of dual porosity systems. This "hump" is very small for large values of ω. The λ term only serves to shift the position of the trough created by the effects of ω. The radial flow regime is still present as a horizontal line on the derivative plot. However, late time radial flow may not be achieved since the effects of λ can last until the beginning of boundary dominated flow. This can be seen in both the cases of $\lambda = 1x10^{-8}$ and of $\lambda = 1x10^{-7}$.

The dual porosity analytic model is a much better representation of shale gas reservoirs than a single porosity system. However, it does not address the presence of hydraulic fractures that are common to shale gas reservoirs. The next series of plots will apply to the common scenario of

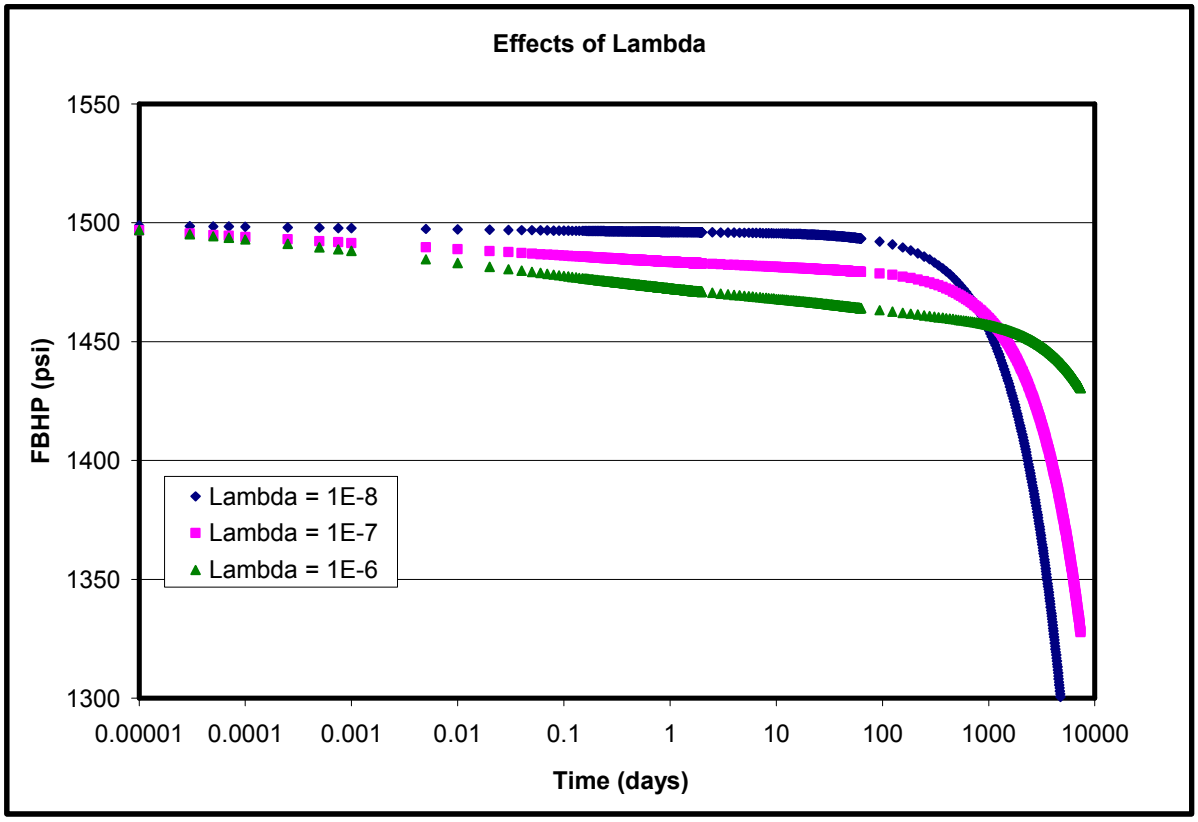

Figure 21 – Wellbore pressure profiles for Model 2 showing the effects of lambda

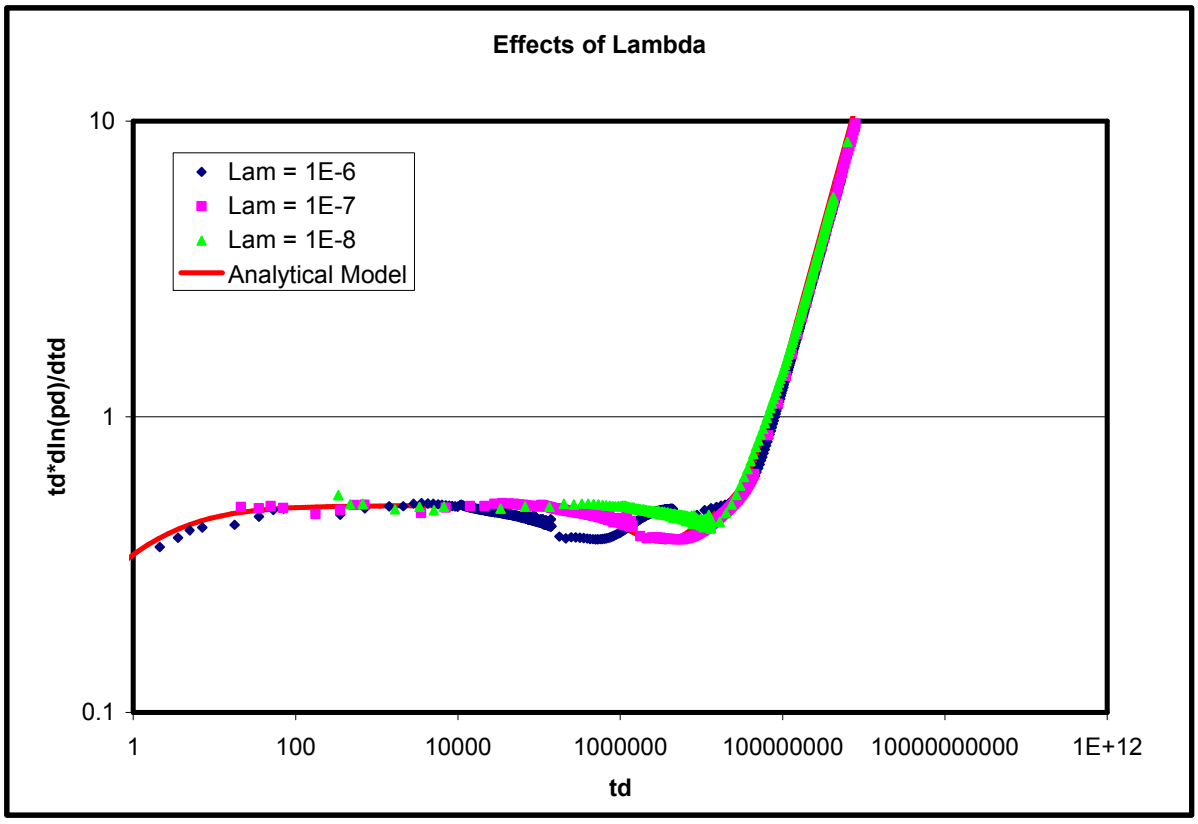

Figure 22 – Diagnostic plot for Model 2 showing the effects of lambda

hydraulically fractured reservoirs. The development of the plotting functions for these systems was discussed earlier. For review, the dimensionless time and pressure variables are presented below.

$$\frac{t_d}{C_{df}} = 0.00634 \frac{\pi k_m t}{\phi_m \mu c_{tm} x_f w} \qquad \text{Eq 105}$$

$$p_{wd} = \frac{k_m h \Delta m(p)}{1422 T q_g} \qquad \text{Eq 106}$$

where

$$\Delta m(p) = m(p_i) - m(p_{wf}) \qquad \text{Eq 107}$$

A hydraulic fracture model (Model 3) was constructed in a different manner than the previous models. As a model, hydraulic fractures are very thin, vertical structures that generally penetrate the entire thickness of a reservoir and extend for several hundred feet horizontally. The width of the fracture itself is rarely more than a fraction of an inch.

In a finite difference simulator, this kind of structure is difficult to create. There is really only one way to achieve the desired result, local grid refinement. For this model, each of the grid cells around the well were subdivided into multiple cells. The refinement was increased closer to the well and the fracture. This resulted in the grid cells that represent the fracture being 4 inches in width. This allowed the permeability to be modified for only a very narrow streak of the model on either side of the well and was the smallest grid size allowed in the model.

Figure 23 shows map views of Model 3. It shows the local grid refinement as it appears on a large scale and on a close up view of the area around the well. The fracture is visible as a thin red line.

The wellbore pressure profiles and type curves for this model and models with different values of C_{df} (Eq 88) are presented in Figure 25 and Figure 26.

The effects of the hydraulic fracture are imbedded in the C_{df} term. These effects are visible in derivative plot in Figure 26 at only early time. They consist of a ¼ slope that is visible for a short length of time depending on the value of C_{df}. The larger values of C_{df} (which happen to coincide with large values of fracture permeability) extend the effects into slightly later time. However, all of the models merge together at late-time to form the zero-slope pseudo-radial flow and then the unit-slope boundary-dominated flow.

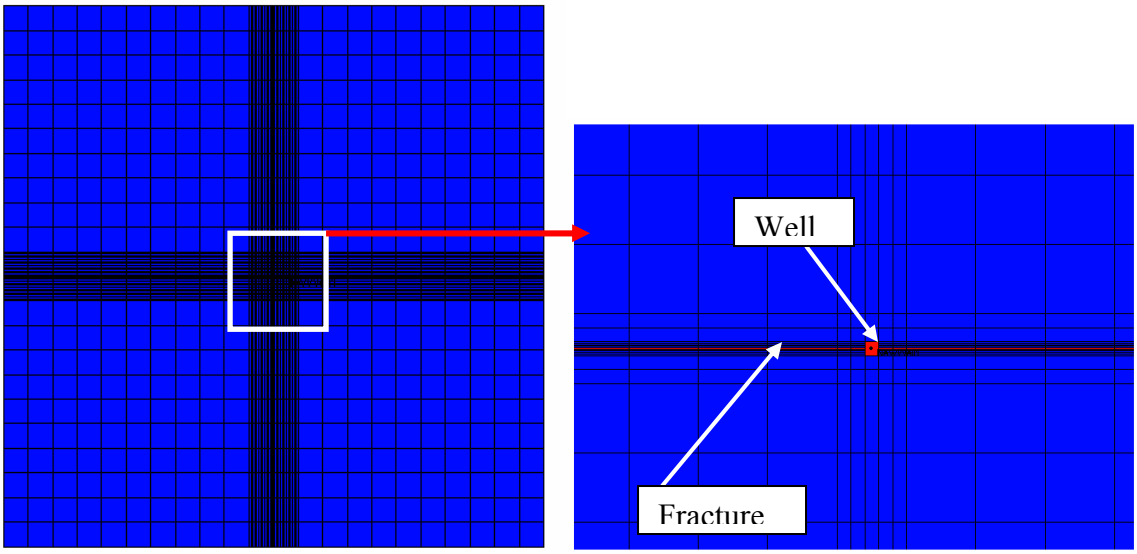

Figure 23 – Aerial views of Model 3

Table 4 – Dataset for Model 3

Height/Net Pay (ft)	40
Outer Radius, r_e (ft)	2604
Well Radius, r_w (ft)	0.25
Porosity, ϕ_m	0.10
x_f (ft)	200(C_{df} = 0.03)
Permeability, k_m(md)	0.5
Permeability, k_{fh}(md)	25 (C_{df} = 0.03)
Initial Pressure, (psia)	1514
Water Saturation, S_w	0.05
Rock Density, (lb/ft^3)	152.95
Temperature, (^{o}F)	225
Gas Gravity	0.6
Gas Composition	100% CH_4

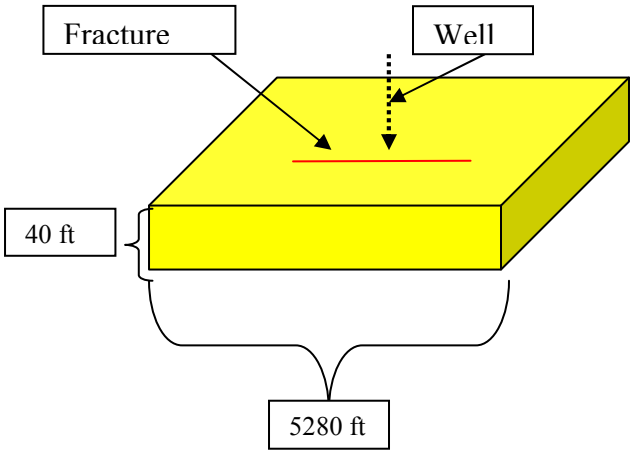

Figure 24 – Depiction of Model 3

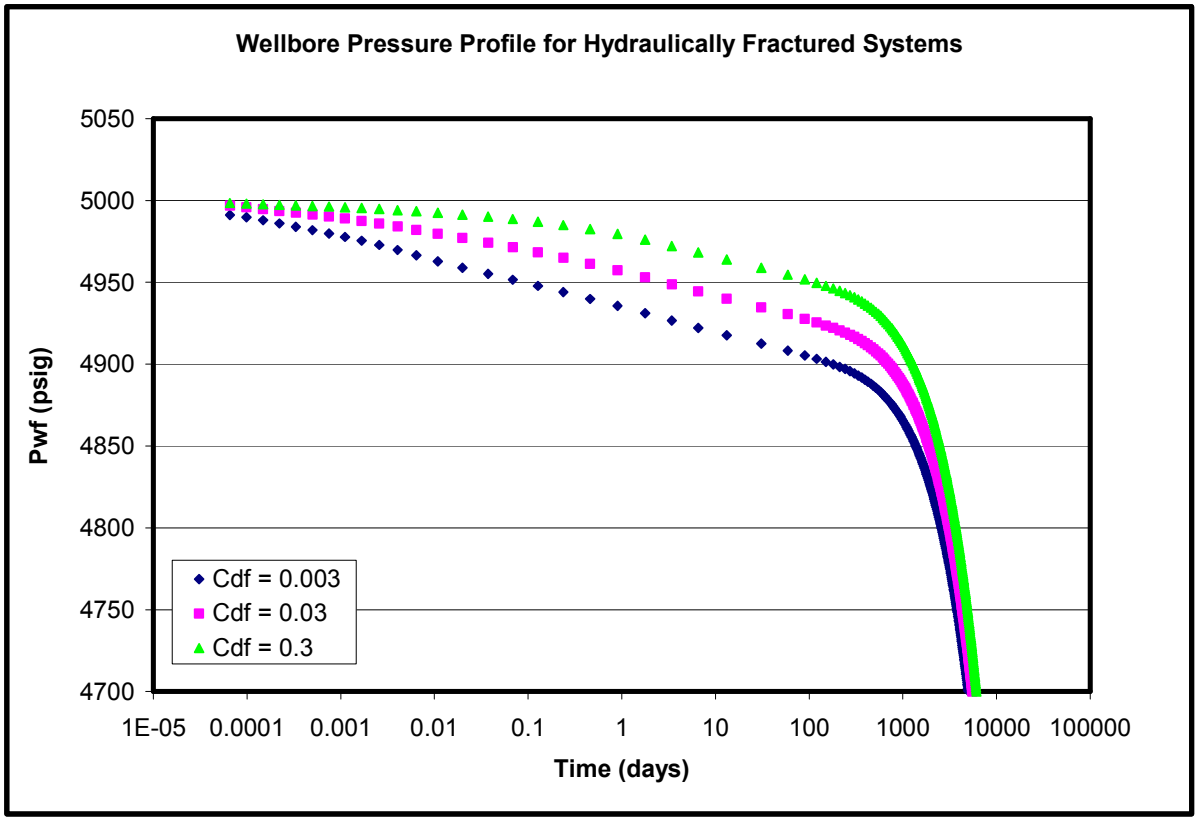

Figure 25 – Wellbore pressure profiles for Model 3 showing the effects of C_{df}

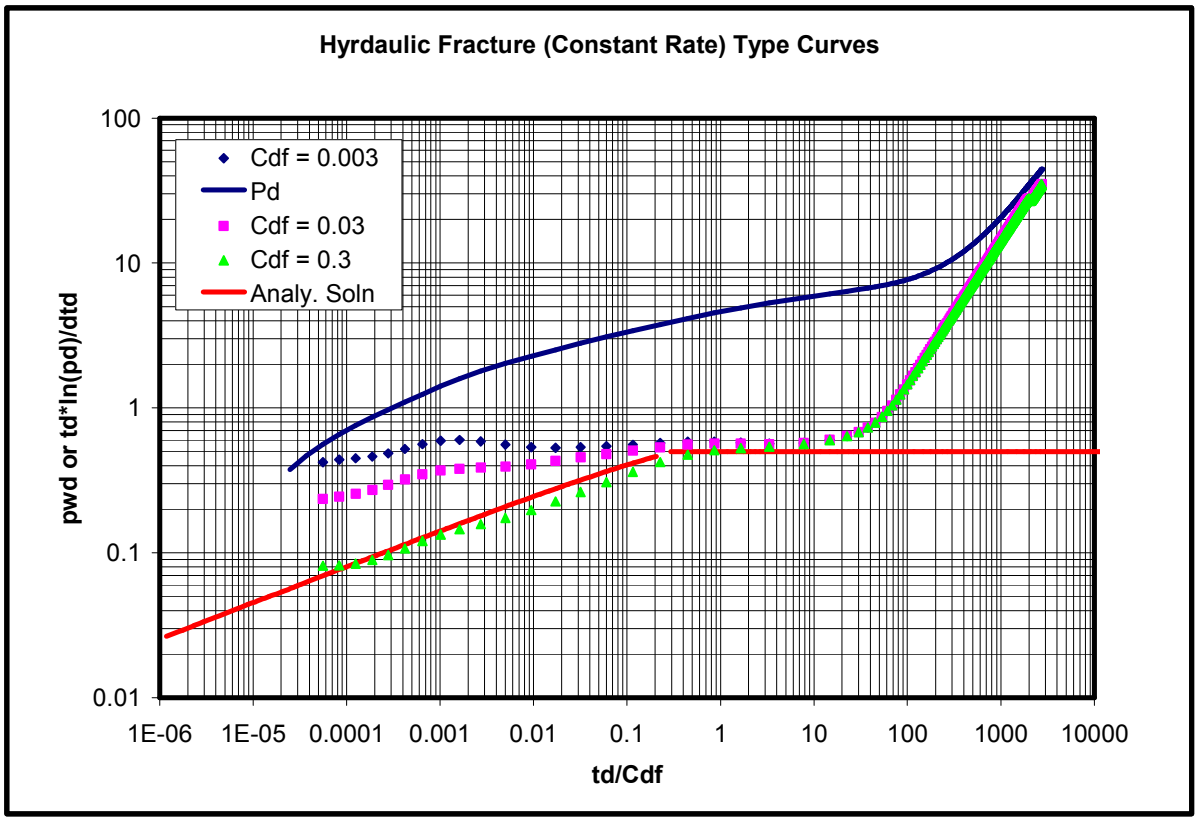

Figure 26 – Diagnostic plot for Model 3 showing the effects of C_{df}

The next complication added to the system is to assume dual porosity systems with hydraulic fractures that are produced at constant rate. The plotting functions were discussed earlier and are essentially a combination of those used for hydraulically fractured systems and those used for dual porosity systems. They are

$$\frac{t_d}{C_{df}} = 0.00634\frac{\pi k_f t}{\phi\mu c_t x_f w} \qquad \text{Eq 108}$$

$$p_{wd} = \frac{k_f h\Delta m(p)}{1422Tq_g} \qquad \text{Eq 109}$$

Model 4 was constructed similarly to Model 3. The exact same grid refinement was used to create the very thin gridblocks necessary for the hydraulic fracture. The only difference is that Model 4 is a dual porosity model was used, so an additional permeability, k_f (natural fracture permeability), was defined. A schematic of the model is shown in Figure 27 and a list of its properties can be seen in
Table 5.

Table 5 – Dataset for Model 4

Height/Net Pay (ft)	40
Outer Radius, r_e (ft)	2604
Well Radius, r_w (ft)	0.25
Porosity, ϕ_m	0.10
Porosity, ϕ_f	0.001 (ω = 0.01)
x_f (ft)	200
Permeability, k_m (md)	0.5
Permeability, k_f (md)	94 (λ = 1E-5)
Permeability, k_{fh} (md)	250
Initial Pressure, (psia)	1514
Water Saturation, S_w	0.05
Rock Density, (lb/ft^3)	152.95
Temperature, (^{o}F)	225
Gas Gravity	0.6
Gas Composition	100% CH_4

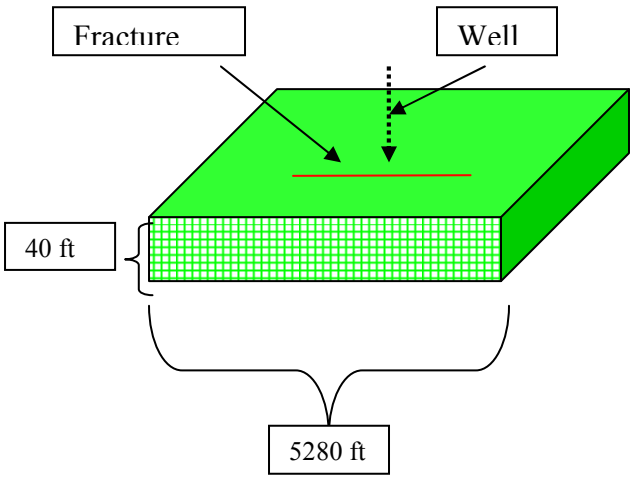

Figure 27 – Depiction of Model 4

The effect of different ratios of x_e/x_f (reservoir half-length to fracture half-length) is shown in Figure 28 and a noticeable vertical shift is seen. The effects of ω and λ are still visible, although it is admittedly hard to see those of ω. This is due to the very rapid drawdown that occurs due to the presence of the hydraulic fracture.

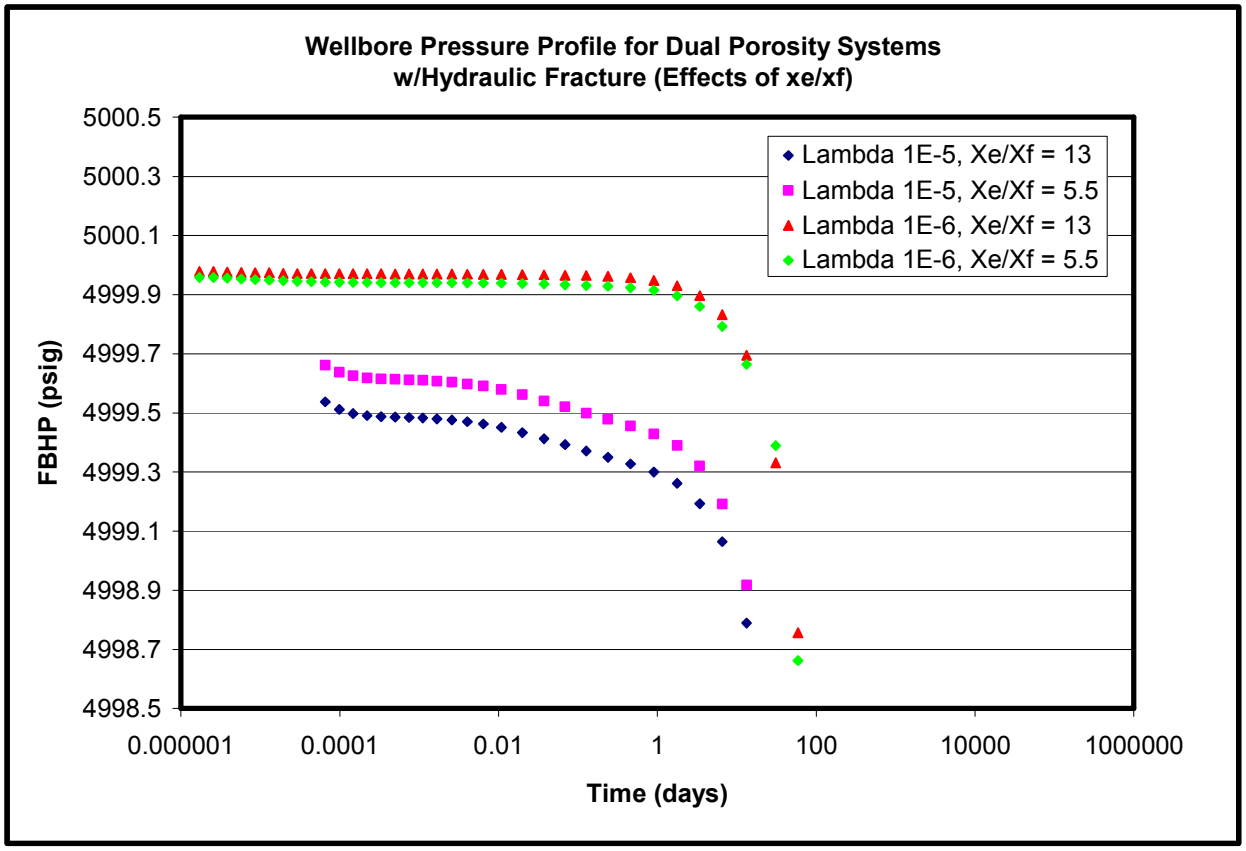

Figure 28 – Wellbore pressure profile for Model 4 showing the effects of fracture half-length

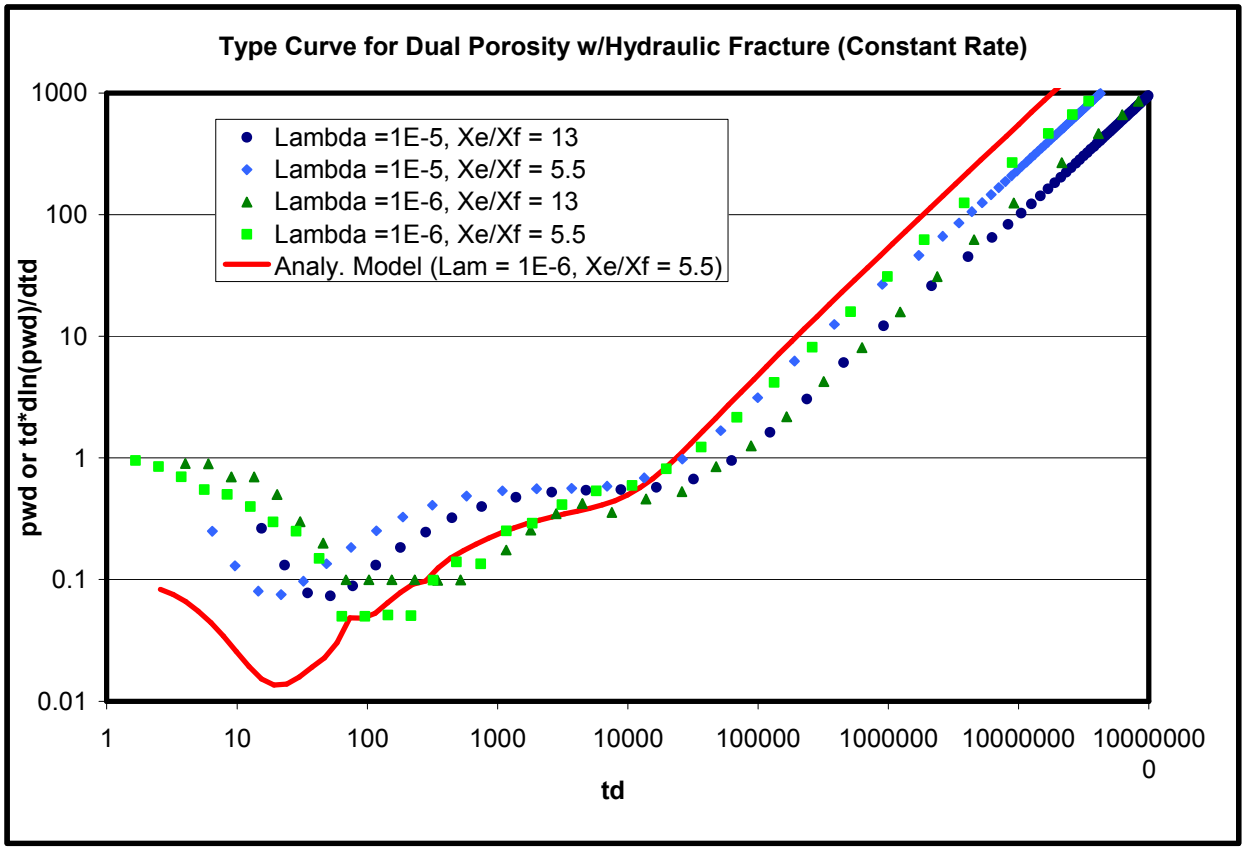

Figure 29 – Diagnostic plot for Model 4 showing the effects of fracture half-length

Figure 29 shows derivative curves for 4 simulation runs. The effects of ω and λ are still the same as they were for dual porosity systems without hydraulic fractures. However, the effect of the hydraulic fracture is a very apparent horizontal shift in the derivative curve. This can be seen when comparing the dotted and lines of similar color (shades of green and shades of blue) in Figure 29. The good thing about Figure 29 is that all reservoirs with the different x_e/x_f ratios will lie on different late-time trends. This allows an analyst to identify both natural and induced fracture properties. In addition, the lack of early time data will not make analysis completely useless. This is very important when using actual production data (rather than well test or simulated data) if one considers that data from such early times are rarely present.

However, Figure 29 shows that the analytical solution (from Aguilera, 1989), the red curve, does not match well to these simulated results. This could be due to the way the simulation model was constructed. The fracture width is larger than it would be in reality, this may mute the effects of the fracture and cause the system to behave more like a dual porosity system. However, Cinco-Ley and Meng (1988) proposed that an accurate, closed-form analytical solution for this system was not possible. They proposed approximate solution for each of the dominant flow regimes.

4.2 Systems Produced at Constant Terminal Pressure

As was noted before, all the examples shown have been systems produced at a constant rate. Since the eventual goal of this work is to analyze production data which is more closely

approximated by production at constant pressure, these graphs are not appropriate for production data analysis. However, constant pressure systems have been shown by other authors to be equivalent to constant rate systems provided that certain adjustments be made to the recorded times and pressures.

These adjustments have been discussed earlier in this work and consist of using an adjusted time instead of time in the dimensionless time function. This is scaled on changes in system compressibility, gas viscosity, and pseudopressure. Then, it is coupled with the concept of material balance time which ratios the production rate to the initial gas in place. Of course, an adjusted pressure (essentially pseudopressure) is used in place of pressure since these are gas systems.

$$t_a = \frac{(\mu c_t)_i z_i G}{q(t) * 2 p_i}[m(p_i) - m(\overline{p})] \qquad \text{Eq 110}$$

A very important concept is often overlooked by other authors is the effect of adjusted time on the dimensionless plotting functions, especially t_d. When adjusted time is combined with dimensionless time, the effects of compressibility are completely eliminated from the dimensionless plotting functions. Viscosity is not completely eliminated as it is still part of the integral that defines pseudopressure. This will be a very important concept when dealing with reservoirs that contain adsorption. The result can be seen below.

$$t_{dA} = \frac{0.00634 k t_a}{\mu_{gi}(\phi c_t)_i A} = 0.00634 \frac{z_i}{2 p_i} \frac{Gk}{A\phi} \frac{[m(p_i) - m(\overline{p})]}{q_g} \qquad \text{Eq 111}$$

The very good thing about using adjusted time in the dimensionless time definition is that dimensionless time and pressure can be calculated and plotted as an equivalent well test (i.e. as constant rate data rather than constant pressure data). This should have the same appearance/shape/flow regimes as a traditional, constant rate well test. Therefore, production data from the field that has been converted using material balance time should overlay constant rate analytical solutions when parameter values that are consistent with the reservoir are found.

The following simulation models produced at constant pressure have identical parameters to their constant rate counterparts. The only difference being they are constrained at a constant flowing bottom-hole pressure (FBHP) rather than at a specific rate. This first graph is the same simple single-porosity system described earlier.

Figure 30 is obtained by using the rate output from the simulation and implementing the concept of adjusted time described above. As expected, these two curves overlay each other exactly. The conversion of a constant pressure solution to a constant rate solution preserves all of the flow regimes.

Figure 31 is a plot of a dual porosity system with $\lambda = 1 \times 10^{-6}$ and $\omega = 0.1$. All other reservoir parameters are kept the same as in the constant rate systems. Figure 31 again illustrates that a constant pressure boundary condition can be converted to a constant rate boundary condition even for dual-porosity systems.

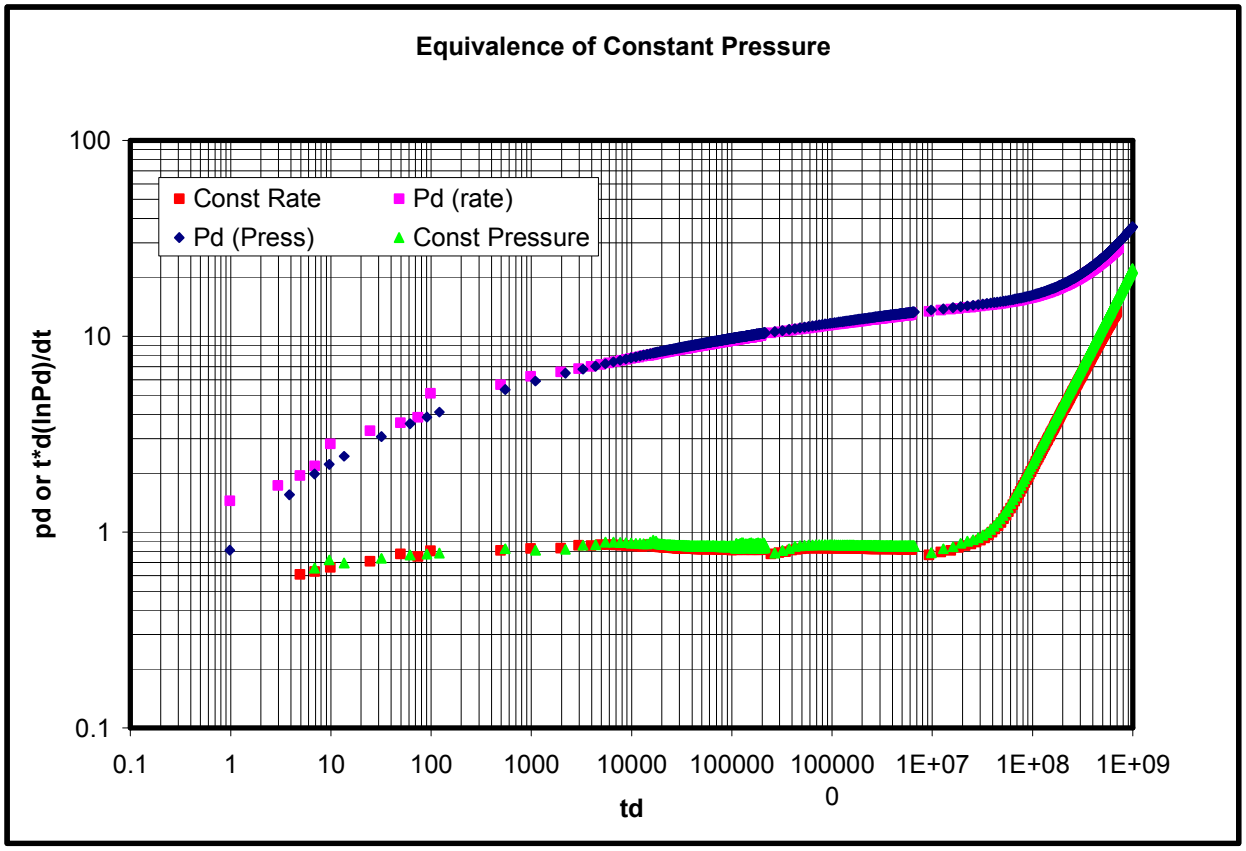

Figure 30 – Diagnostic plot showing the equivalence of constant rate and constant pressure derivative curves

Figure 32, Figure 33, and Figure 34 isolate the effects of the dual porosity parameters λ and ω in constant pressure systems. The rate-decline type curves are the dimensional equivalent of wellbore pressure profiles for constant rate systems. The x-axis is the log(t) and the y-axis is normalized rate. Plotting the data in this way (Figure 32 and Figure 33) yields plots that look very similar to Fetkovich's decline curves for liquid systems. Note that the plotting functions are quite different though. The equation for normalized rate is

$$q_{norm} = \frac{q_g}{m(p_i) - m(p_{wf})}. \qquad \text{Eq 112}$$

Figure 32 and Figure 33 show the effects of lambda and omega on dimensional type curves for constant pressure systems. Note the difference in character of the dimensional plots in Figure 32 and Figure 33 and the dimensionless plot in Figure 34. In the opinion of this author, having a unified late-time curve for a given dimensionless radius makes Figure 34 much easier to read. Admittedly, a similar effect can be achieved using a Fetkovich style plot.

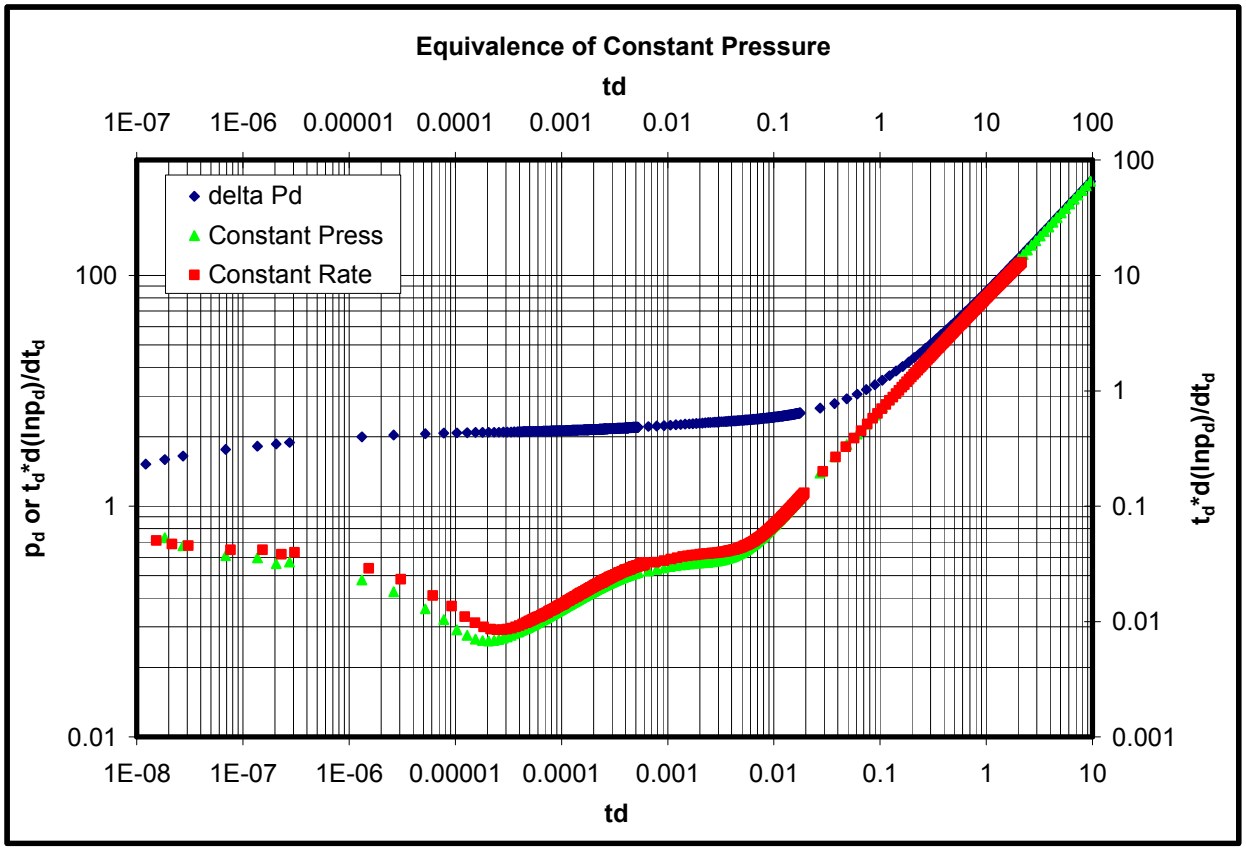

Figure 31 -- Diagnostic Plot showing the equivalence of constant rate and pressure systems in a complex medium

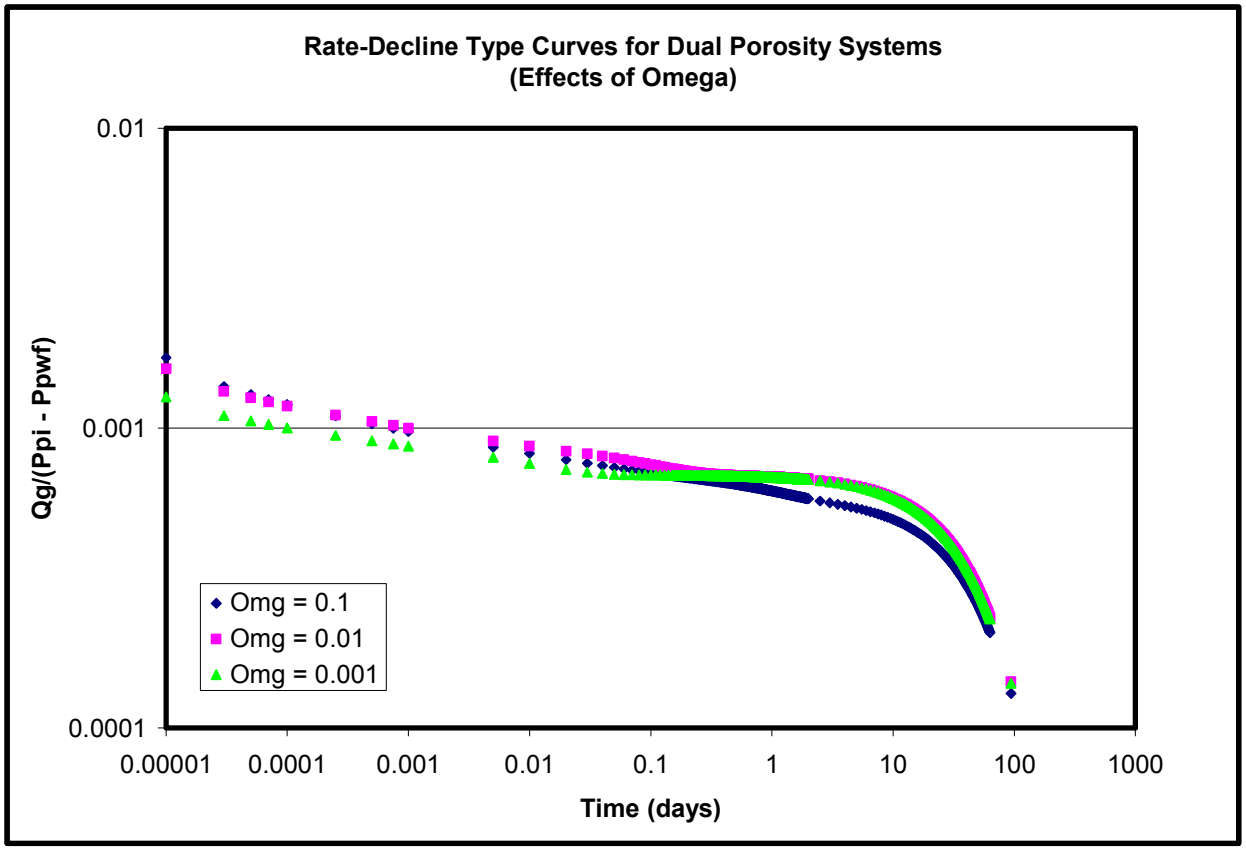

Figure 32 -- Rate-decline plot showing the effects of omega

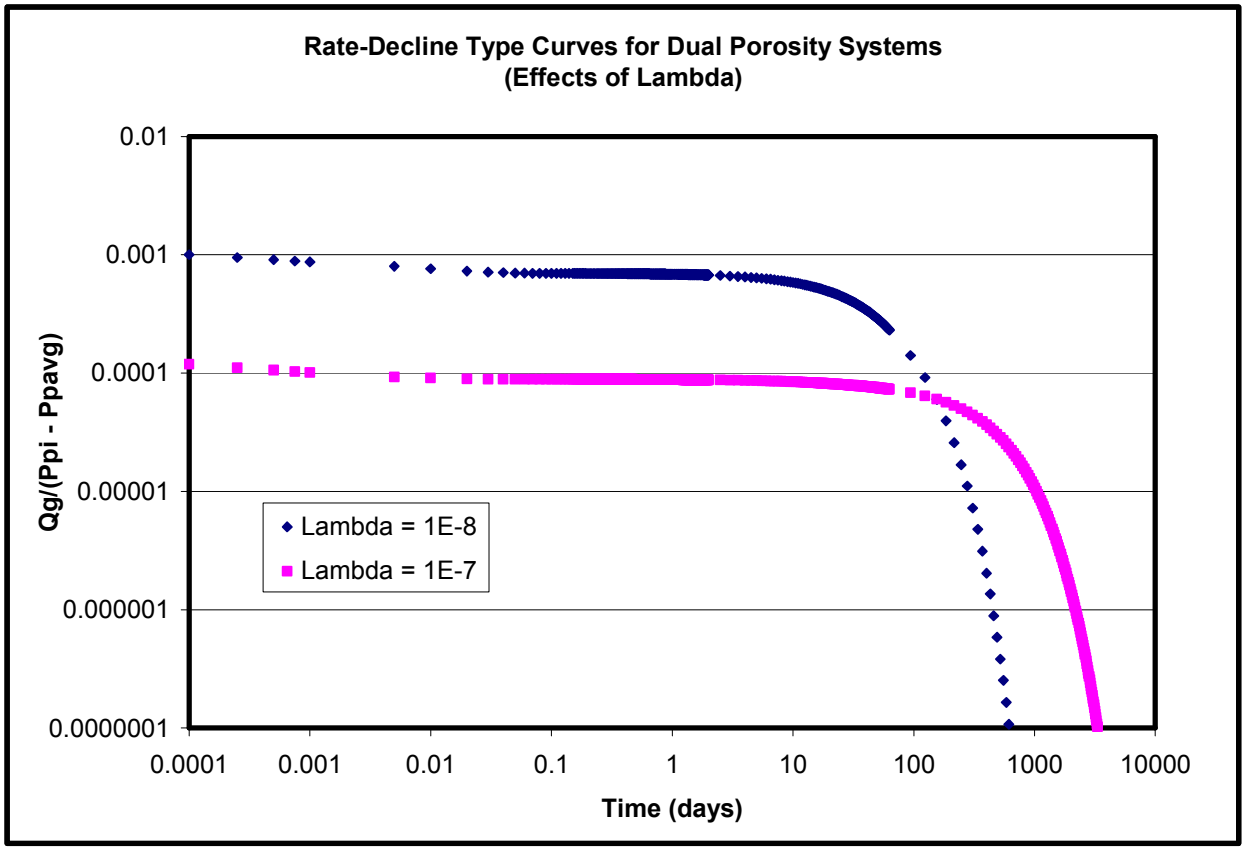

Figure 33 – Rate-Decline plot showing the effects of lambda

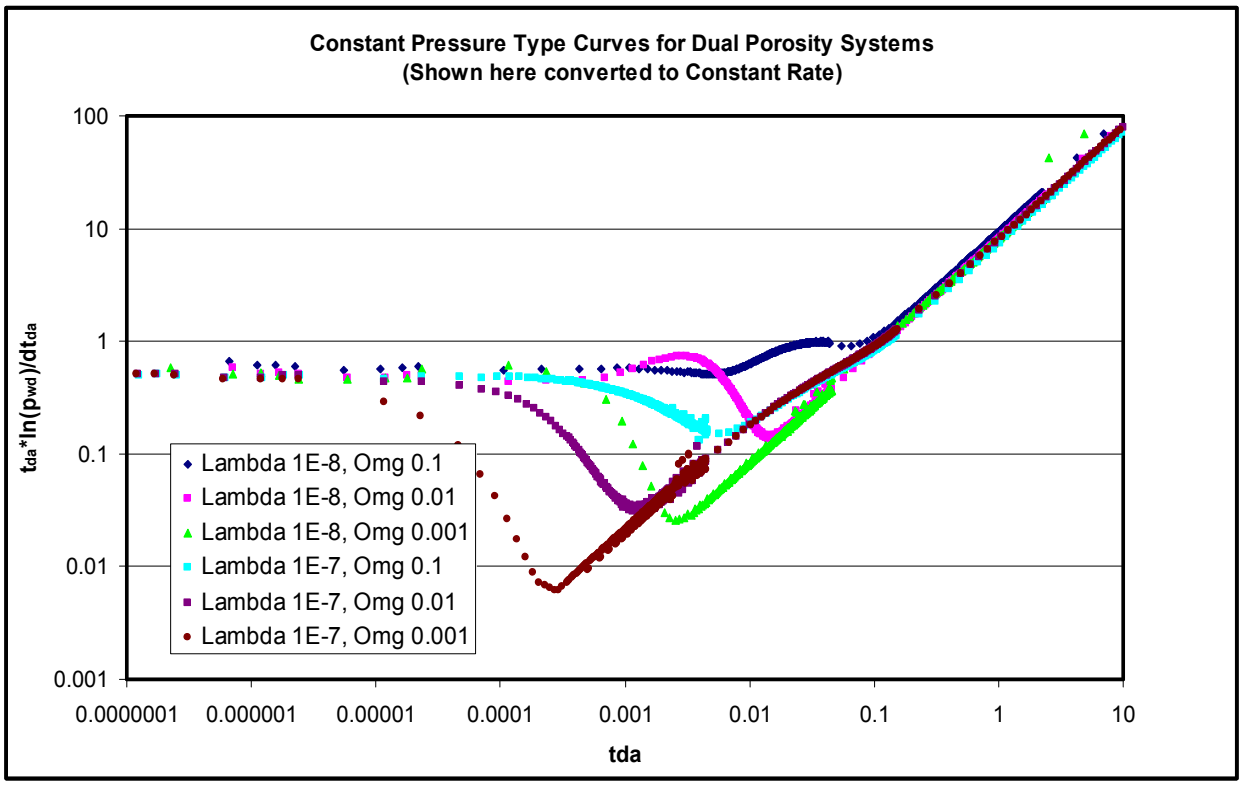

Figure 34 – Derivative type curve for constant pressure systems. Shown here converted to an equivalent constant rate system

The effects of λ and ω in constant-pressure systems after the systems are converted to constant-rate are shown in Figure 34, and are essentially the same as they are in constant-rate systems. This is to be expected since the technique of material balance time was used.

Figure 35 and Figure 36 are simulated data for single porosity hydraulically fractured systems produced at constant pressure. The models used to create these datasets are identical to those used for constant rate, hydraulically fractured systems with the exception of the boundary condition used at the well. The technique of material balance time was used to convert the constant pressure data to constant rate data, so it could be displayed on pressure-transient style plots. The equation for t_{da} is slightly different for hydraulically fractured systems than for the systems discussed previously. Recall that the x-axis plotting function for this type of system is t_d/C_{df}. This means that there will be additional terms in the equation for t_{da}.

$$t_{dA} = \frac{0.00634 k_{fh} t_a}{\mu_{gi} (\phi c_t)_i A} \frac{\pi k_m x_f}{k_{fh} w} = 0.01002 \frac{z_i}{p_i} \frac{x_f}{w} \frac{G k_m}{A \phi} \frac{[m(p_i) - m(\bar{p})]}{q_g} \qquad \text{Eq 113}$$

where

$$C_{df} = \frac{k_{fh} w}{\pi k_m x_f} \qquad \text{Eq 114}$$

The rate-decline type curves were created by plotting dimensionless rate versus dimensionless time. Normalized rate was not used in this case in order to compare the simulated results to an analytical solution.

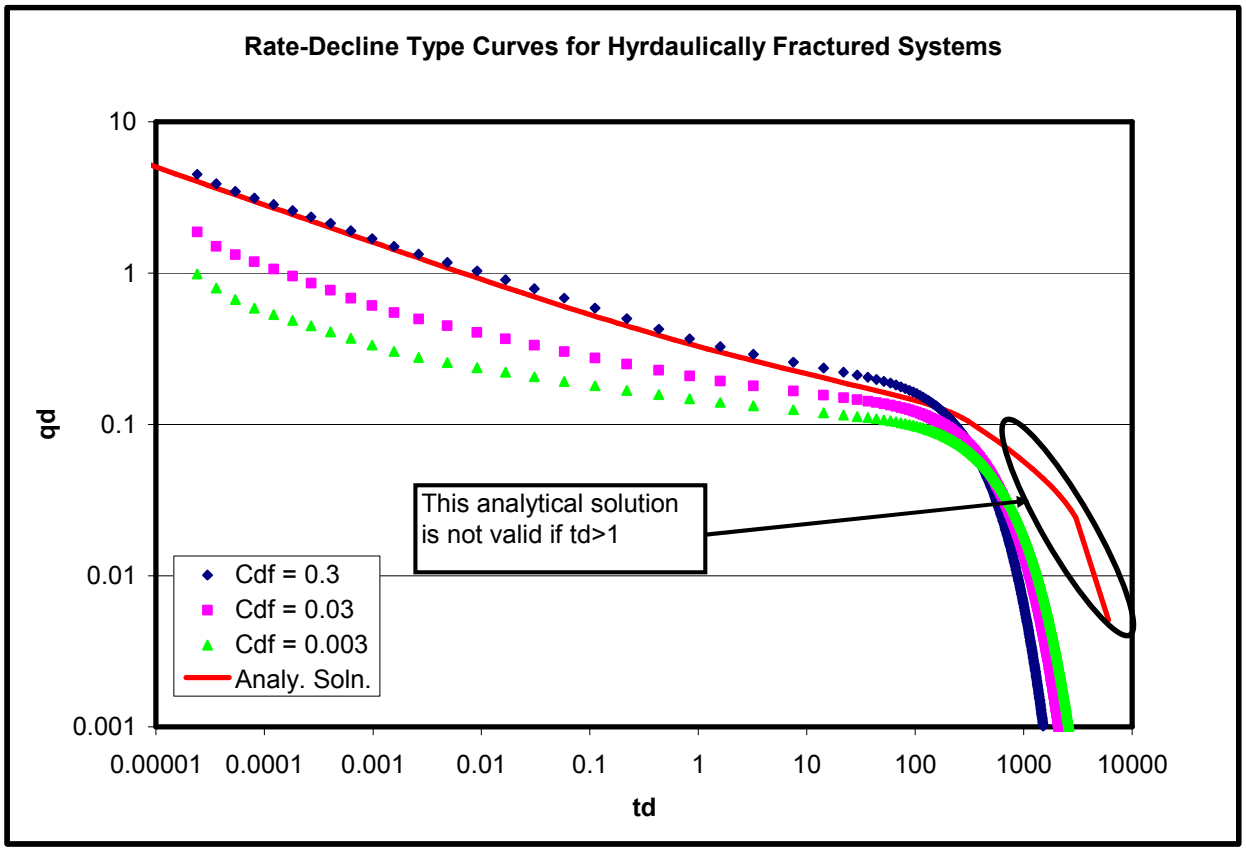

Figure 35 – Rate-Decline type curves for constant pressure systems showing the effects of dimensionless fracture conductivity

The analytical solution (the solid red line) seen in Figure 35 does not overlay the late-time portion of the simulated dataset because a closed-form solution for hydraulically fractured reservoirs was not available in literature, and deriving one was beyond the scope of this work. The analytical solution shown is for early time only, and is not valid for $t_d > 1$.

The effects of changing dimensionless fracture conductivity on constant pressure systems converted to an equivalent constant rate system are the same as they are for constant rate systems. This is to be expected since the technique of material balance time was used.

Figure 37 and Figure 38 refer to double porosity systems with hydraulic fractures produced at constant pressure. These are the most complicated systems that will be examined in this work.

Again, material balance time was used to convert the constant pressure systems to equivalent constant rate systems. The equation for material balance time as it applies to this type of system is

$$t_{dA} = \frac{0.00634 k_{fh} t_a}{\mu_{gi} (\phi c_t)_i A} \frac{\pi k_f x_f}{k_{fh} w} = 0.01002 \frac{z_i}{p_i} \frac{x_f}{w} \frac{G_i k_f}{A \phi} \frac{[m(p_i) - m(\bar{p})]}{q_g} \qquad \text{Eq 115}$$

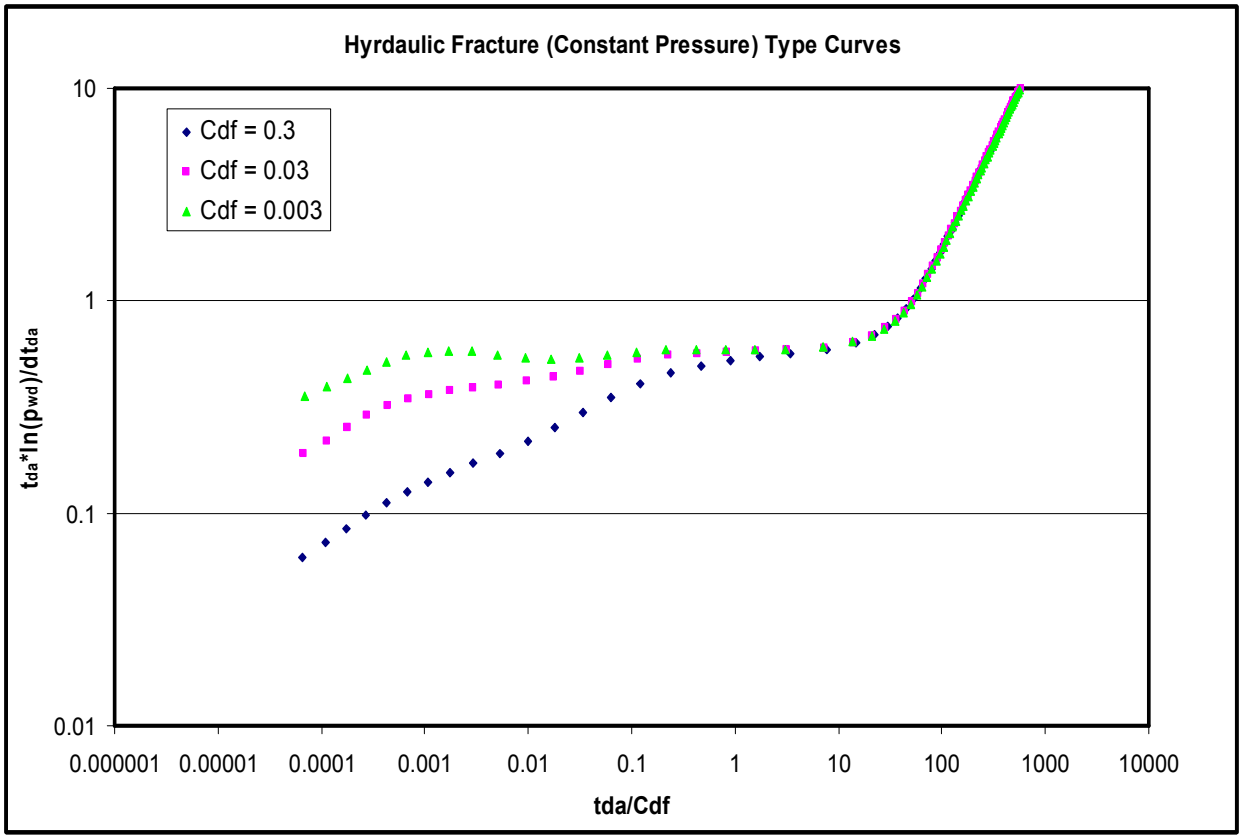

Figure 36 – Diagnostic plot for a constant pressure system showing the effects of dimensionless fracture conductivity. Shown here converted to an equivalent constant rate system

Again, Figure 37 and Figure 38 show the effects of changing fracture half-length in a dual porosity system with hydraulic fractures. The effects are the same as they are in constant rate systems. The use of the t_{da} conversion does not affect the appearance of the curves. Of course, the plotting functions (t_{dxf} in t_{da}) must be adjusted accordingly to reflect accurate scaling.

4.3 Low Permeability Systems Gas Systems

The previous graphs represent the performance of systems with parameters that are not realistic for shale gas systems. In particular, the permeability, porosity, and production rate are not representative of what is being encountered in the field. However, all of the plots that have been shown contain dimensionless pressures and times. This means that any system with the same

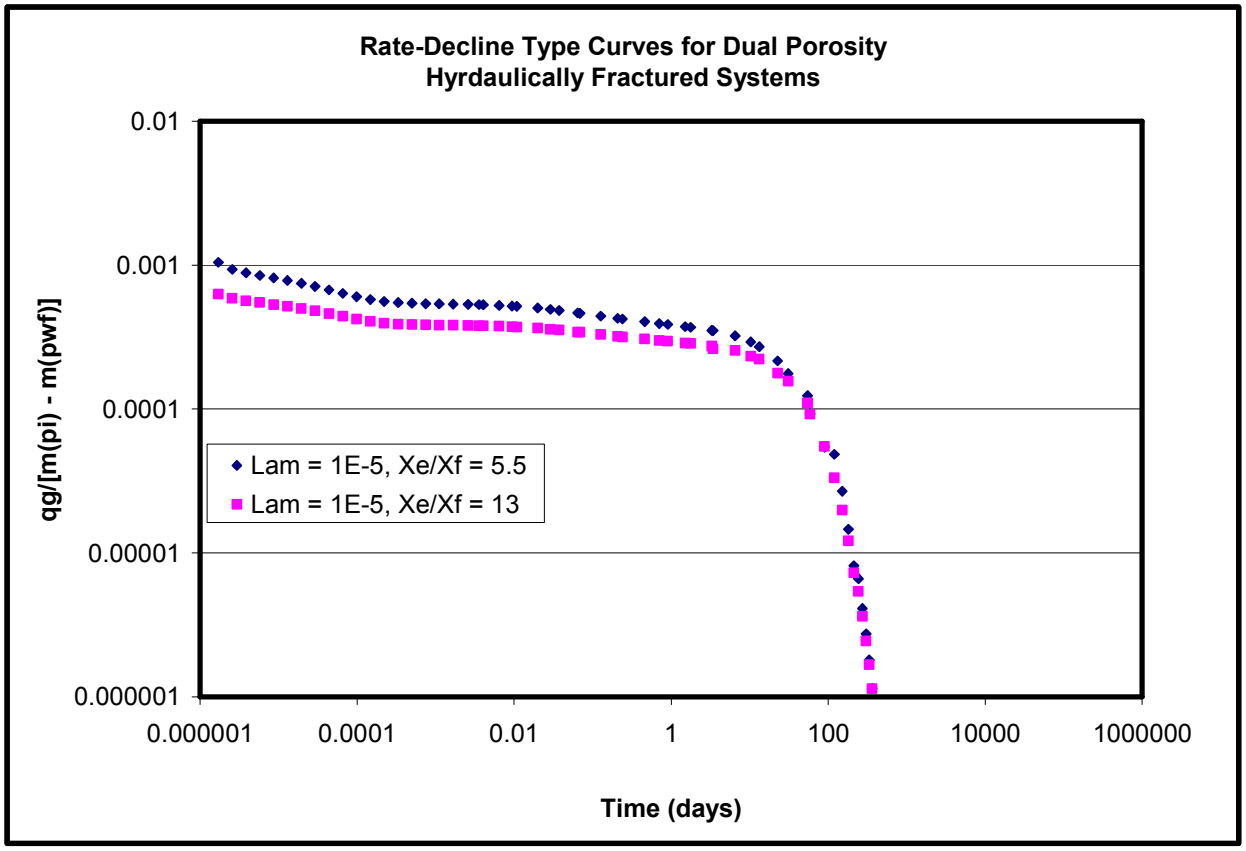

Figure 37 – Rate-Decline type curve showing the effects of changing fracture half-length in a dual porosity system with a hydraulic fracture.

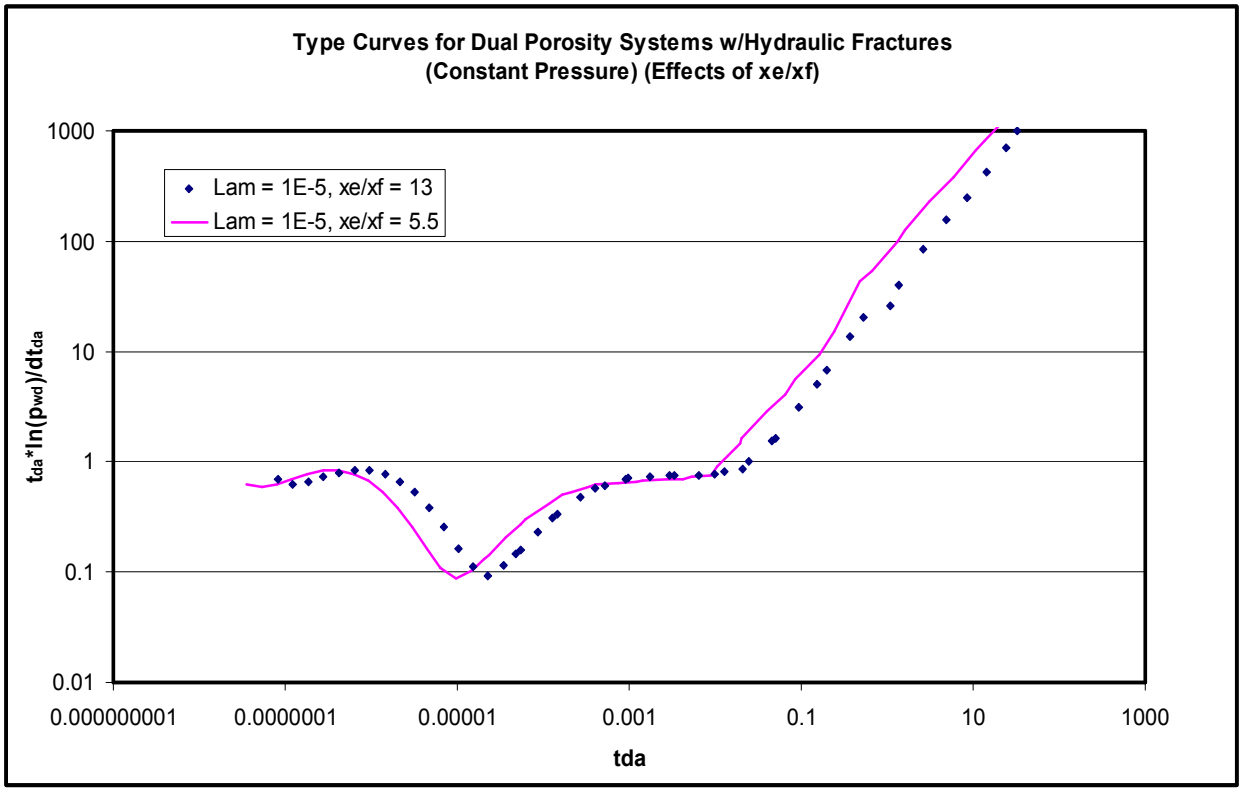

Figure 38 – Diagnostic plot for a constant pressure system showing the effects of changing fracture half-length. Shown here converted to an equivalent constant rate system.

dimensionless parameters (as well as λ and ω in the case of dual-porosity systems) will plot in exactly the same place on a graph of dimensionless pressure vs. dimensionless time. Nonetheless, the conversion to dimensionless variables must be done in the same manner. In the following cases, the simulation results of a system (Model 5) with realistic parameters for shale gas systems is shown ($\lambda = 1x10^{-8}$, $\omega = 0.1$).

Table 6 – Dataset for Model 5

Height/Net Pay (ft)	200
Outer Radius, r_e (ft)	2500
Well Radius, r_w (ft)	0.25
Porosity, ϕ_m	0.05
Porosity, ϕ_f	0.0055 (from ω)
Permeability, k_m(md)	0.01
Permeability, k_f(md)	19 (from λ)
Initial Pressure, (psia)	1514
Water Saturation, S_w	0.05
Rock Density, (lb/ft^3)	152.95
Temperature, (^oF)	120
Gas Gravity	0.55
Gas Composition	100% CH_4

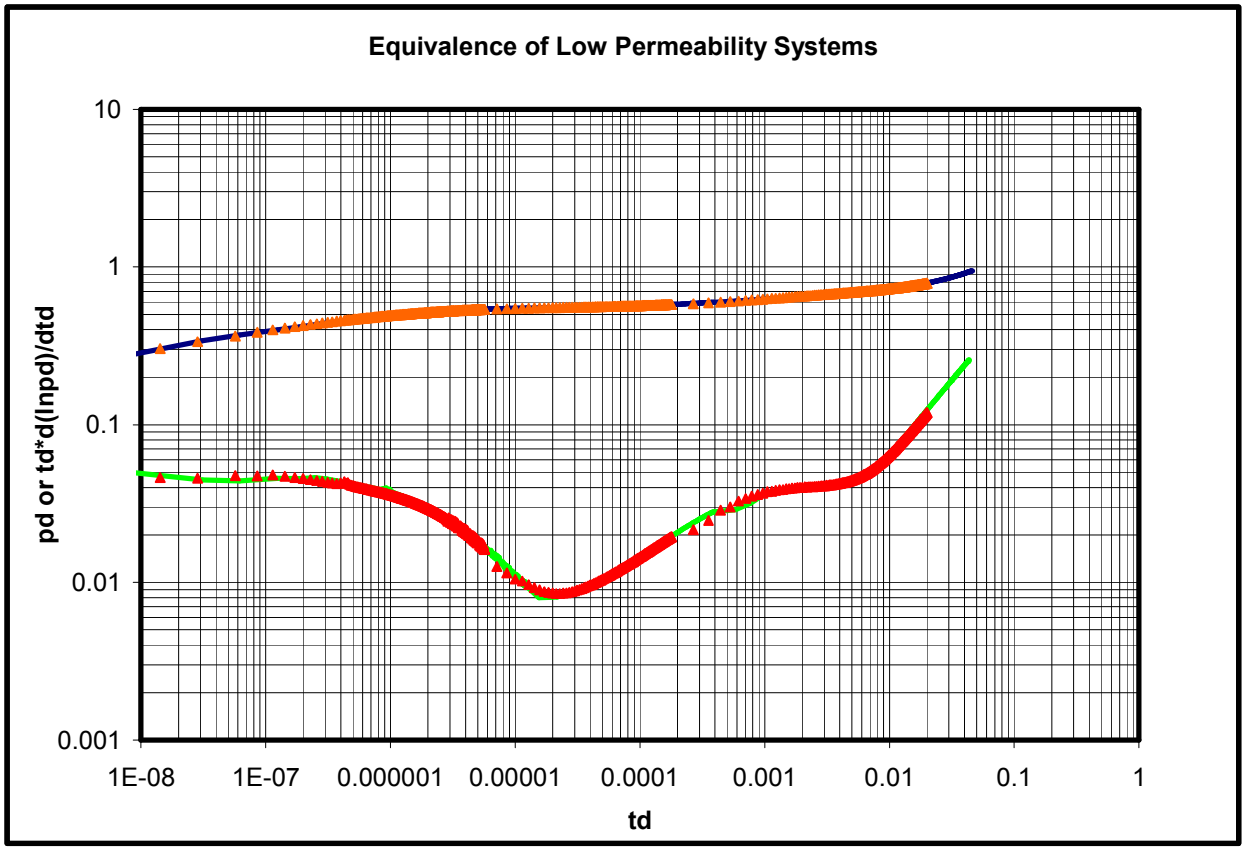

Figure 39 – Diagnostic plot showing that a shale gas system behaves identically to a "normal" reservoir on a diagnostic plot

The solid lines in Figure 39 represent the unrealistic system that has been used until now. The dotted line is the system with realistic parameters of a shale gas reservoir. Clearly, it is exactly equivalent in dimensionless space to the system with less realistic parameters. This is to be expected and has been shown before by other researchers. Nonetheless, it was necessary to show that shale gas systems still fit the expected models with their unusually low values of porosity and permeability.

5. SIMULATION MODELING OF ADSORPTION

The goal for this section is to show the effect of adsorbed gas on the type curves used for constant rate and constant pressure production. It will be shown that systems with adsorbed gas cannot be matched correctly to current analytical solutions if nothing is done to account for the adsorbed gas. However, if certain steps are taken, adsorption systems can be matched to the solutions for non-adsorbed systems.

5.1 Adsorption Systems Produced at Constant Terminal Rate

All previous systems that have been mentioned do not contain any adsorbed gas. Since all of the real shale gas systems have adsorbed gas (Montgomery, et al., 2005), it is necessary to add this component to the simulation models. The simulator requires that the adsorption data be entered has an isotherm. It then interpolates, as necessary, between the data points to calculate the amount of adsorbed gas at any time. Typically, adsorbed values are obtained from lab work in the form of Langmuir Pressure (p_L) and Langmuir Volume (v_L). An isotherm can be constructed using the Langmuir equation:

$$v_{ads}(scf/ft^3) = \frac{v_L p}{p_L + p} \qquad \text{Eq 116}$$

Adsorption data for all of the models in this chapter is not representative of real shale gas systems. The values in this chapter were selected to ensure that the effects of adsorption were highlighted. For the purposes of these next cases, the adsorbed values used were

Table 7 – Langmuir properties

Langmuir Pressure (psia)	214
Langmuir Volume (SCF/ft^3)	61.2
Rock Density (g/cm^3)	2.45

These properties were chosen to try to investigate effects of adsorption and are not representative of shale gas systems encountered in the field. Figure 41 and Figure 42 compare a dual-porosity system ($\lambda = 1x10^{-7}$, $\omega = 0.01$) to a dual porosity system with the same matrix and fracture properties but also with adsorbed gas. The two models were given identical physical and reservoir properties except for adsorption being specified for one system. These simulation models were constructed to be almost identical to the dual porosity models presented earlier, except that some contain adsorbed gas.

The effects of adsorption are clear in Figure 42. There is a horizontal shift on the derivative curve. There also is a smaller apparent ω (greater dip at td $\approx$ 0.003) caused by the method in which ω is used to calculate the matrix and fracture porosities for the two systems. Recall that ω is

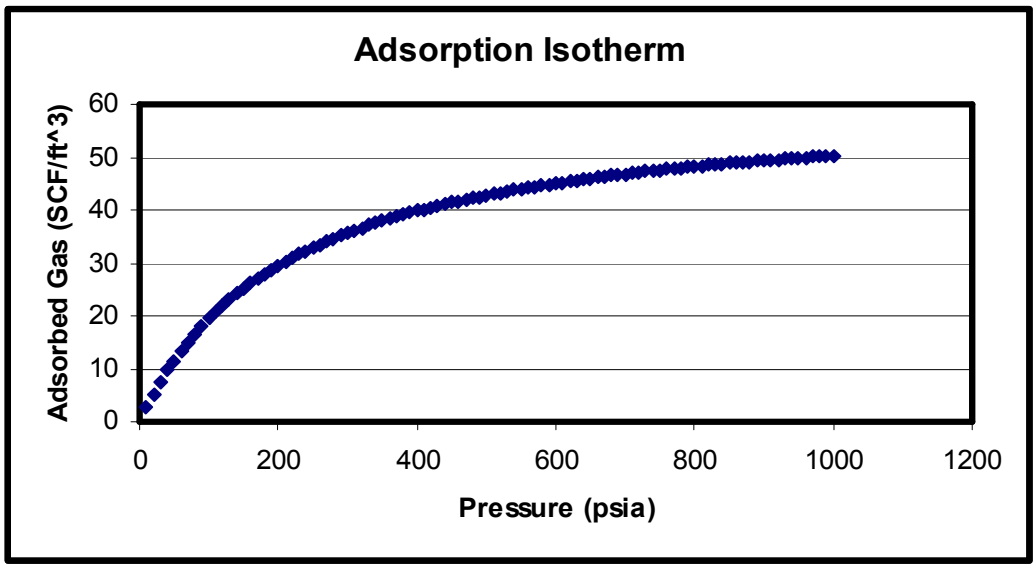

Figure 40 – Langmuir isotherm used in simulation models

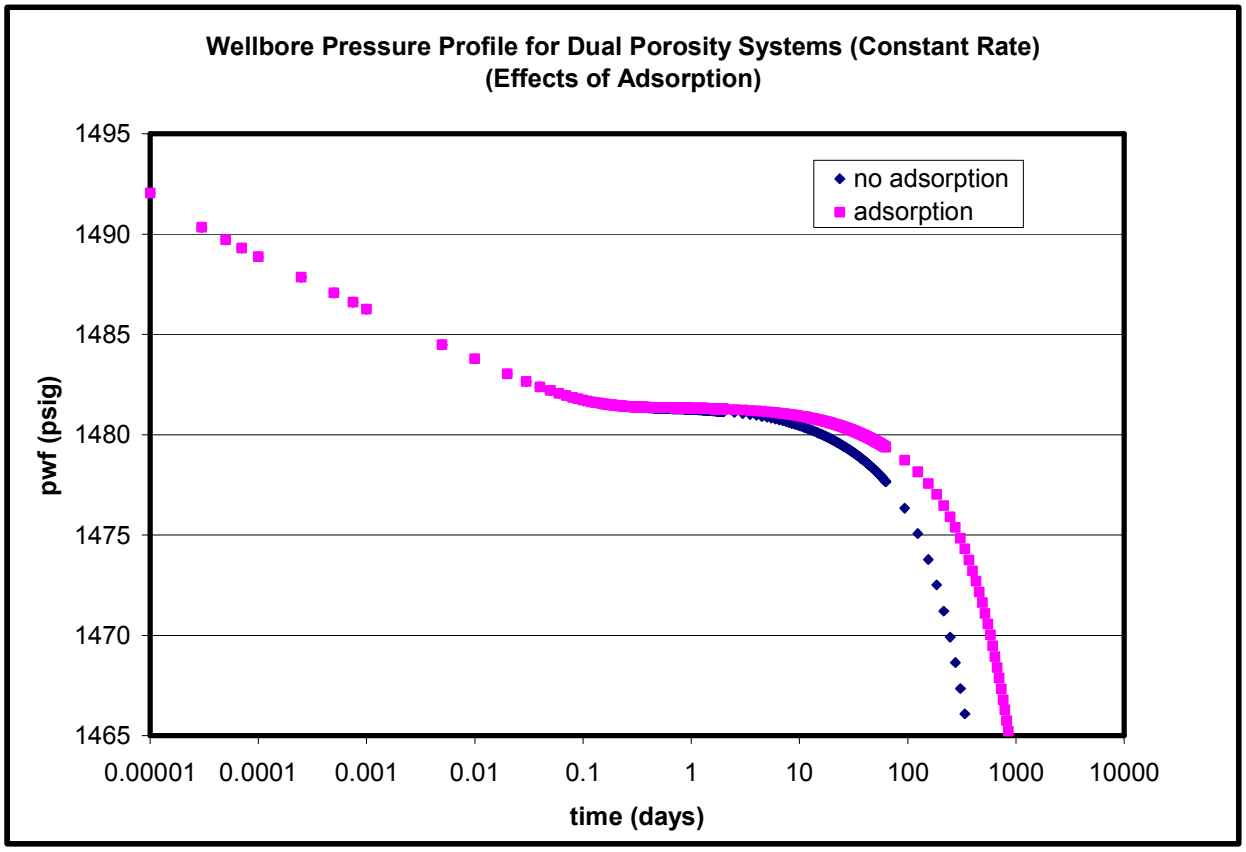

Figure 41 – Wellbore pressure profiles for dual porosity systems showing the effects of adsorption

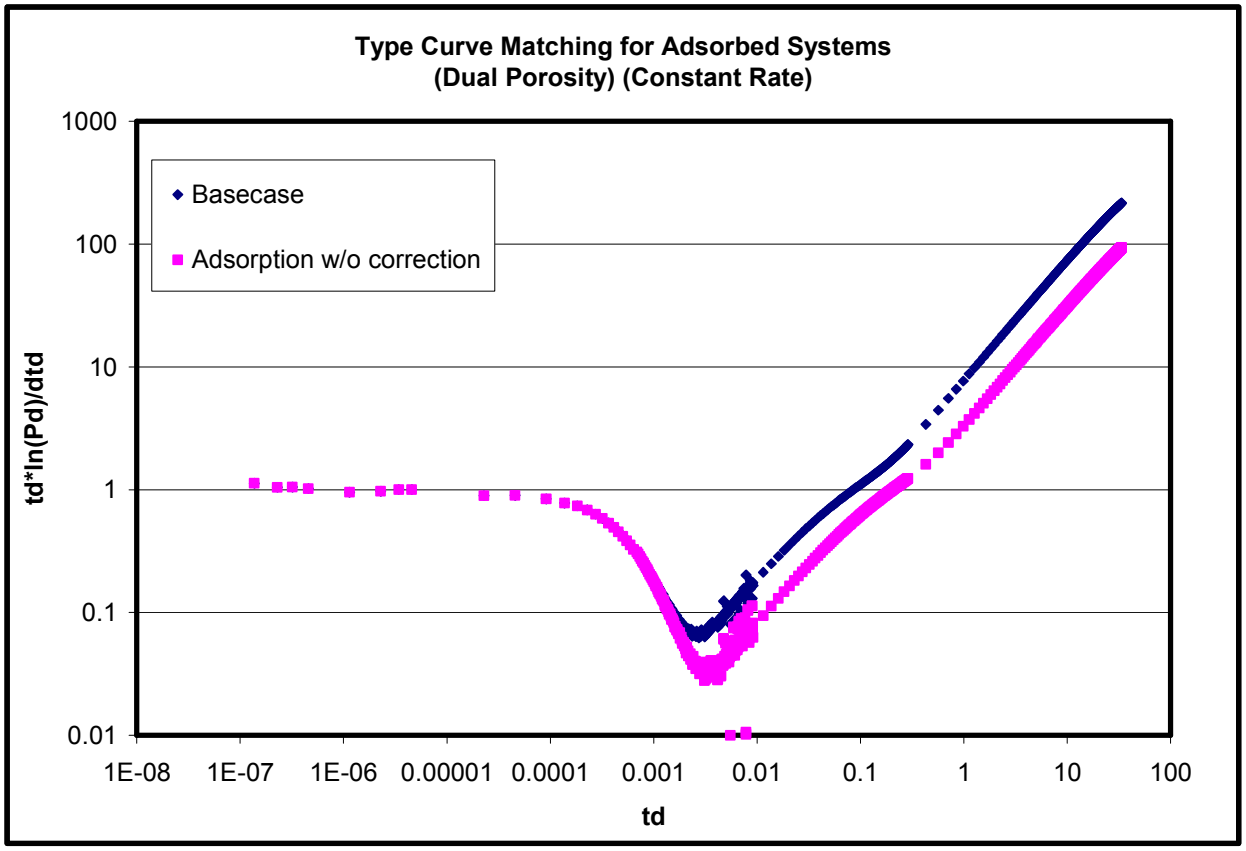

Figure 42 – Diagnostic plot for dual porosity system that shows the effects of adsorption.

$$\omega = \frac{(\phi c_t)_f}{(\phi c_t)_f + (\phi c_t)_m} \qquad \text{Eq 117}$$

The systems have identical drainage area, thickness, fracture and matrix porosities, and initial pressure. Adsorbed gas is found only in the matrix. This so, the ω for the simulated model with adsorption is different because the compressibility with adsorption is larger. The denominator in the equation for ω is larger because of adsorption (Eq 100, total compressibility for a system with adsorption). A system with ω = 0.01 in no adsorption would have ω = 0.0045 with the adsorption given in Table 7.

The horizontal shift is also due to the altered compressibility. There are only two things that can (reasonably speaking) shift the dimensionless time without shifting the dimensionless pressure (i.e. radial flow has not moved vertically). They are system compressibility and system porosity. Since the two models have identical porosity (both are dual porosity models), compressibility must be the cause. So, any accurate analysis of a constant rate system must include a definition of compressibility that accounts for adsorption. Spivey and Semmelbeck (1995) proposed handling adsorption by using an adjusted system compressibility that has been described earlier.

$$c_t = S_w c_w + (1 - S_w) c_g + \frac{p_{sc} V_L p_L T z}{\phi T_{sc} z_{sc} (p_L + \bar{p})^2} + c_f \qquad \text{Eq 118}$$

If this equation for compressibility is used in the equation for dimensionless time, the horizontal shift seen in the previous graph should disappear. Then, the boundary-dominated flow portions of the type curves will overlay. This is shown in Figure 43 where the orange data points overlay the blue data points at late-time but are shifted to left for early-time. The early time portions will not overlay because of the shift in ω caused by adsorption that was discussed earlier.

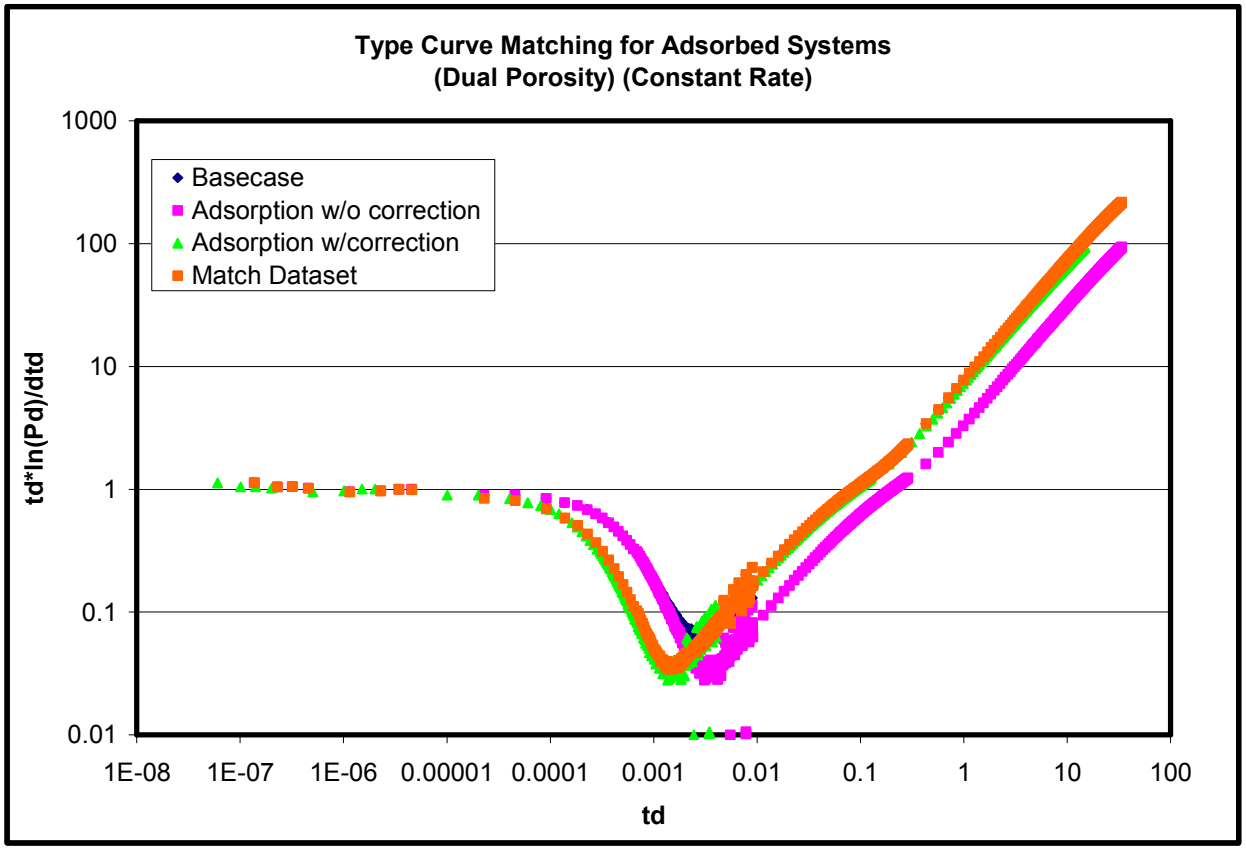

Figure 43 – Diagnostic plot showing the matching process for adsorbed systems

The "Match Dataset" in Figure 43 requires explanation. The goal was to have an adsorbed system overly a non-adsorbed system by applying the correction for adsorption in the form of an adjusted system compressibility proposed by Bumb and McKee (1988) and later expounded upon by Spivey and Semmelbeck (1995). Also, this process would show what potential errors are made when adsorption is not accounted for.

First, a simulation dataset that contains no adsorbed gas was analyzed (i.e. the known simulation model parameters were used to calculate the plotting functions). This is the "Basecase" in Figure 42 and Figure 43. Second, another simulation model with adsorbed gas was analyzed without using the correction for system compressibility outlined earlier. This is the "Adsorption w/o

correction" in Figure 42 and Figure 43. There is a horizontal shift to the right in this dataset caused by adsorption. Third, the same dataset used in making the "Adsorption w/o correction" was analyzed using the method described previously to account for adsorption. This causes the dataset to shift back to the left and overlay the "Basecase" at late-time. This is the "Adsorption w/correction" in Figure 43. Lastly, a new simulation model ("Match Dataset") was constructed to overlay the adsorbed dataset. The "Match Dataset" represents a non-adsorbed system with the same effective ω as the adsorbed system. Any match of the production data would yield reservoir parameters that coincide with this analytical solution. The only parameter changed to attain this match was ω (made smaller). Since the larger compressibility results in a smaller effective ω, it was necessary to build a non-adsorbed simulation model to match all portions (early and late time) of the adsorption system.

Note that neither the "Adsorption w/o correction" dataset nor the "Adsorption w/correction" dataset overlay the "Basecase" at both early and late-time. The "Adsorption w/o correction" dataset overlays the "Basecase" at early-time despite the presence of adsorbed gas because the p_L used in this model is relatively small. Therefore, adsorption is only a late-time effect. The "Adsorption w/correction" in Figure 43 is an adsorbed system that has been corrected for adsorption using an effective system compressibility that accounts for adsorption (Eq 118). However, the larger system compressibility caused by adsorption has resulted in this system having a different ω. So, it will not overlay the "Basecase" at early-time. It should be mentioned that the horizontal shift caused by adsorbed gas is very slight and may or may not be visible when actual production data is used. In addition, this shift can easily be mistaken for something else such as a small increase in porosity. Finally, failing to recognize the presence of adsorption can lead to erroneous estimates of ω.

Figure 44 and Figure 45 pertain to hydraulically fractured systems that contain adsorbed gas. The hydraulically fractured simulation models were constructed almost identically to the hydraulically fractured systems presented earlier except that some contain adsorbed gas. The adsorption isotherm and its parameters (v_L and p_L) are identical to the ones used for the dual porosity systems.

The effects of adsorption on hydraulically fractured systems are simpler than for dual porosity systems. Since there is no fracture-matrix storativity term in these systems, the only effect of adsorption is a horizontal shift in the derivative curve. This is corrected using Eq 100.

Figure 44 and Figure 45 show the effects of adsorption on a hydraulically fractured system. Note the horizontal shift caused by adsorption in Figure 45. Again, the green curve represents a system that has been corrected for adsorption using Eq 100. The pink curve does not have this correction. Also note that there is a secondary, indirect effect of adsorption like there was in a dual porosity system. The horizontal shift caused by adsorption could result in a slightly larger value of C_{df}.

Figure 46 and Figure 47 pertain to dual porosity systems with hydraulic fractures that contain adsorbed gas. These models were constructed almost identically to the dual porosity systems with hydraulic fractures presented earlier except that they contain adsorbed gas. The adsorption isotherm and its parameters (v_L and p_L) are identical to the ones used for dual porosity systems.

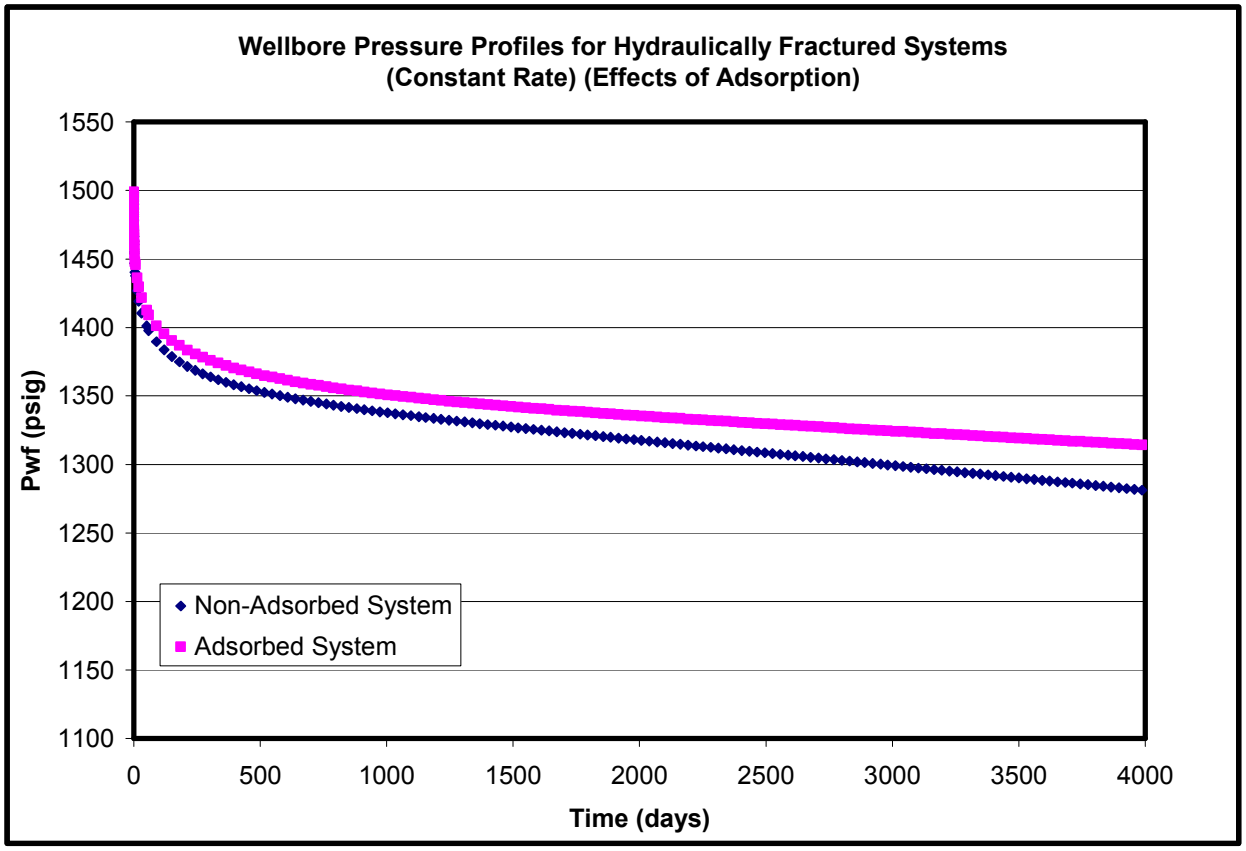

Figure 44 – Wellbore pressure profile for hydraulically fractured systems produced at constant rate. Note the significant change in the late-time (low pressure) behavior of the adsorbed case.

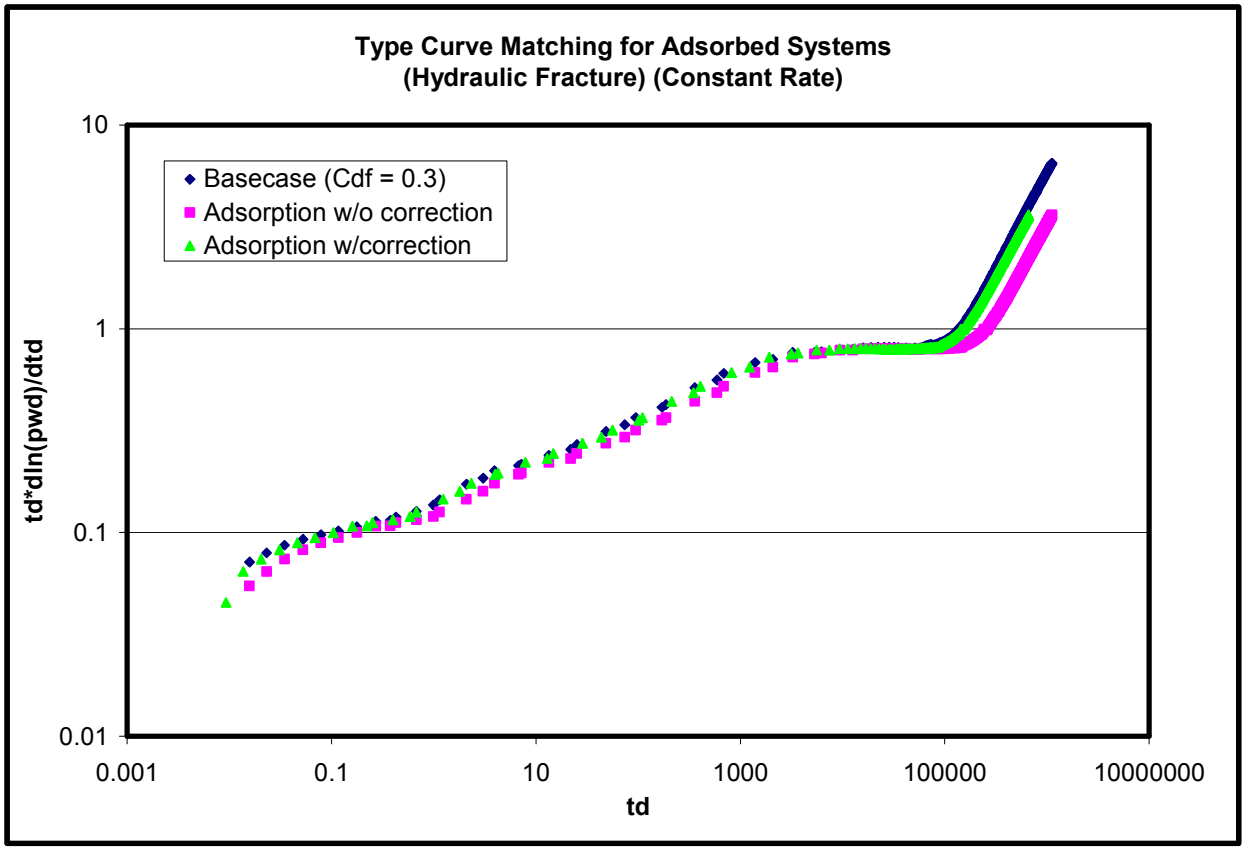

Figure 45 – Diagnostic plot for hydraulically fractured systems produced at constant rate. Note the horizontal shift caused by the presence of adsorbed gas (uncorrected dataset).

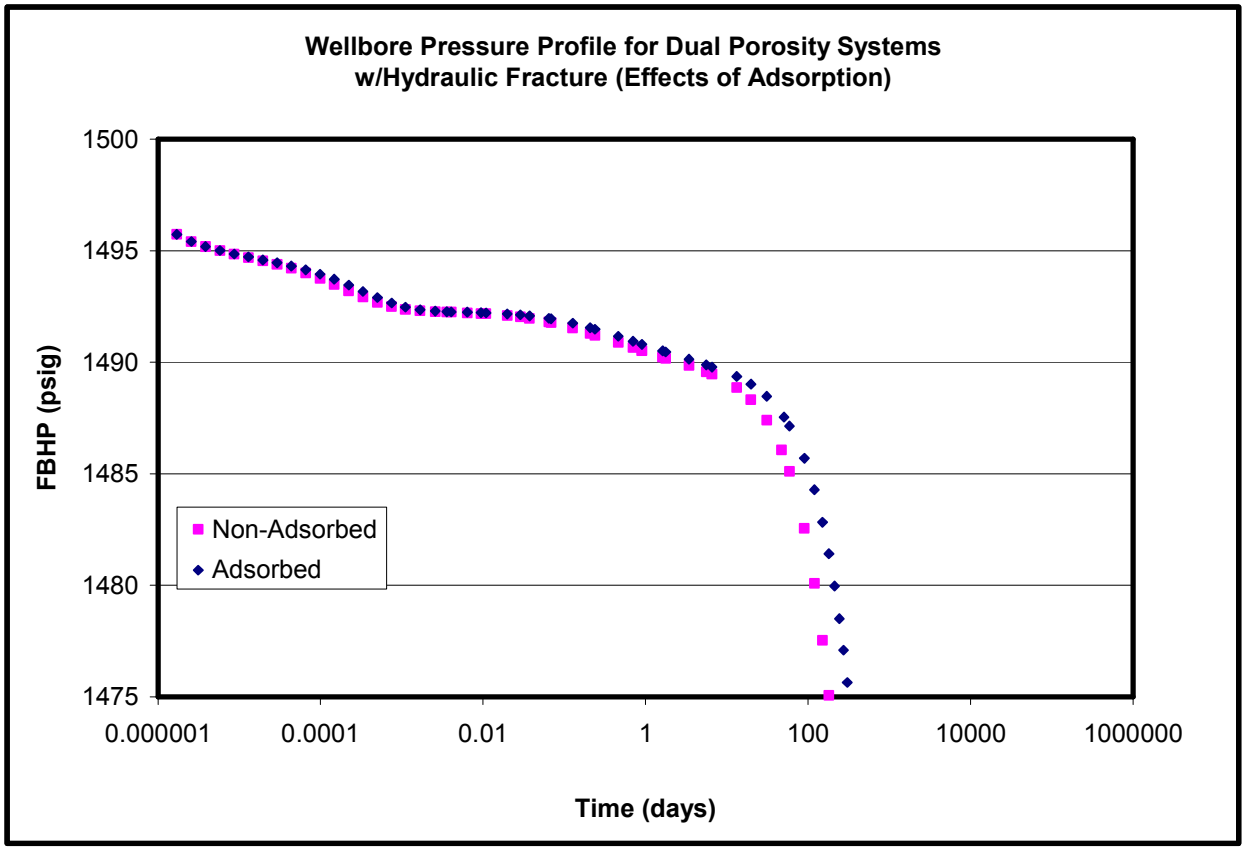

Figure 46 – Wellbore pressure profiles for a dual porosity system with a hydraulic fracture. Note that there is almost no early time effect. The near well performance is already so great due to the hydraulic fracture that the additional adsorbed gas has little to no impact on performance.

Note that there is almost no early time effect. The near well performance is already so great due to the hydraulic fracture that the additional adsorbed gas has little to no impact on performance.

The effect of adsorption is very minimal on both the wellbore pressure profiles and the derivative plots. There is also no shift in ω as was seen with dual porosity systems without a hydraulic fracture. Somewhat depending on λ, ω predominately affects early time performance. Since adsorbed gas tends to cause one to see an apparent smaller ω, the performance characteristics of the large conductivity of the hydraulic fracture obscure the effects of ω. However, the corrected compressibility does allow for better a match to be obtained between the non-adsorbed and adsorbed systems.

5.2 Adsorption Systems Produced at Constant Terminal Pressure

Earlier, the equivalence between constant pressure and constant rate was discussed. However, once adsorption is considered, things become more complicated. The presence of adsorption in a system produced at constant pressure does not allow for a "correction" to be applied, in the form of a new definition for compressibility, in order to get adsorption systems to behave like non-adsorbed systems. This is primarily due to the definition of material balance time which is used to convert constant pressure systems to an equivalent constant rate system. The Palacio and Blasingame (1993) definition of material balance time is

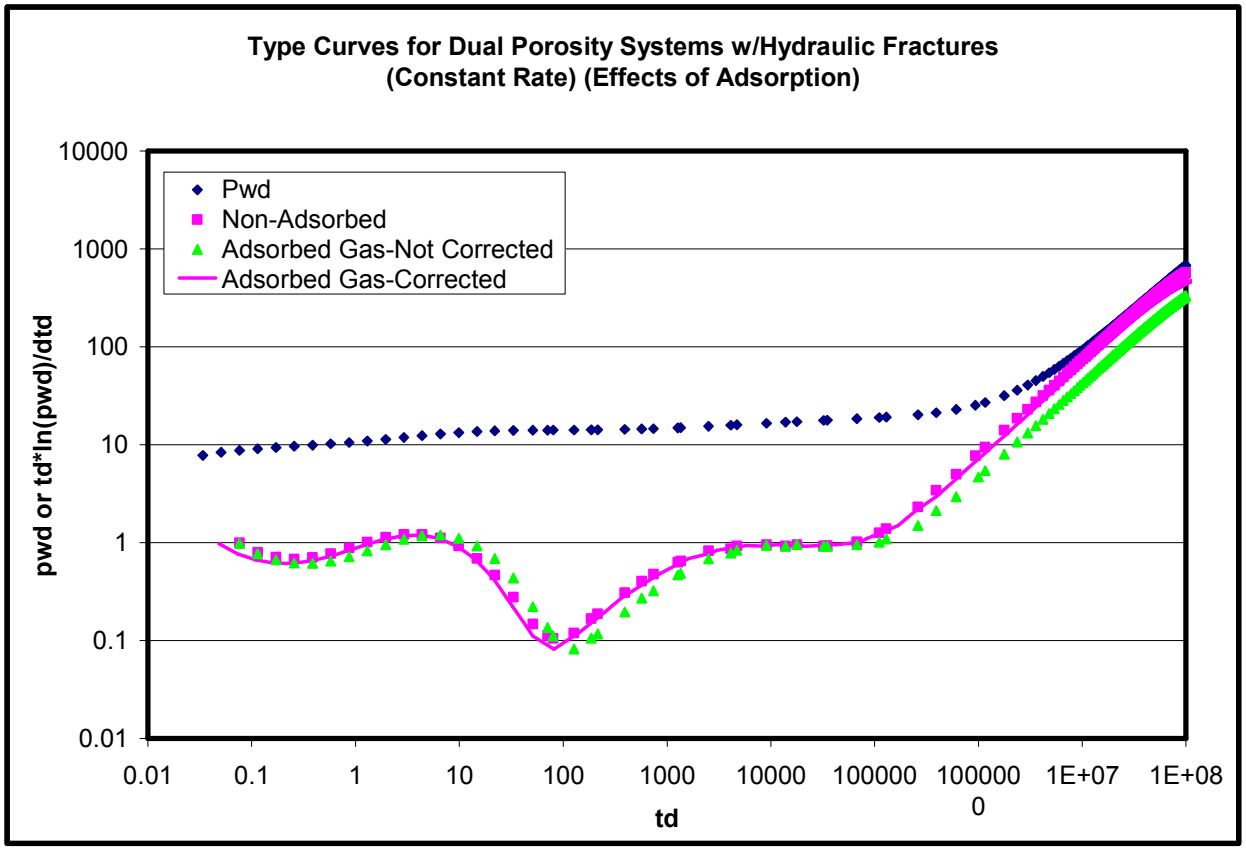

Figure 47 – Diagnostic plot for dual porosity systems with a hydraulic fracture. Again, note that there is almost no early time effect of adsorption. There is also no shift in omega as was seen with dual porosity systems without a hydraulic fracture. Somewhat depending on lambda, omega is predominately affects early time performance. Since adsorbed gas tends to cause one to see an apparent smaller omega, the huge conductivity of the hydraulic fracture counteracts this.

$$\bar{t}_a = \frac{\mu_{gi} c_{ti}}{q_g}\left(-\frac{Gz_i}{p_i}\right)\int_0^t \frac{\bar{p}}{z}\frac{c_g}{\mu_g(\bar{p})c_t(\bar{p})}\frac{dp}{dt}dt \qquad \text{Eq 119}$$

The only assumption made so far is that the single-phase, gas material balance equation applies. This requires that the reservoir be volumetric and the only source of energy for production come from gas expansion. This begs the question of whether or not it would be meaningful to introduce the new definition of compressibility into G (original gas in place). It would be meaningful, but it would not change the definition of t_a since G_i is a constant and is removed from any integral expression.

The next step in computing t_a is typically to assume that total system compressibility (c_t) is equal to gas compressibility (c_g). For non-adsorbed systems, this is usually a reasonable assumption. For systems with significant amounts of adsorbed gas, this represents a serious error in two ways. The first error being that total system compressibility is now most accurately represented

by the equation for c_t from Spivey and Semmelbeck (1995). This new c_t is in no way equal to c_g for reservoirs with large amounts of adsorbed gas. So, c_t and c_g should be left inside the integral which will require an iterative solution. Since the solution is already iterative, these additional calculations require only a minimal amount of additional effort.

The second error that is referred to above is the indirect result of compressibility being removed from the pressure integral. Recall that production data analysis is frequently done using the dimensionless time variable (t_{da}) as the x-axis plotting function. The equation for t_{da} is (Cox, et al. 2002)

$$t_{da} = \frac{kt}{(\mu c_t)_i \phi A} \qquad \text{Eq 120}$$

To incorporate material balance time, substituted $\bar{t}_a$ for t where

$$\bar{t}_a = \frac{\mu_{gi} c_{ti}}{q_g} \left(\frac{G z_i}{2 p_i} \right) \left(m(p_i) - m(\bar{p}) \right) \qquad \text{Eq 121}$$

Combining and simplifying

$$t_{da} = \frac{z_i}{2 p_i} \frac{kG}{\phi A} \frac{[m(p_i) - m(\bar{p})]}{q_g} \qquad \text{Eq 122}$$

The equation given above is what is typically plotted on the x-axis. It is apparent that compressibility is no longer in the equation for t_{da} in the traditional evaluation. So, this brings to light a very important point. It appears that any attempt to account for the behavior of systems that have significant amounts of adsorbed gas is futile in dimensionless space with the new definition of compressibility that was proposed by Bumb and McKee (1988) and Spivey and Semmelbeck (1995). That is not to say that the definition is incorrect. Spivey and Semmelbeck (1995) showed that it worked quite well for systems when the rate-time analysis was done in real/dimensional space. It is simply that compressibility is not in the equation for t_{da}.

However, it was shown earlier that one of the assumptions that is typically used in the development of t_a is incorrect for adsorbed systems. If this assumption is not made, then the definitions of t_a and t_{da} are

$$\bar{t}_a = \frac{\mu_{gi} c_{ti}}{q_g} \left(- \frac{G z_i}{p_i} \right) \int_0^t \frac{\bar{p}}{\bar{z}} \frac{c_g}{\mu_g(\bar{p}) c_t(\bar{p})} \frac{dp}{dt} dt \qquad \text{Eq 123}$$

$$t_{da} = \frac{z_i}{2p_i}\frac{kG}{\phi A}\frac{[m_{ct}(p_i) - m_{ct}(\bar{p})]}{q_g} = t_{da\,new} \qquad \text{Eq 124}$$

Eq 124 for t_{danew} does not make the assumption that allows compressibility to be eliminated from the integral. This new integral is essentially pseudopressure with the ratio (c_g/c_t) left inside. This new integral is represented with the group $(m_{ct}(p_i) - m_{ct}(\bar{p}))$.

Figure 48 and Figure 49 are intended to show the effects of adsorbed gas on a dual porosity system. All of the models used to generate the datasets are identical to the dual porosity models presented earlier except that these are produced at a constant flowing bottomhole pressure and they contain adsorbed gas. All of the datasets were converted to constant rate using the modified material balance time function described above.

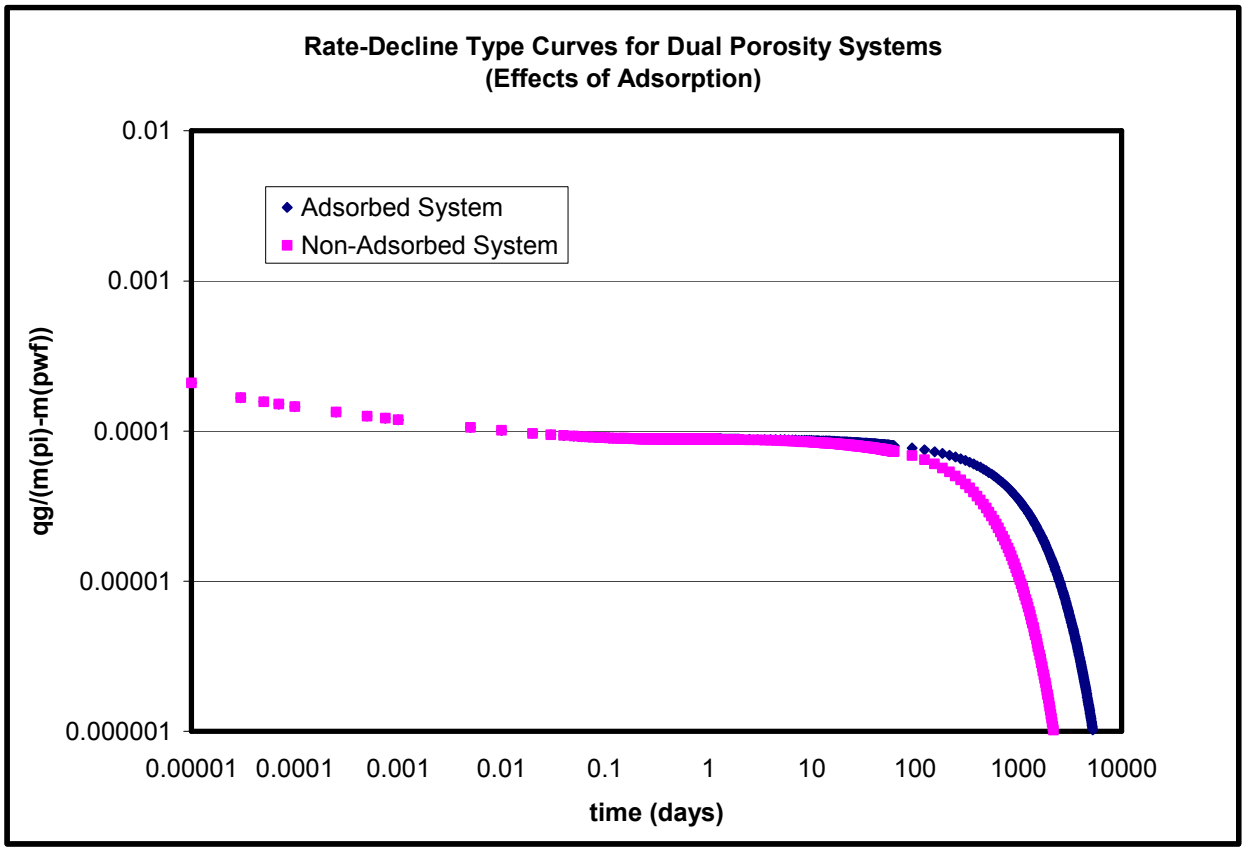

Figure 48 – Rate-decline type curves for dual porosity systems showing the effects of adsorption. Note that the majority of the effect comes at late-time (i.e. lower pressure).

The effect of adsorption on dual porosity systems produced at constant pressure is the same as those produced at constant rate and can be seen in Figure 48 and Figure 49. This is to be expected since the equivalence of the systems was shown earlier. Adsorption results in a smaller "apparent" ω and a horizontal shift of the type curve.

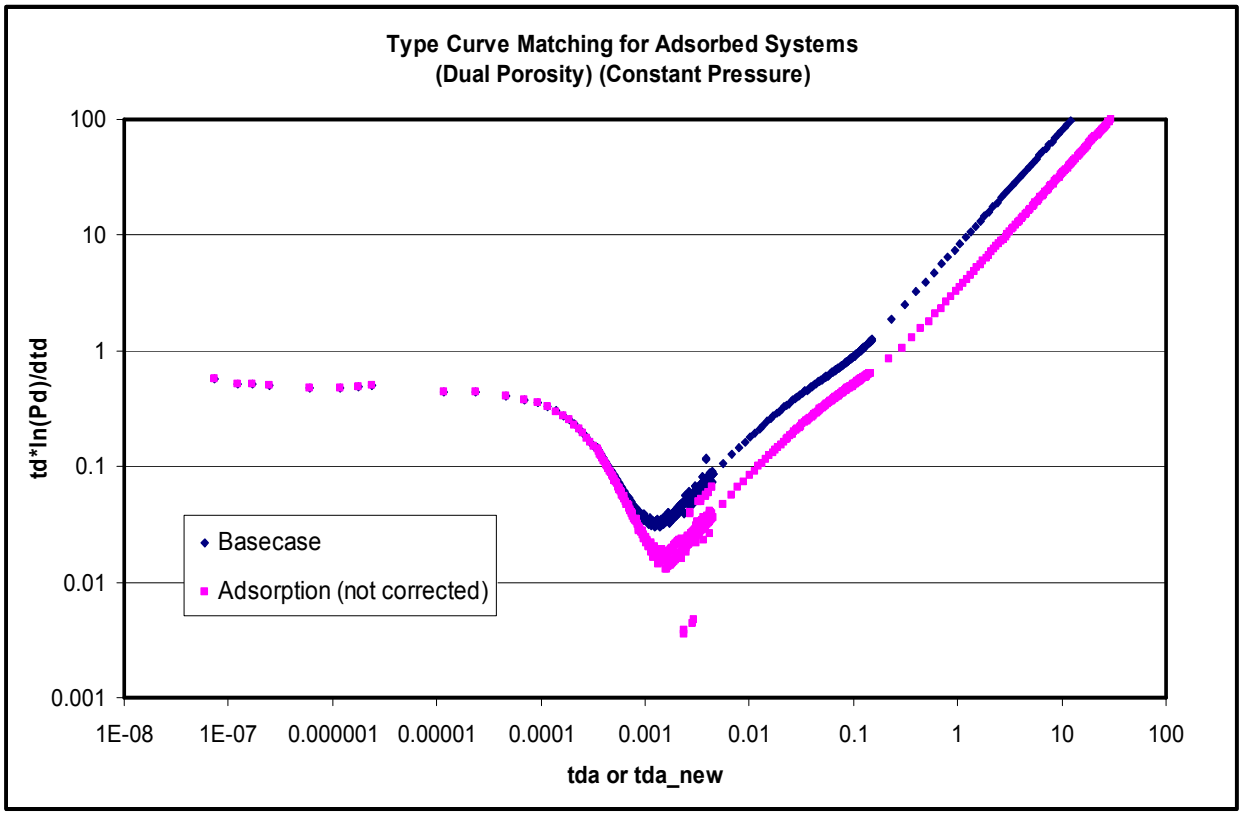

Figure 49 – Diagnostic plot for constant pressure dual porosity systems show here converted to an equivalent constant rate. Note the horizontal shift and the smaller apparent omega both caused by adsorption.

Figure 50 and Figure 51 explain the differences in the constant pressure type curves for adsorbed systems when compared to those for constant rate. Adsorbed systems produced at a constant rate can be matched simply by correcting the system compressibility and ω. The goal here is to show how to make an adsorbed system overlay (appear identical to) a non-adsorbed system. Therefore, an adsorbed system could be matched to an analytical solution. The question to be answered is what parameters will result from the match. When using material balance time, the match is often to the term $kG/(\phi A)$ assuming than initial pressure, flowrate, and bottomhole pressure are confidently known.

Figure 50 demonstrates that a simple correction of system compressibility is not sufficient to allow the system with adsorption to overly the system without adsorption. This is due to the use of material balance time to "convert" the constant pressure systems to an equivalent constant rate system. Recall the definition of material balance time.

$$t_{da}new = \frac{z_i}{2p_i}\frac{kG}{\phi A}\frac{[m_{ct}(p_i) - m_{ct}(\overline{p})]}{q_g} \qquad \text{Eq 125}$$

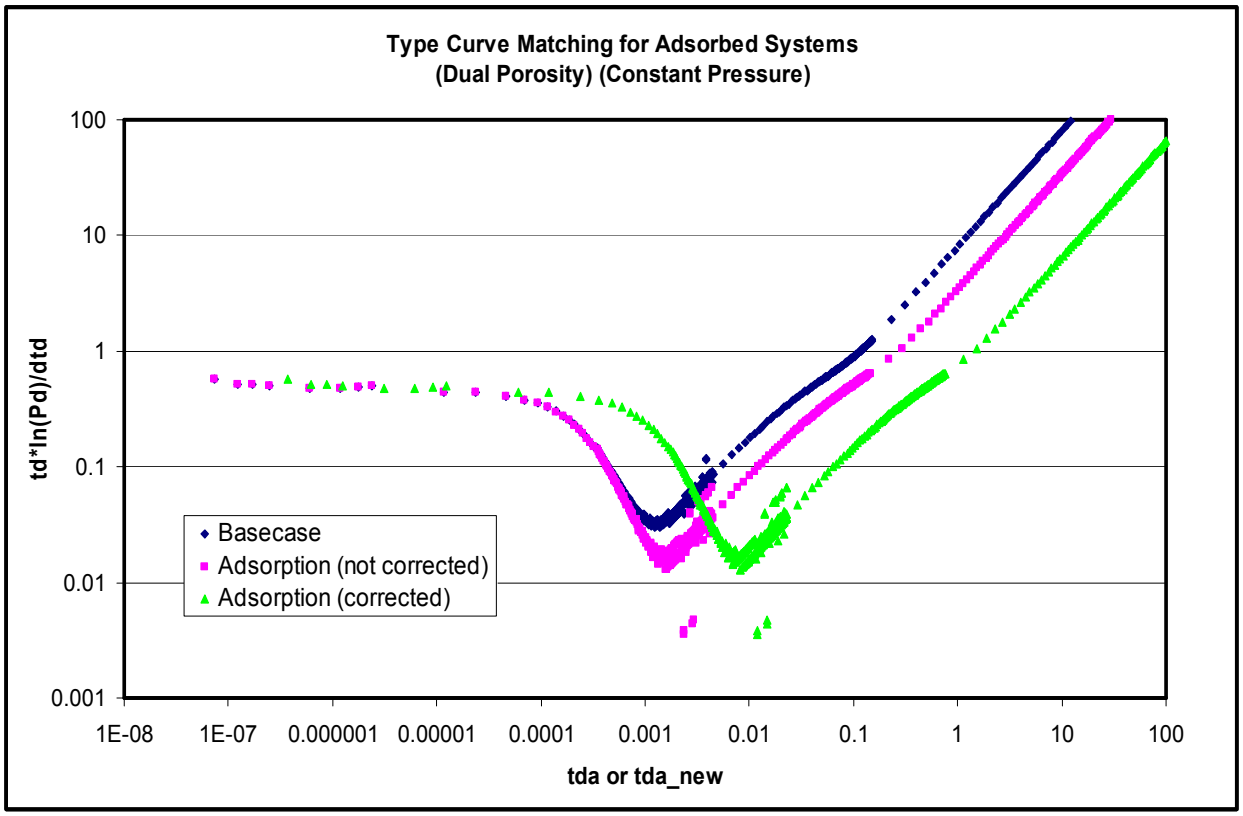

Figure 50 – Diagnostic plot for dual porosity systems with adsorption. The matching process for constant pressure systems is very different than for constant rate systems.

Think of the "Basecase" in Figure 50 as the analytical solution. It has no adsorption since most analytical models do not account for this. The pink series in is the result of calculating the dimensionless plotting functions without accounting for adsorption in any way (i.e. our initial gas in place is only free gas and there is no correction for compressibility). The green series is the result of including adsorption when calculating the plotting functions (i.e. the adsorbed gas is included in the gas in place ($G = G_{tot}$) and there is a correction for system compressibility).

The large increase in original gas in place (G_{tot}), which is due to the presence of adsorbed gas, causes a large increase in t_{danew}. This increase is not offset by a similar decrease in the third term $[\Delta m(p)/q]$ of the equation. All other parameters being the same, the result is that a system with adsorbed gas will not overlay a system without adsorbed gas. It is not possible to get a match with correct reservoir parameters.

Figure 51 shows the results of a method to achieve a match between a system with adsorbed gas and one without adsorbed gas. The "Basecase" represents the system without adsorbed gas. The data from the adsorption model is presented in three ways. The first is "uncorrected"; the conversion to material balance time does not include the adjusted system compressibility that accounts for adsorption. In addition, it assumes G is only free gas. Second, the "correct" dataset

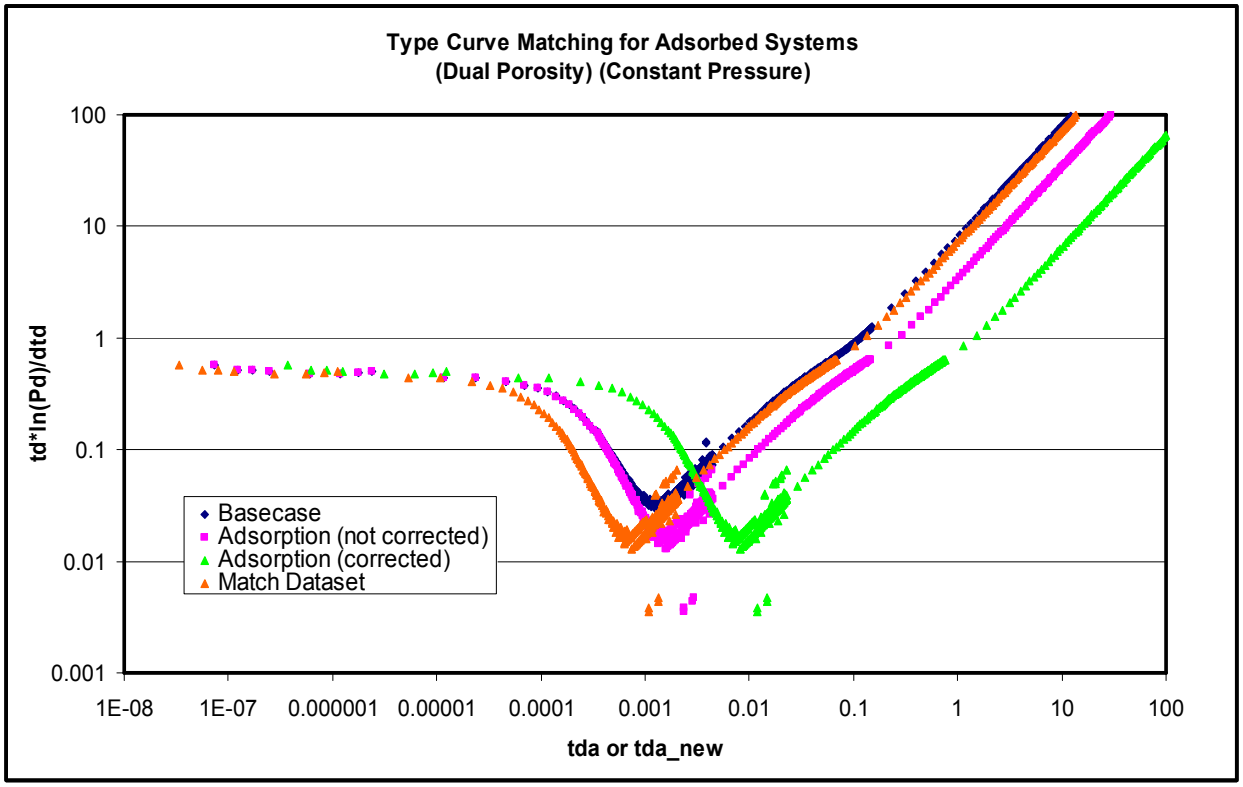

Figure 51 – Diagnostic plot for dual porosity systems produced at constant pressure shown here converted to an equivalent constant rate. The "Match Dataset" represents the system with the parameters necessary to overlay an analytical solution without adsorption.

uses the correction for adsorption and assumes $G = G_{tot}$. The match is achieved by using the adjusted system compressibility and taking G to be only the free gas, not the sum of free gas and adsorbed gas. This method will allow a match to correct reservoir parameters but to an "incorrect" gas in place. It should be noted that the match is only to the term $kG/(\phi A)$, assuming that p_i, q_g, and p_{wf} are accurately known. Therefore, one must be very sure of the other three parameters (p_i, q_g, and p_{wf}) in the above term to come away with the correct match. A summary of the match terms for the datasets in Figure 51 can be seen in Table 8.

Table 8 – Matching results for dual porosity systems with adsorption.

	Basecase	Adsorbed System (not corrected)**	Adsorbed System (corrected)	Match Dataset
$kG_i/(\phi A)$	0.2	0.2	2.24	0.2

Does not overlay the "Basecase" because the third term of t_{danew} does not include the adjusted system compressibility for an adsorbed system. Thus, it is too large. Therefore, any overlay of uncorrected production data to an analytical solution will result in an incorrect match term $kG/(\phi A)$.

Table 8 seems to indicate that the "Adsorbed System (not corrected)" attained a correct match since the match term $kG/(\phi A)$ is identical to the "Basecase" match term. However, it does not overlay the "Basecase" because the third term of t_{danew} does not include the adjusted system compressibility for an adsorbed system. Thus, it is too large. Therefore, any overlay of uncorrected production data to an analytical solution will result in an incorrect match term $kG/(\phi A)$. This highlights the importance of knowing p_i, q_g, and p_{wf} before embarking on this type of analysis.

Figure 52 and Figure 53 refers to hydraulically fractured systems with adsorbed gas that were produced at constant pressure. The same method that was applied to dual porosity systems will be applied to these systems. However, t_{da} is different for these systems, so the match will be to a different set of terms. The equation for t_{da} is

$$t_{dA} = 0.01002 \frac{z_i}{p_i} \frac{x_f}{w} \frac{Gk_m}{A\phi} \frac{[m_{ct}(p_i) - m_{ct}(\bar{p})]}{q_g} \qquad \text{Eq 126}$$

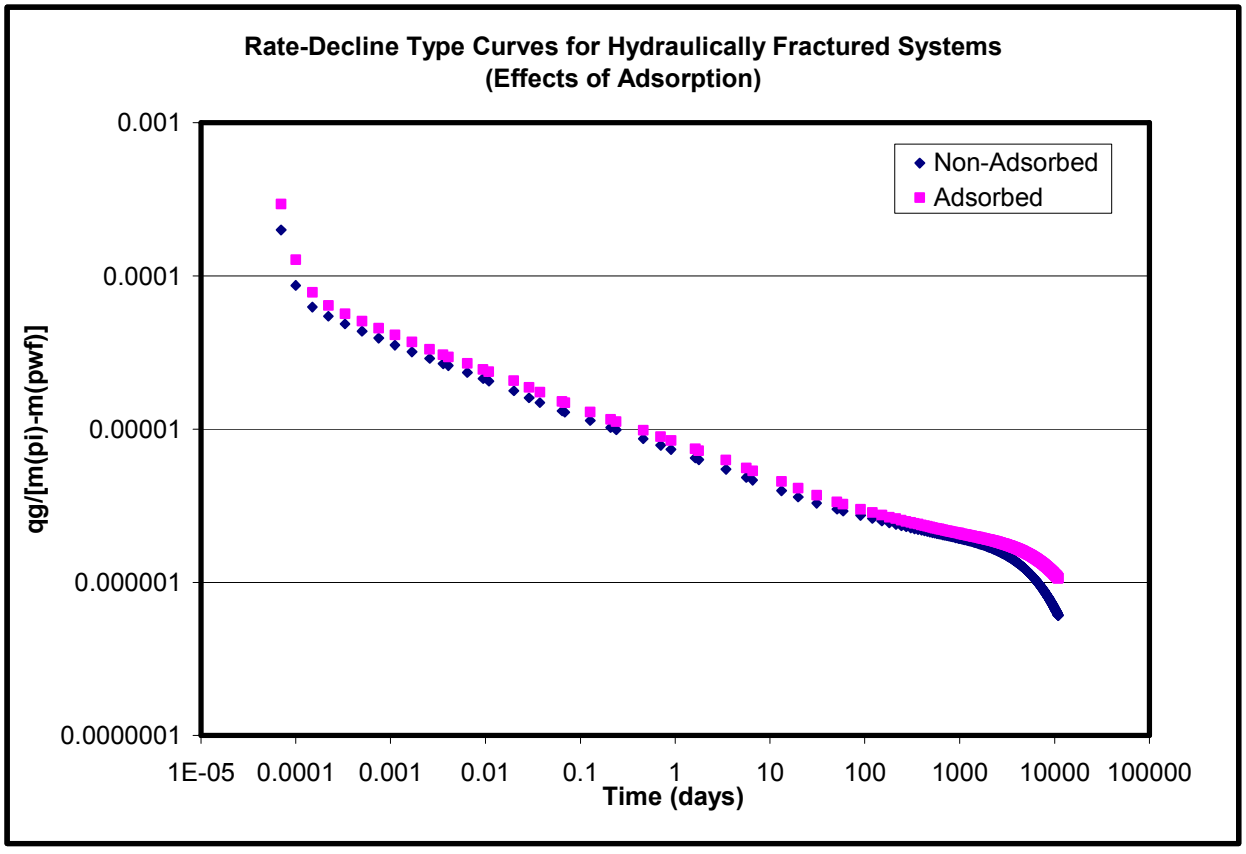

Figure 52 – Rate-decline type curve for a hydraulically fractured system with adsorbed gas produced at constant pressure. Note again that the effect of adsorption is predominately at late time.

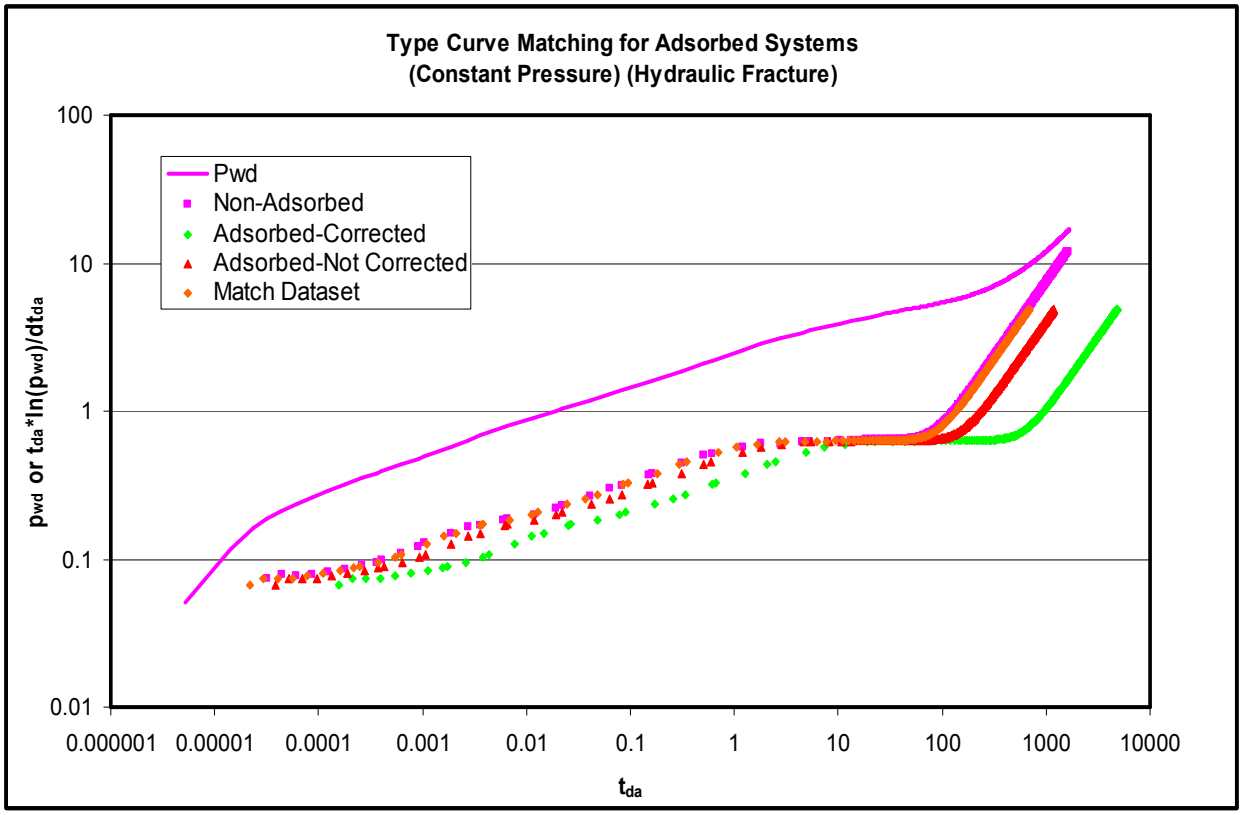

Figure 53 – Diagnostic plot for hydraulically fractured systems with adsorbed gas produced at constant pressure. Shown here converted to an equivalent constant rate system. Note that the "Adsorbed-Corrected" system does not overlay the "Non-Adsorbed" basecase system since it the plotting functions were calculated using total gas in place rather than just free gas in place.

Just like before, the uncorrected adsorbed system will not overly the non-adsorbed system if the correct reservoir properties are used. Recall that there is no difference between the adsorbed and non-adsorbed cases except for the presence of adsorption. When the correction for adsorption is applied, the derivative curve shifts sharply to the right due to the much larger original gas in place (caused by adsorbed gas). Assuming that, p_i, q_g, and p_{wf} are accurately known, the match term is $kGx_f/(\phi Aw)$. The "Match Dataset" is achieved by again taking G_i to be only the free gas in the adsorbed system instead of the sum of the adsorbed and free gas.

Finally, the effects of adsorption on dual porosity systems with hydraulic fractures will be documented. Figure 54 shows rate profiles that were generated from a model which was run at constant terminal pressure rather than constant rate. As has been shown for the systems examined previously, constant pressure systems must be handled differently than constant rate systems when production data analysis is performed. The model used to generate the following rate profiles is identical to that used before for this type of system except that it now contains adsorbed gas. The dimensionless time plotting functions used in Figure 55 is

$$t_{dA} = 0.01002 \frac{z_i}{p_i} \frac{x_f}{w} \frac{Gk_f}{A\phi} \frac{[m(p_i) - m(\bar{p})]}{q_g} \qquad \text{Eq 127}$$

Figure 54 and Figure 55 are type curves for a dual porosity system with hydraulic fractures produced at constant terminal pressure. They show the effects of adsorbed gas on these types of systems.

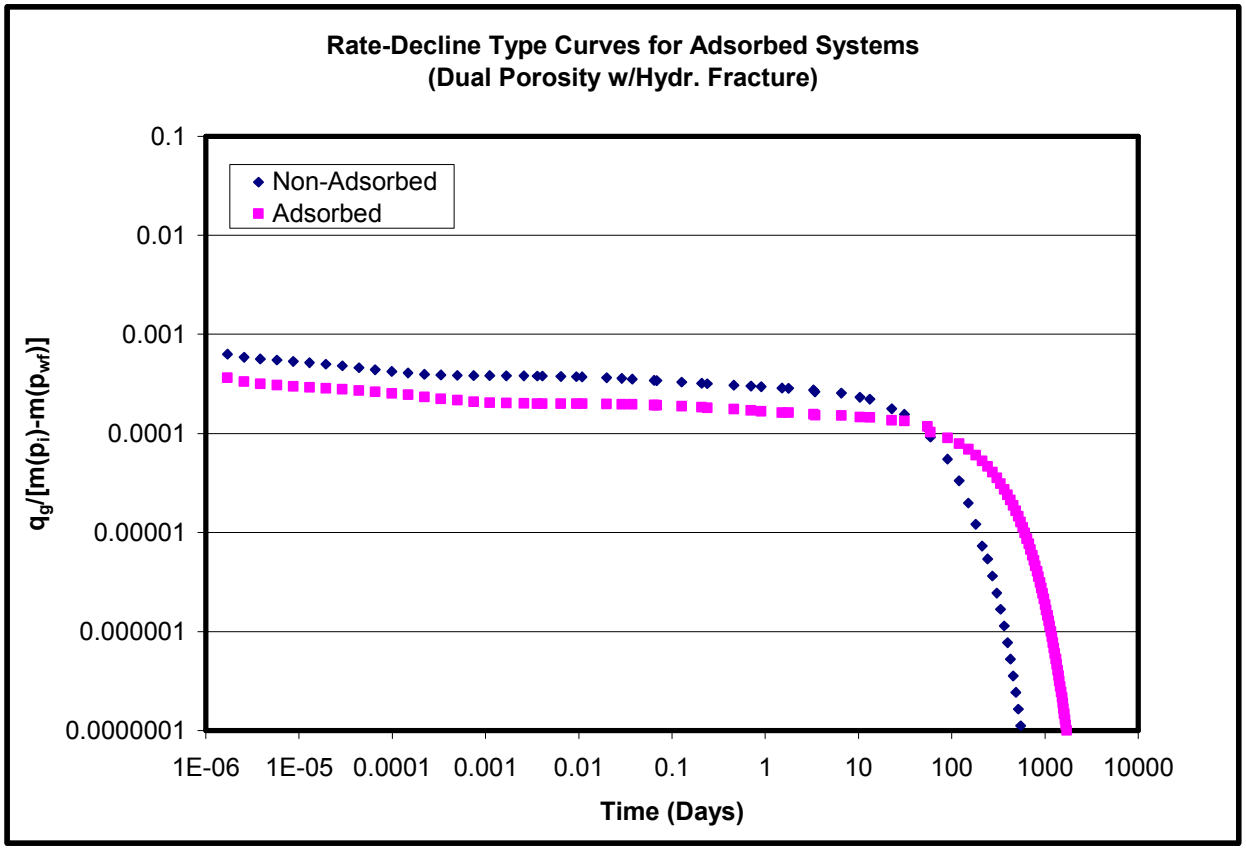

Figure 54 – Rate-decline type curve showing the effect of adsorbed gas on dual porosity systems with hydraulic fractures produced at constant pressure. There is a slight shift on this graph caused by adsorption at both late and early time. However, the scale on this plot is extremely small and this effect will probably not be visible on the diagnostic plot. The presence of the hydraulic fracture should mute nearly all early time effects of adsorption and the dual porosity matrix.

There is a slight shift on this graph caused by adsorption at both late and early time. However, the scale on this plot is extremely small and this effect will probably not be visible on the diagnostic plot. The presence of the hydraulic fracture should mute nearly all early time effects of adsorption and the dual porosity matrix.

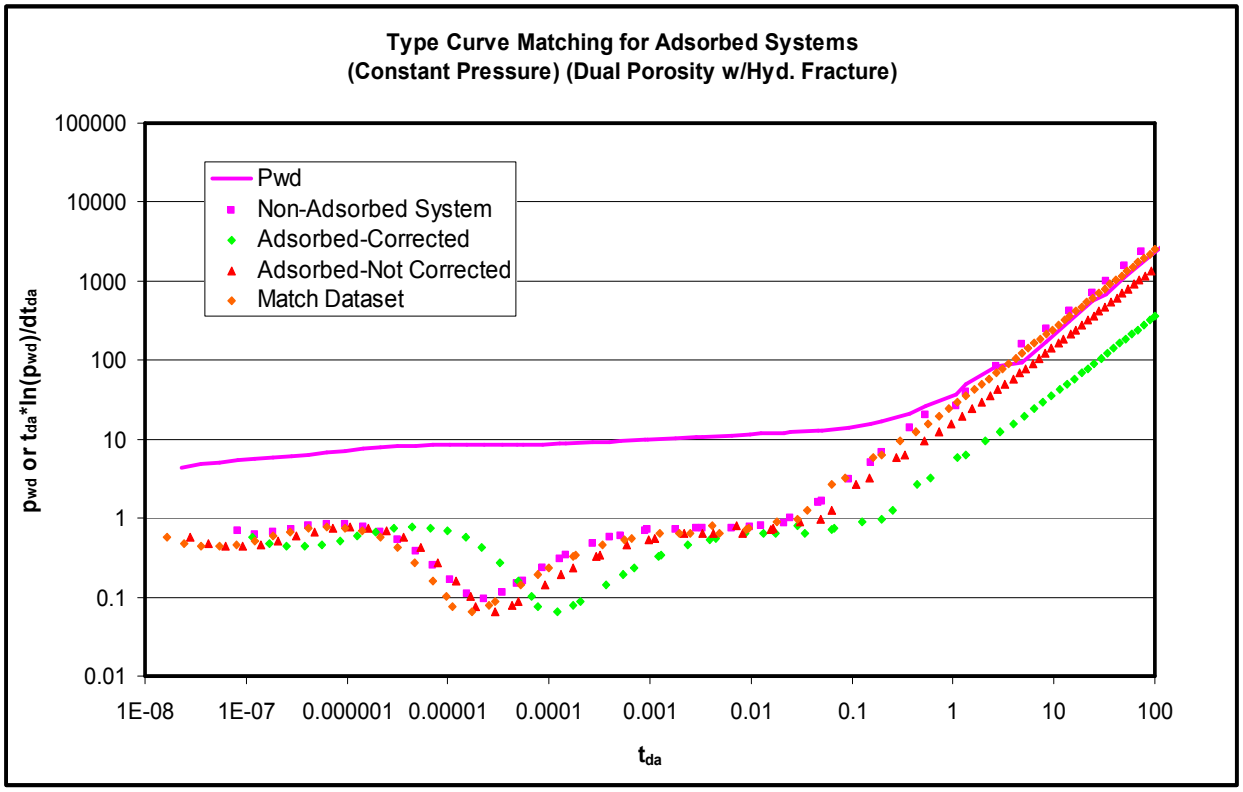

Figure 55 – Diagnostic plot showing the effects of adsorption on dual porosity systems with hydraulic fractures produced at constant pressure. Shown here converted to an equivalent constant rate system. Interestingly, the "Adsorbed-Not Corrected" system overlays the non-adsorbed system until late-time. Nearly all early time effects of the adsorbed gas have been muted.

Figure 55 shows the effects of adsorption on dual porosity systems produced at constant pressure. Interestingly, the "Adsorbed-Not Corrected" system overlays the non-adsorbed system until late-time. Nearly all early time effects of the adsorbed gas have been muted. As expected, the horizontal shift caused by adsorption in the "Adsorbed-Not Corrected" is very clear. Also as expected, there is a large horizontal shift in the "Adsorbed-Corrected" system since its plotting functions were calculated with G_{tot} (adsorbed plus free gas). The only dataset that overlays the entire "Non-Adsorbed" system is the match dataset. It uses free gas to calculate its plotting functions and corrects for adsorbed gas by including the adjusted total system compressibility described earlier. This "matching" procedure is identical to that used for all of the systems discussed previously in this work.

In summary, it has been shown that the analytical solutions present in literature are perfectly accurate in reproducing the results of simple and complicated numerical models. This means that it is completely justifiable to use these analytical models to perform production data analysis on real data. It was shown that simple and complicated constant rate and constant pressure systems are equivalent provided some relatively simple steps are taken. These are not new or surprising conclusions; they are merely steps along a path towards a goal. What is new is that the effects of adsorption on four common reservoir systems have been documented. Also, a

matching procedure has been outlined that allows a real production dataset from a reservoir that has adsorbed gas to be matched to an analytical model. This matching procedure required the modification of existing methodology to adapt to the complexities of adsorbed systems. Next, this procedure will be applied to actual field datasets to examine its viability, strengths, and shortcomings.

6. TRIAL CASES

The effects of adsorption have been documented on production data type curves. In addition, a new definition of material balance time has been proposed that prevents system compressibility from being eliminated in the dimensionless plotting function t_{danew}. Thus, the effects of adsorption can now be better accounted for when using dimensionless plotting functions for production data analysis.

6.1 Simulation Example Well

This next discussion will explain how the techniques described previously are applied in production data analysis. For this discussion, a simulated dataset will be used so that data reliability and accuracy do not cause problems (the model will be discussed later). The methodology for matching production data to an analytical, type curve solution will be discussed. However, an analyst rarely has a complete understanding of the reservoir in question when the analysis of the production data is performed. So, the same set of production data will be analyzed using different analytical models (single porosity, dual porosity, and dual porosity w/hydraulic fracture). The effect of these different analysis styles will be noted in the match parameters. The important question being whether or not any additional insight is gained from using a more complicated model.

In addition, the effects on match parameters of correcting system compressibility to account for adsorbed gas will be investigated. Is it really necessary to correct for adsorption when using the various analytical models? If so, what mistakes are made when adsorbed gas is not accounted for?

Shale gas systems were described in detail earlier. Presently, reservoir descriptions of common shale gas reservoirs are considered to be dual porosity reservoirs with adsorbed gas in the matrix portion only. In addition, shale gas wells are typically stimulated by hydraulic fracturing. Therefore, the simulation model used for this section is a representation of these features. Production comes from a single well located in the center of the model which can be seen in Figure 56. Local grid refinement was used to create the hydraulic fracture, and resulted in a fracture width of 4 inches. Aerial views of the grid that show the local grid refinement can be seen in Figure 23. The reservoir parameters can be found in Table 9 and the relative permeability curves can be found in Figure 57 and Figure 58.

Lastly, the rate profile generated by the simulation model is shown in Figure 59. The flowing bottomhole pressure was set at 914 psia to achieve starting rates close to 1 MMSCF/day. The model was run for 10 years with daily production data being recorded for the first 3 months followed by monthly data points for the remaining time. This same rate profile will be analyzed with the various types of analytical models mentioned before in Chapter 4 and Chapter 5.

6.1.1 Analysis as a Single Porosity System with Adsorbed Gas

The most common system used in production data analysis is a single porosity system because these reservoirs are very common and relatively simple to analyze. So, in this analysis, 3 different styles of type curves will be used. First, a plot of q_d vs. t_d will be analyzed to determine a match. Second, a Fetkovich plot will be used which plots q_{Dd} vs t_{Dd}. Lastly, a plot of p_{wd} vs.

Table 9 – Simulation Example Well Dataset

Height/Net Pay (ft)	40
Length (x & y) (ft)	5280
Well Radius, r_w (ft)	0.25
Porosity, ϕ_m	0.10
Porosity, ϕ_f	0.001 ($\omega = 0.01$)
x_f (ft)	480 ($C_{df} = 0.03$)
Permeability, k_m(md)	0.01
Permeability, k_f(md)	1.875 ($\lambda = 1x10^{-5}$)
Permeability, k_{fh}(md)	2500 ($C_{df} = 0.3$)
Initial Pressure, (psia)	1514
Water Saturation, S_w	0.05
Rock Dens., (g/cm^3)	2.45
p_L (psia)	635
v_L (scf/ton)	89
Temperature, (^{o}F)	225
Gas Gravity	0.6
Gas Composition	100% CH_4
Initial BHP (psia)	914

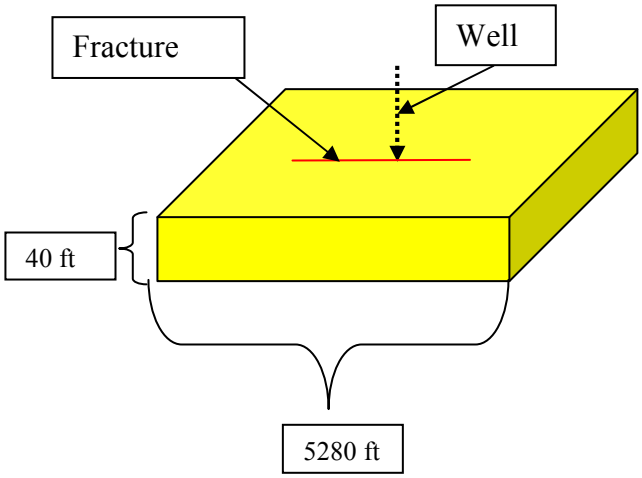

Figure 56 – Depiction of Simulation Example Well Model

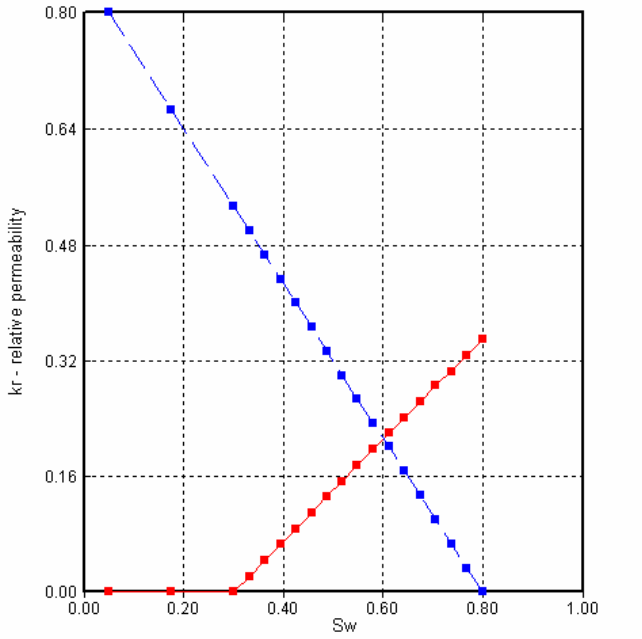

Figure 57 – Oil-Water Relative Permeability Curve for Simulation Example Well

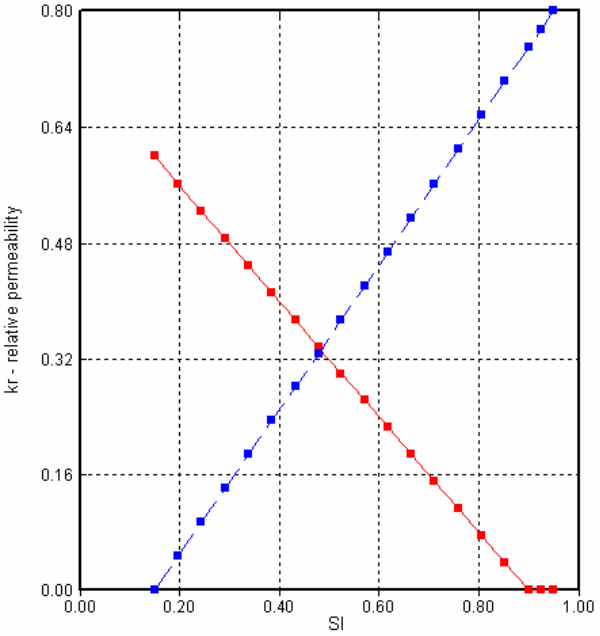

Figure 58 – Gas-Oil Relative Permeability Curve for Simulation Example Well

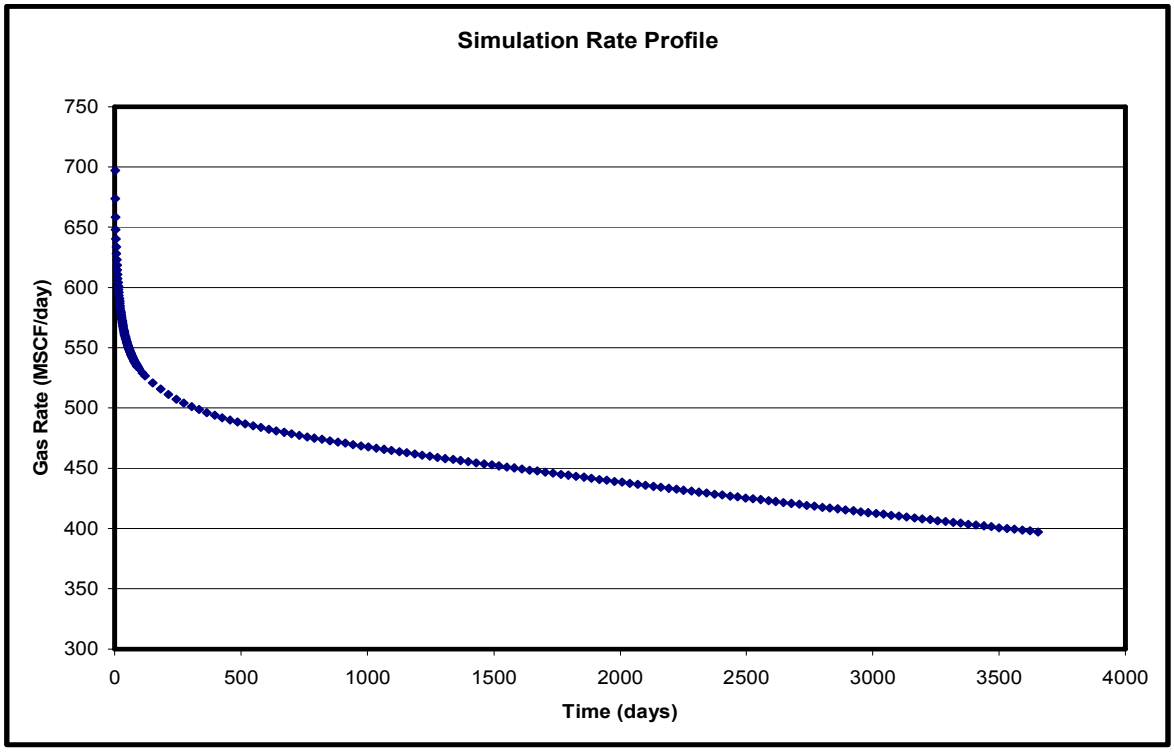

Figure 59 – Rate Profile for Simulation Example Well

t_{da_new} will show if there are any benefits to by using this approach. This is referred to as Gas Production Analysis (GPA) (Cox, et al. 2002). In addition, all of the analysis done in this section

will treat the models as if adsorbed gas is present and correct for it. The next section will detail the effects of analyzing the system without correcting for adsorbed gas.

It should be noted that the method to achieve the match with the various sets of type curves mentioned above is different than what is traditionally done. Traditionally, the production data and/or pressure functions are plotted against a real-time function on one graph and the analytical dimensionless solutions, or type curves, are plotted on another. These two graphs are overlayed to achieve a match. This overlay and the resulting match points are used to estimate the reservoir parameters of interest. Here, the match is achieved by changing reservoir parameters, chiefly permeability, porosity, and drainage radius, and then converting the rate or pressure data into dimensionless format to obtain a match. So, every time one of these parameters is changed the plotting functions are recalculated to reflect this new data. The new plotting functions are then plotted against the analytical dimensionless solution for the model of interest (for example, a single porosity analytical solution) to obtain a match. A similar recalculation procedure is also required for all methods that involve material balance time.

In this particular case, a dual porosity system with hydraulic fractures is being simplified since it is being viewed as a single porosity system. So, all the properties for both natural and man-made fractures influence the rates obtained from the flow simulation, but do not appear in the conversion of the data into dimensionless format. First, the outcome of the q_d vs. t_d will be examined. The values of all of the relevant parameters were changed until an appropriate match was obtained to a single porosity analytical solution type curve. The values in Table 10 are the values that were matched to the single porosity analytical solution.

Table 10 – q_d vs. t_d match results for single porosity system with adsorbed gas

s_g =	0.6		**INITIAL DATA**		
r_e =	2640	ft			
r_w =	0.25	ft			
A =	2.79E+07	ft^2			
h =	40	ft			
v_b =	1.12E+09	ft^3			
s_w =	0.05	fraction			
phi =	0.15	fraction			
t_{res} =	225	^oF			
p_i =	1514.70	psia			
p_L =	635	psia	ρ_m =	2.45	g/cm^3
v_L =	89	scf/ton	6.81	scf/ft^3	
z =	0.929				
b_{gi} =	0.012	rcf/scf	2.117	rbbl/mscf	
$OGIP_{free}$ =	13374898	MSCF			
$OGIP_{ads}$ =	4545700	MSCF			
Total =	17920598	MSCF	G/A =	0.48	
k_m (md) =	1.15	k_m (nd) =	1150000		

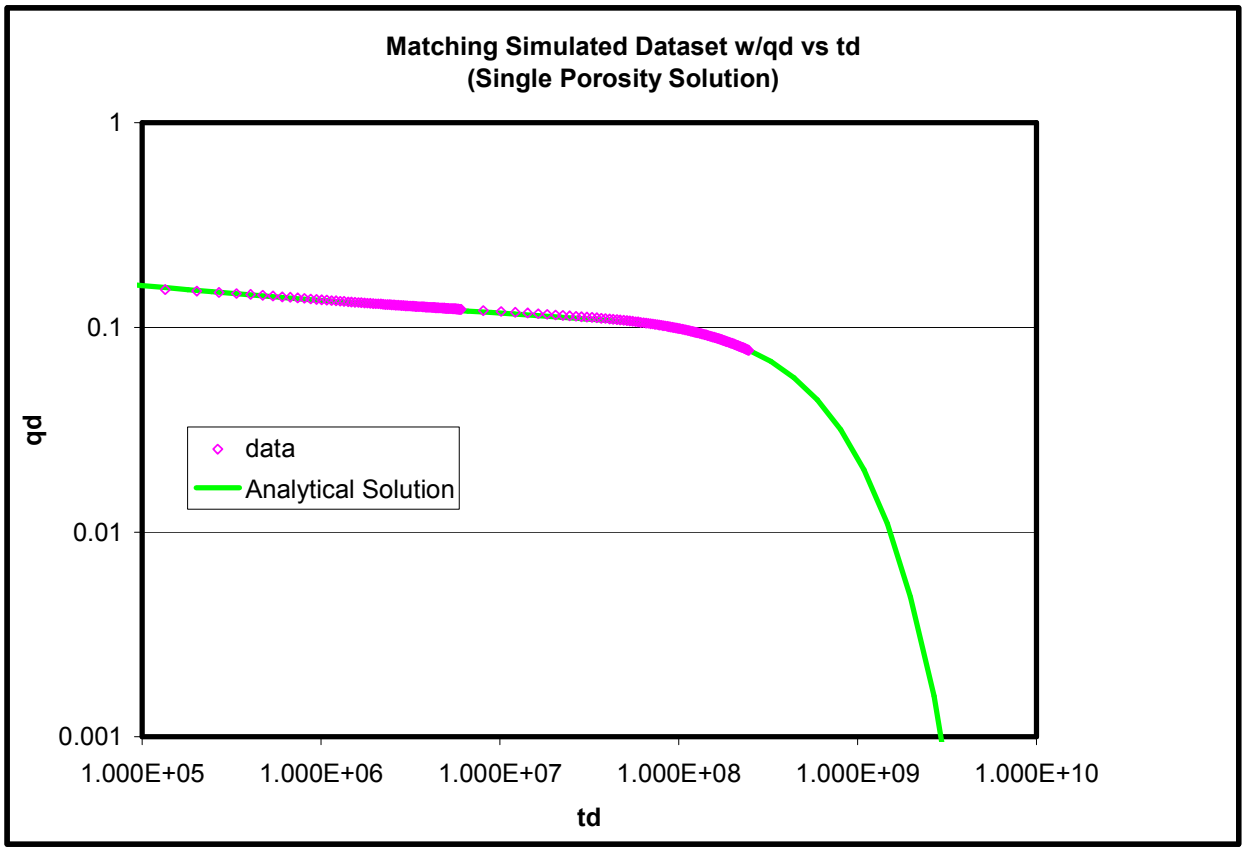

Figure 60 – match for q_d vs t_d method for single porosity system with adsorbed gas

Figure 60 shows the match to a single porosity analytical solution from the data table presented earlier. The important thing to note is that the data only makes it to the very edge of the decline-curve portion of the graph (the stem). Recall that this is 10 years of production data. Because the data never really progresses down the decline-curve stem, there is a high level of uncertainty in the match. Changes in the parameters for t_d that would move the data towards the lower values of t_d would also show a reasonable match.

Figure 61 shows the match obtained with single porosity Fetkovich type curves. The same matching procedure that was described earlier was applied here as well. Note that the match data are identical to that that was obtained from the q_d vs. t_d method as is the quality of the match. Table 11 shows a summary of the parameters used in the matching the data to the analytical model.

Again, note that for 10 years of production the data does not make it to the decline-curve stems. This results in a critical lack of a definitive *b* value for this system, and makes forecasting cumulative production/recovery difficult with this method. The transient portion of the match would also be in question if the system parameters from the simulation model were not known and used as a starting point. Given the input data as a starting point, an approximate *b* value of 0.5 can be estimated from this match.

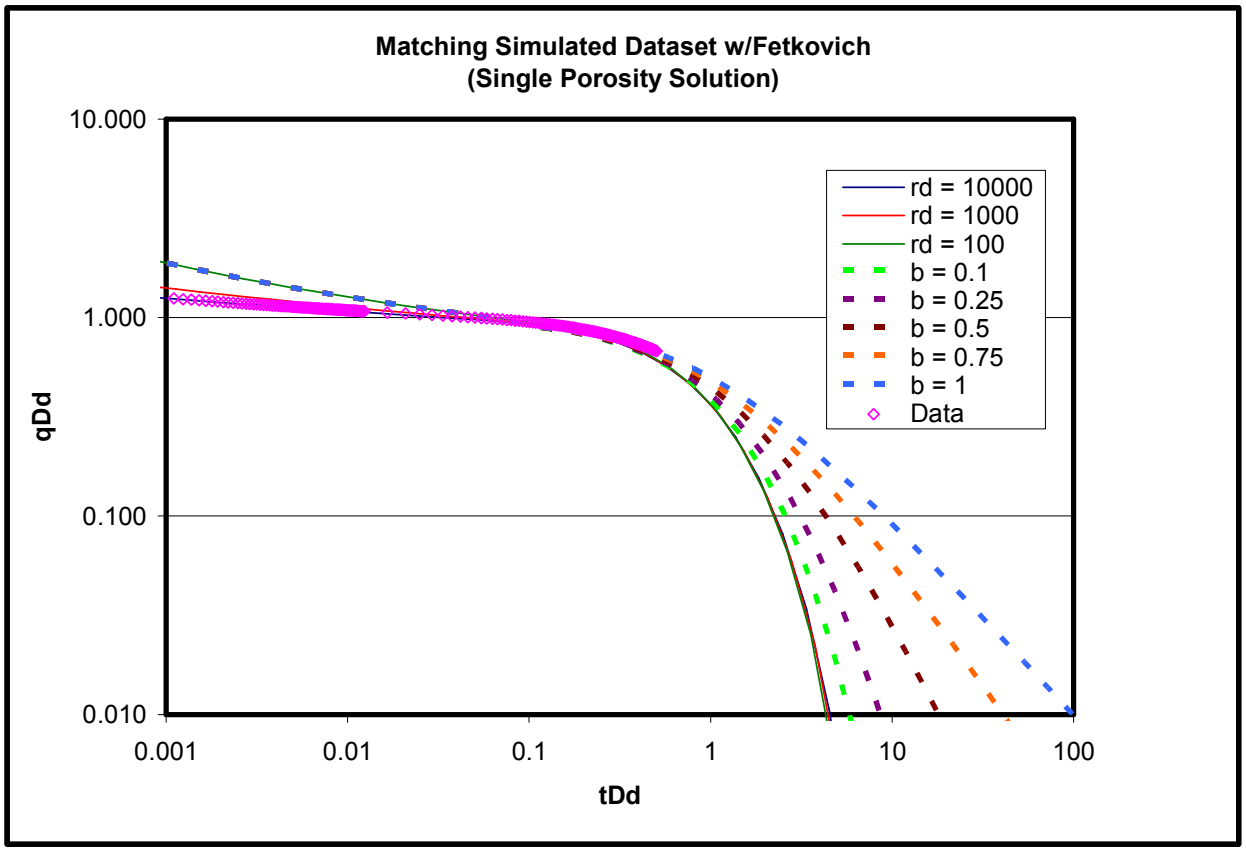

Figure 61 – match for Fetkovich method for single porosity system with adsorbed gas

Table 11 shows a summary of the match data for the GPA method. There are some differences between this match data and that obtained from the previous two methods. Chiefly, the drainage radius and porosity obtained from this match are correct when they are compared to the simulator input data. There is also a very slight difference in the permeability obtained from the previous two methods when compared to this method, but that can be considered negligible.

Figure 62 shows the match achieved using the GPA method with a single porosity analytical solution. Boundary-dominated flow is clearly reached which makes the match much more reliable and useful.

There are some common observations that apply to all of these plots. Since this system was assumed to be a single porosity system when it is actually a dual porosity system with hydraulic fractures, the very early time behavior will not overlay the type curves. However, it was shown previously that the only parameter obtained from very early time behavior is ω. It was also shown that the bottomhole pressure drop over which this parameter is obtained is very small (<10 psi) for the dual porosity systems of interest. In reality, bottomhole pressures are usually obtained from multiphase flow correlations using tubing head pressure and fluid composition. Since the accuracy of real production data, especially tubing head pressures, is rarely less than 10 psi, it is doubtful that ω could ever be obtained with any certainty for this particular system.

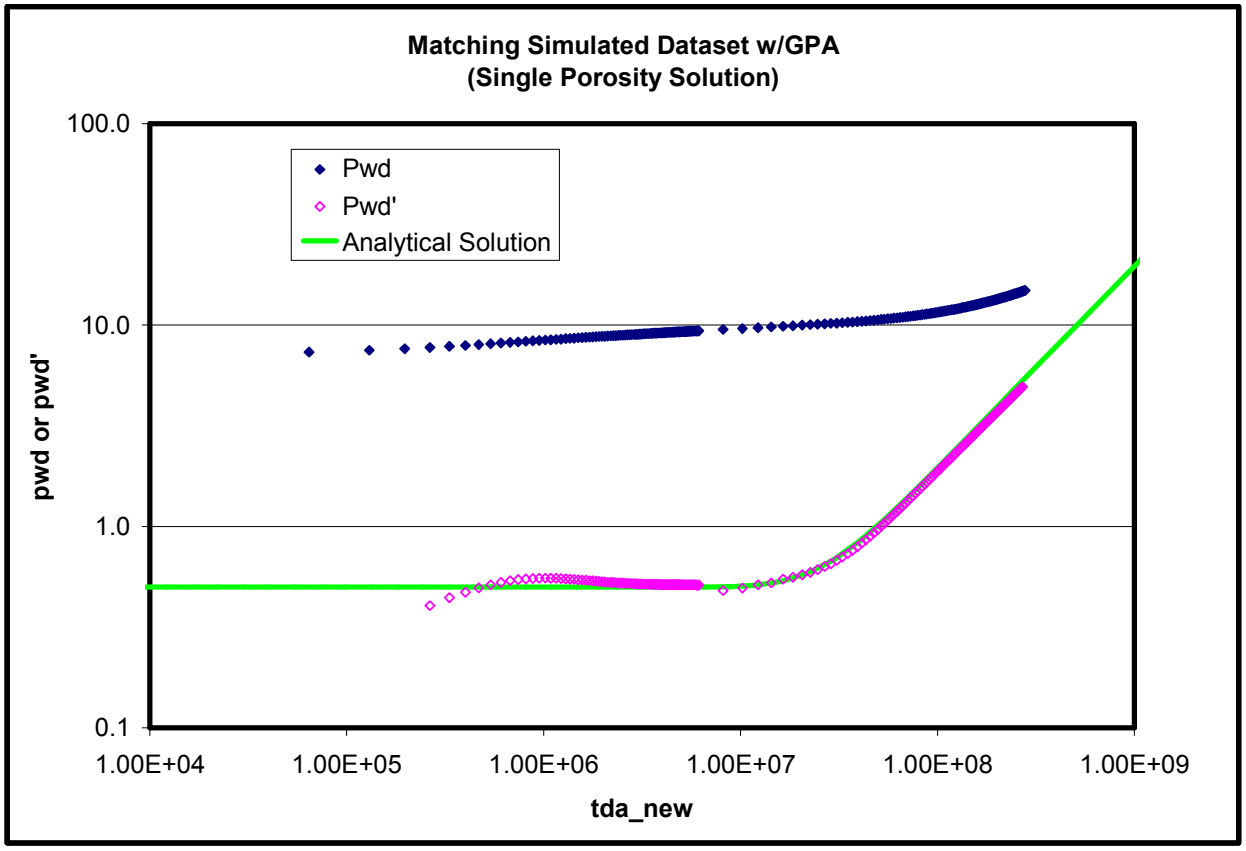

Figure 62 – match for GPA for single porosity system with adsorbed gas

Another observation common to the different analyses is that the permeability obtained is neither matrix permeability nor fracture permeability. This is to be expected since this system is incorrectly assumed to behave as a single porosity system.

Table 11 is a summary of the matching results achieved by the various styles of type curves that were used.

Table 11 – Summary of matching results for single porosity system with adsorbed gas

	Drainage radius, re (ft)	Porosity (ϕ_m)	Eff. Sysetm Permeability, k (md)	G/A*	Match Term ($kG/\phi A$)
q_d vs t_d	3000	0.15	1.2	0.48	n/a
Fetkovich	3000	0.15	1.2	0.48	n/a
GPA (p_{wd} vs t_{da_new})	2640	0.15	1.15	0.48	3.68
Actual (from model)	2640	0.1	1.8 (k_f), 0.01 (k_m)	0.32	5.76**

Using free gas only. G/A with adsorbed gas is 0.49 for the model and 0.64 for the matches
** based on k_f **

Considering that this system was assumed to be a single porosity system, these results are quite good. As was mentioned before, the variation in permeability is to be expected. In addition, the different drainage radius and porosity values obtained from the first two methods can most likely be explained by the data not reaching the decline portion of the type curves. This is where the match becomes more unique and transient effects no longer dominate the data.

Another important thing to note about the above table is the G/A values reflect the non-adsorbed gas only. It was shown earlier that it is necessary to match to only the free gas when dealing with adsorbed systems. The original adsorbed gas in-place can be obtained from the adsorption parameters used to calculate the compressibility that was used in the match.

6.1.2 Analysis as a Single Porosity System without Adsorbed Gas

Here, the simulated production data will be analyzed as if there is no adsorbed gas present. More correctly stated, it will be analyzed as if the analyst does not know that the adsorbed gas is present. Therefore, no correction to the total system compressibility will be used to account for the adsorbed gas; everything else will remain the same including the assumption that this is a single porosity system. Again, the same three styles of type curves will be used in this set of analysis.

First, the match using q_d vs. t_d can be seen in Figure 63. As before, the data does not yet reach the decline-curve stem of the type curve. Therefore, there is a high degree of uncertainty in the match.

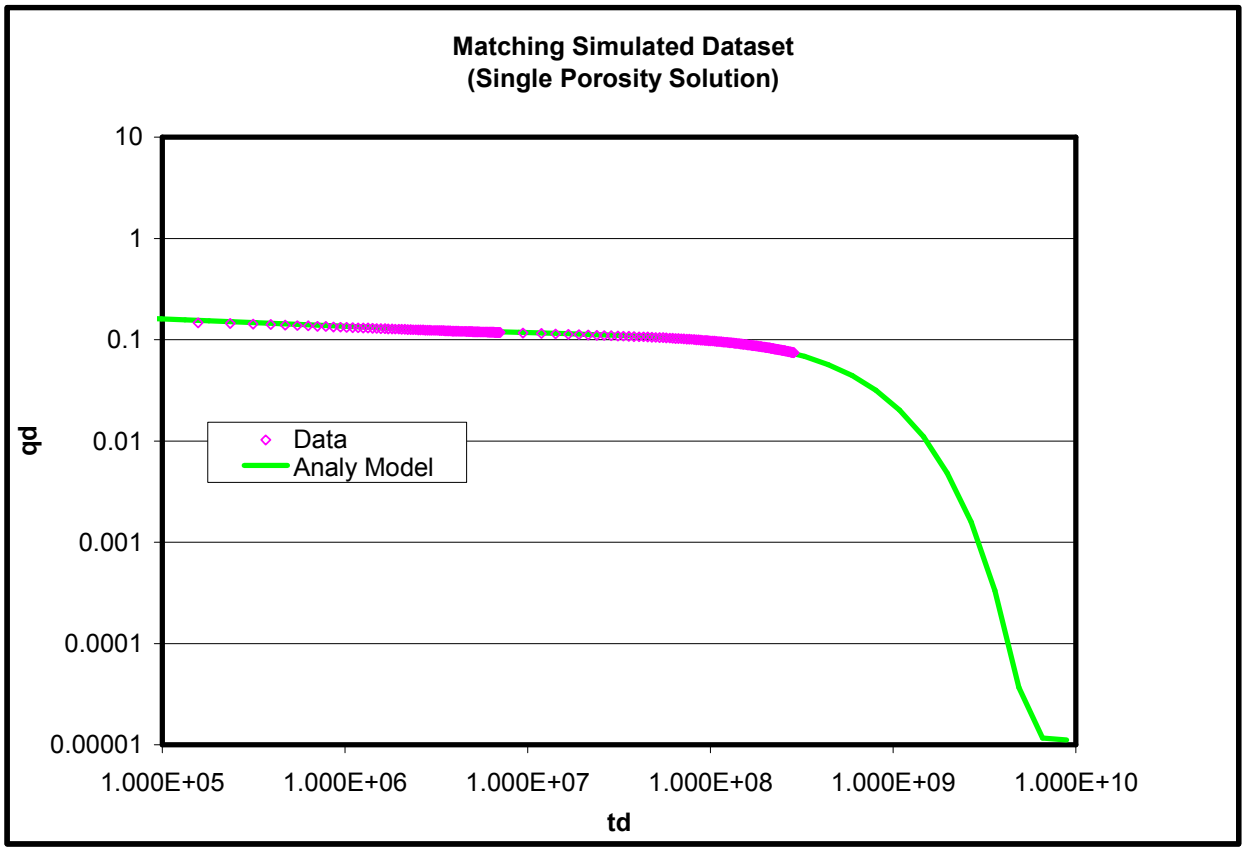

Figure 63 – match results for q_d vs. t_d single porosity system without adsorbed gas

The visual quality of the match is the same as it was when adsorption was considered in the matching process, and the drainage radius that was obtained from this match is also the same as what was obtained previously when system compressibility was corrected for adsorption. A summary of the results from this match can be seen in Table 12.

Second, the results from the Fetkovich style type curve analysis can be seen in Figure 64. Again, the data does not yet reach the decline-curve portion of the type curve. Therefore, there is a high degree of uncertainty, and no b value can be obtained yet.

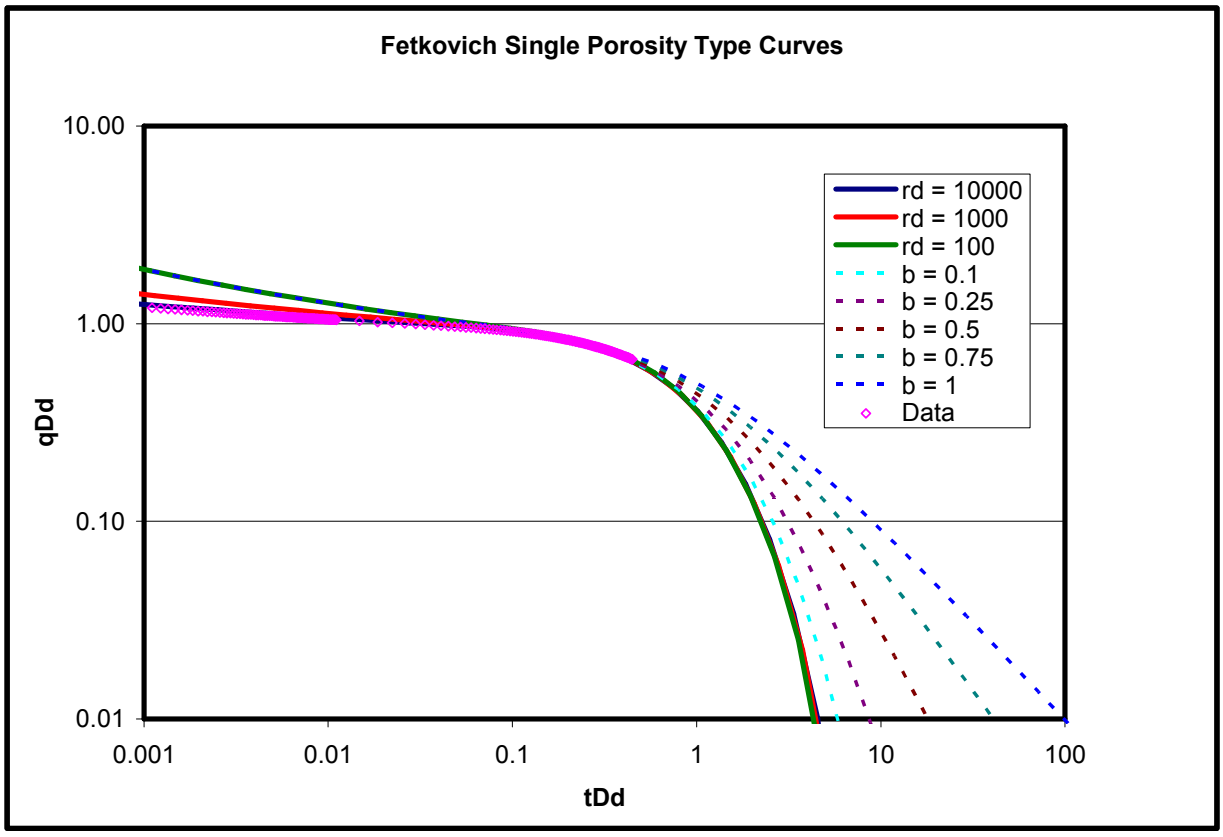

Figure 64 – match for Fetkovich method for single porosity systems without adsorbed gas

As with the q_d vs. t_d type curve, the drainage radius obtained from this match is the same as what was obtained when adsorption was accounted for, and the quality of the match is also the same as before. A summary of the results from this match can be seen in Table 12.

Lastly, GPA was used to analyze the data, and the results can be seen in Figure 65. The data still reaches the boundary-dominated portion of the type curve. As expected, not accounting for adsorption has no effect on whether or not the data reaches this flow regime.

The match quality is the same as it was when adsorption was accounted for. The drainage radius obtained is the same as it was when adsorption was not accounted for. A summary of the results from this match can be seen in Table 12.

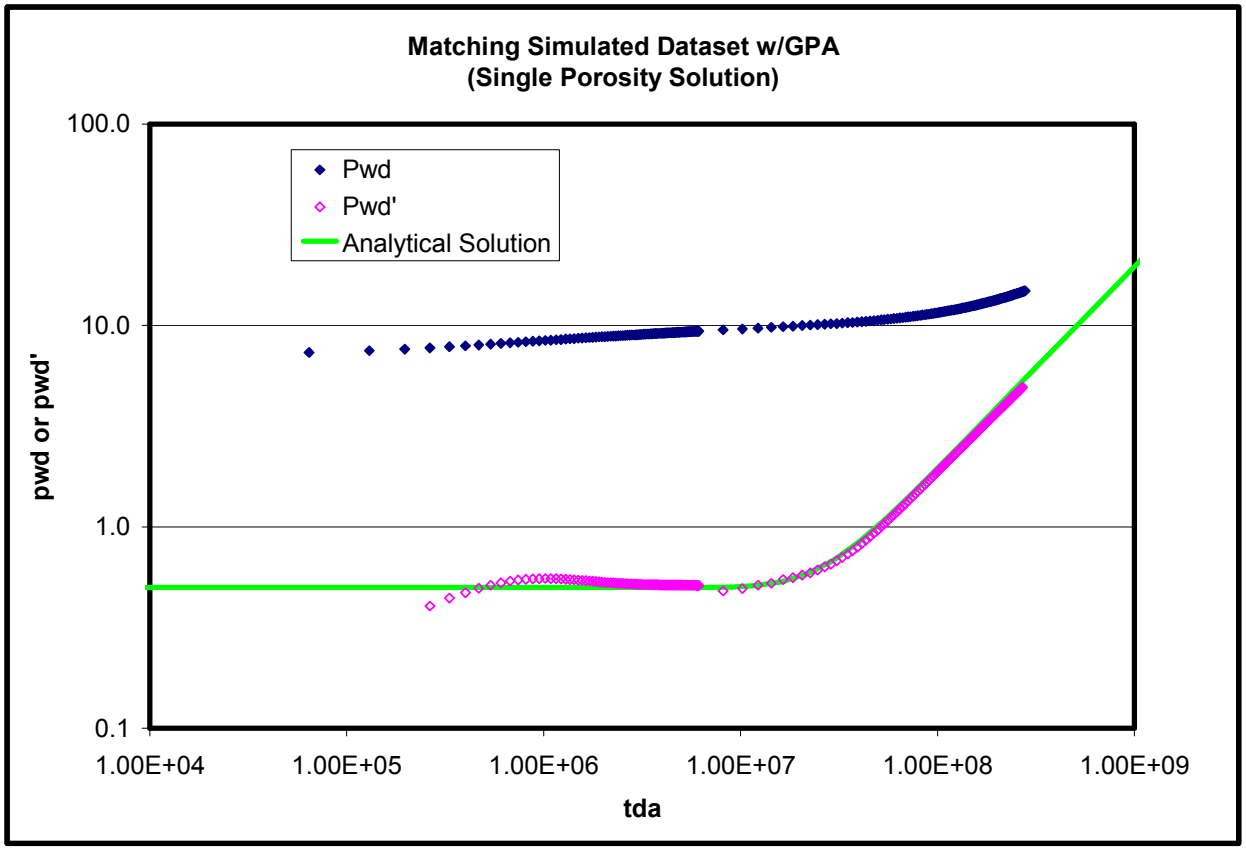

Figure 65 – match for GPA method for single porosity system without adsorbed gas

Table 12 – Summary of matching results for single porosity systems without adsorbed gas

	Drainage radius, re (ft)	Porosity (ϕ_m)	Eff. Sysetm Permeability, k (md)	G/A*	Match Term ($kG/\phi A$) *
q_d vs t_d	3000	0.15	1.19	0.48	n/a
Fetkovich	3000	0.15	1.19	0.48	n/a
GPA no adsorp.	2640	0.15	1.15	0.48	3.68
GPA w/adsorp.	2640	0.15	1.15	0.48	3.68
Actual (from model)	2640	0.1	1.8 (k_f), 0.01 (k_m)	0.32	5.76**

*Using free gas only. G/A with adsorbed gas is 0.49 for the model and 0.64 for the matches. But it is not possible to obtain this from this analysis since the correction for compressibility was not used. Therefore, p_L and v_L cannot be verified *
Using fracture permeability

Table 12 can be used to compare the results of using the correction for adsorption and not using it. The theoretical benefit of using the correction for compressibility to account for adsorption is it allows the analyst to determine the adsorption properties and thus the volume of adsorbed gas. However, it was shown that the shift caused by adsorption when adsorption properties for the Barnett Shale are used is not detectable. This is due to the placement of v_L and p_L in the equation for total system compressibility which can be seen in Eq 102. The effects of adsorption on

system compressibility is smallest when v_L is small and p_L is small when compared to reservoir pressure. Therefore, it is not possible to accurately obtain adsorption properties in this scenario. However, for a larger value of v_L (as was shown in Chapter 5), adsorption can effect the analysis. Since not correcting for adsorption has no impact on the outcome of the analysis, the correction for system compressibility does not need to be applied in this specific scenario. However, it serves as a valuable diagnostic tool to determine when adsorption becomes significant. It is advisable to always compare analysis using the correction to not using it for systems that have or may have adsorbed gas.

An important point to address is how does adsorption affect the method in which the analysis is performed and the outcome of the analysis. First, recall that every analysis using GPA is done using free gas as the value used in the material balance time calculation because none of the analytical models in this work are capable of accounting for adsorbed gas. There are two ways to do an analysis on a system with adsorbed gas. The analyst can disregard it and know that either the drainage radius or the system porosity obtained from the analysis may be too large. This will only be the case if the system has a large v_L and a small p_L. Adsorption can also be dealt with by using the correction for total system compressibility put forth by Bumb and McKee (1988). In doing so, the outcome of the analysis will be correct for any value of the adsorption parameters (provided they are accurate values).

However, it should be noted that both G/A and $kG/\phi A$ were both calculated using free gas only. The G/A for the analysis and the model would be much larger if the total gas was used. However, it is not possible to obtain the total G/A from this type of analysis without using the correction for system compressibility to account for adsorption. This is a result of p_L and v_L not being present in the dimensionless plotting functions. Therefore, they cannot be matched directly or indirectly. In addition, if pressure, porosity, and water saturation are the same, two reservoirs should have the same match G/A regardless of drainage radius.

6.1.3 Analysis as a Dual Porosity System with Adsorbed Gas

Here, the simulated data will be analyzed as a dual porosity system with adsorbed gas. The adsorbed gas will be accounted for using the new material balance time method with the correction for compressibility put forth by Bumb and McKee (1988). The same three styles of type curves will be used in this analysis.

First, the match using q_d vs. t_d can be seen in Figure 66. As before, the data does not yet reach the decline-curve stem of the type curve. Therefore, there is a high degree of uncertainty in the match.

The visual quality of the match is the same as it was when a single porosity model was used. Because the data never really progresses down the decline-curve stem, there is a high level of uncertainty in the match. Changes in the parameters for t_d that would move the data towards lower values of t_d would also show a reasonable match. A summary of the results from this match can be seen in Table 13.

Second, the results from the Fetkovich style type curve analysis can be seen in Figure 67. Again, the data does not yet reach the decline-curve portion of the type curve. Therefore, there is a high degree of uncertainty, and no b value can be obtained yet.

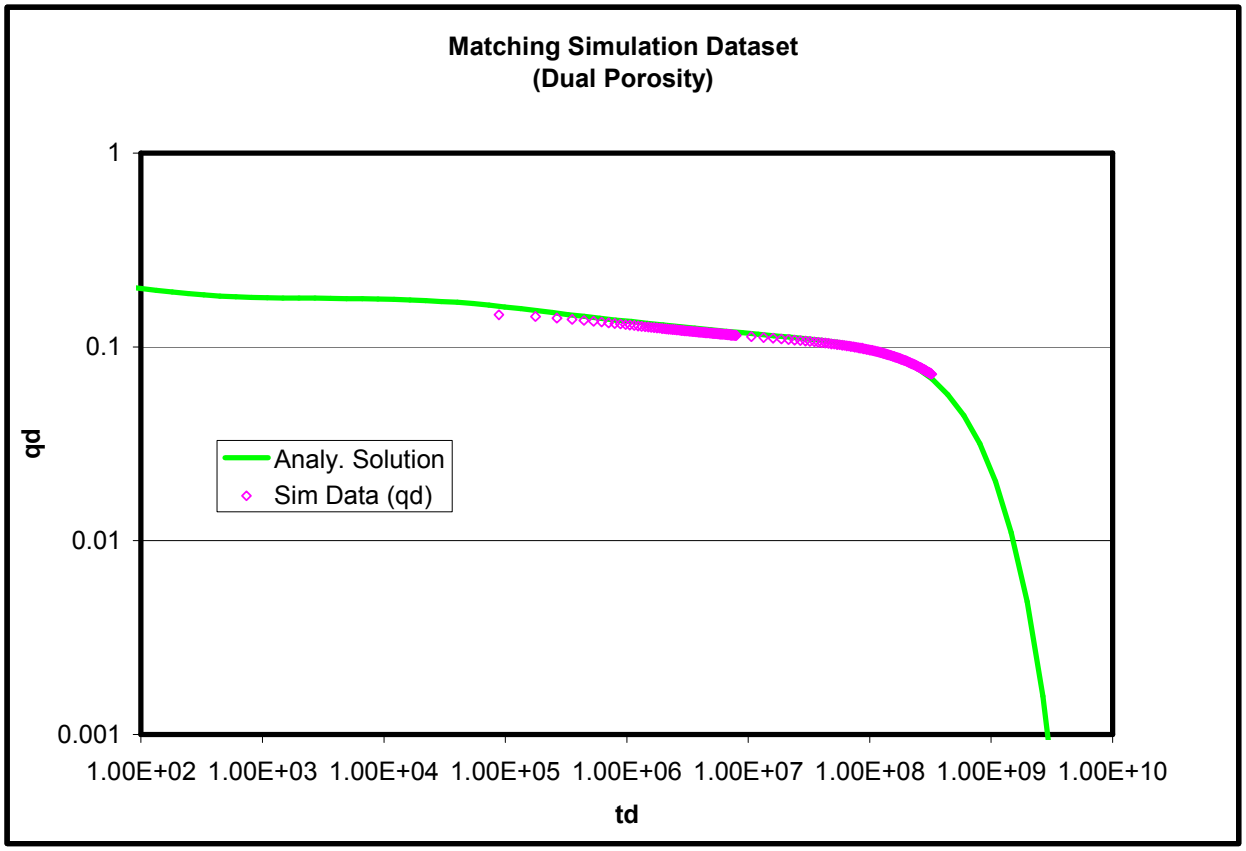

Figure 66 – match q_d vs. t_d method for dual porosity systems with adsorbed gas.

The visual quality of the match presented in Figure 67 is good. The data just begins to start down the depletion stems. While it is not possible to give a definitive b value, an approximate value of 0.25 is indicated. The results from this match can be seen in Table 13.

Lastly, GPA was used to analyze the data, and the results can be seen in Figure 68. The data still reaches the boundary-dominated portion of the type curve. The match resulting from using a dual porosity model offers the same visual quality as that of a single porosity model. There is some indication of what the value of ω might be with the dual porosity model. But, the data does not go back far enough in time to allow for an accurate determination of ω. The results from this match can be seen in Table 13.

Table 11 and Table 13 are a good comparison of what benefits can be obtained from using a more complex analysis. Table 13 presents a summary of the results obtained from "matching" the simulated dataset to a dual porosity analytical model. The only substantial difference between Table 11 and Table 13 is the presence of both matrix and fracture permeability. However, even the dual porosity model does not capture the true fracture permeability. It should

be noted that the dual porosity analytical model was developed using an effective total system permeability. Therefore, any match to the analytical models is obtained using effective system permeability. Otherwise, this dual porosity model gives almost identical G/A and match term values as the single porosity case did.

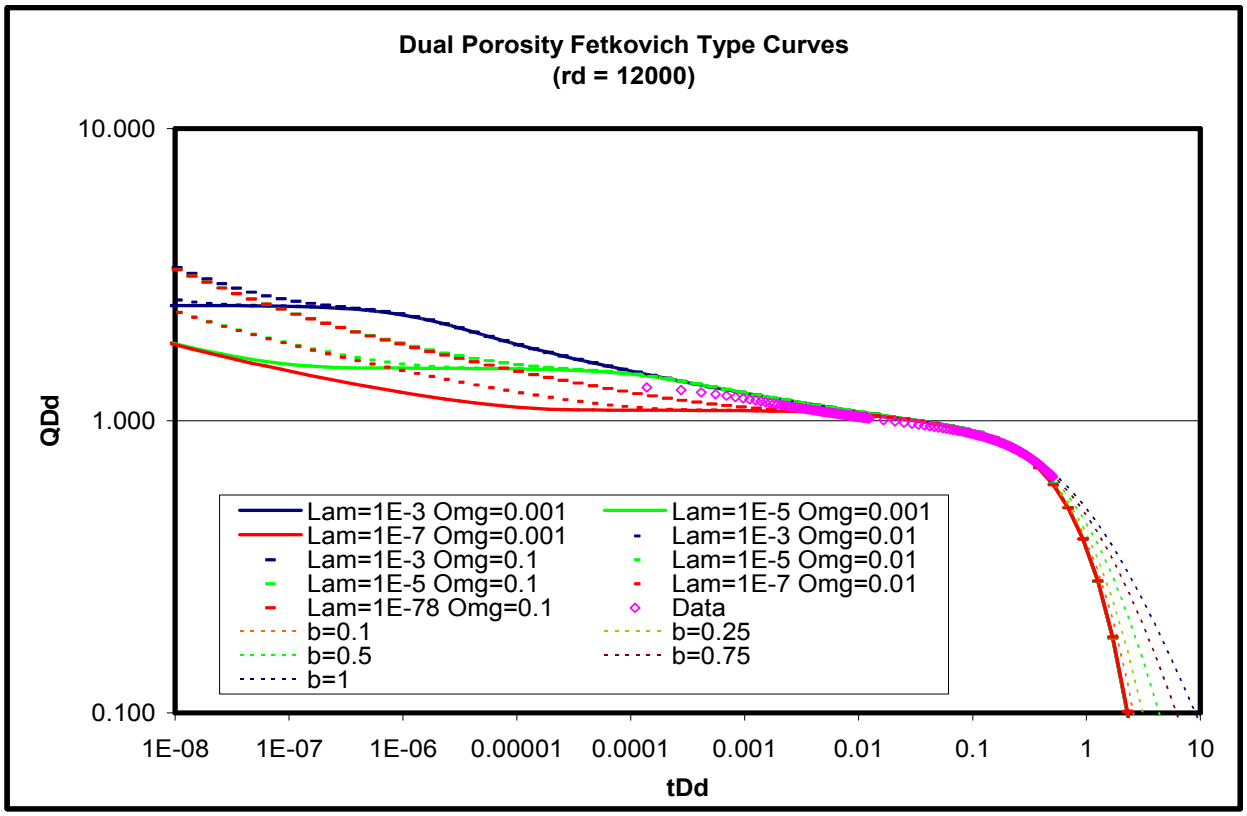

Figure 67 – match for Fetkovich method for dual porosity systems with adsorbed gas.

Table 13 – Summary of matching results for dual porosity systems with adsorbed gas.

	Drainage radius, r_e (ft)	ω	λ	G/A*	Match Term $(kG/\phi A)$ *
q_d vs t_d	3000	0.01	1×10^{-5}	0.32	n/a
Fetkovich	3000	0.01	1×10^{-5}	0.32	n/a
GPA (p_{wd} vs t_{da_new})	2640	0.008	1.75×10^{-5}	0.32	3.52
Actual (from model)	2640	0.01	1×10^{-5}	0.32	5.76**

Using free gas only. G/A with adsorbed gas is much larger
Using fracture permeability

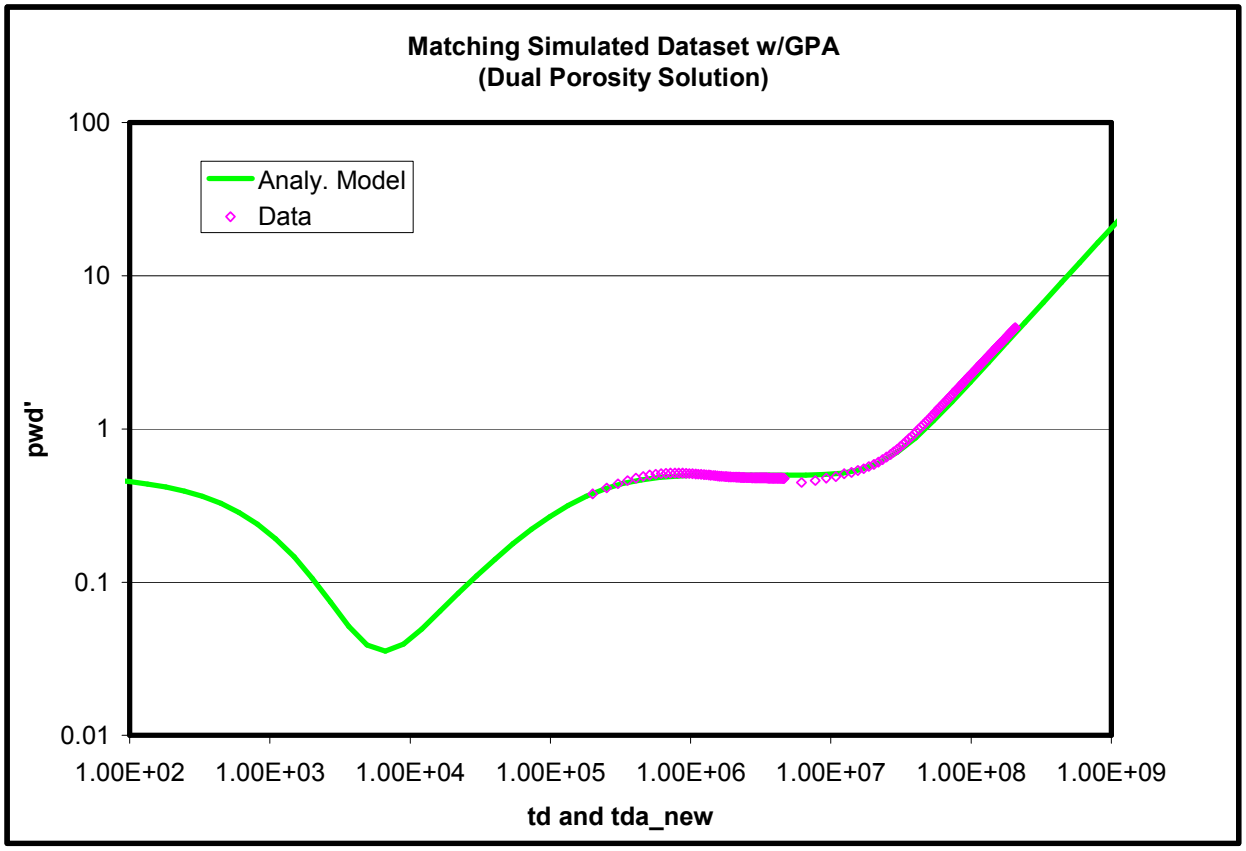

Figure 68 – match for GPA method for dual porosity system with adsorbed gas.

6.1.4 Analysis as a Hydraulically Fractured System with Adsorbed Gas

Here, the simulated data will be analyzed as a hydraulically fractured system with adsorbed gas. The adsorbed gas will be accounted for using the new material balance time method with the correction for compressibility put forth by Bumb and McKee (1988). Only two analysis styles were examined for this type of system. GPA and q_d vs. t_d were used, but Fetkovich analysis was not. The analytical model used for a hydraulically fracture system is not a complete solution. It has a boundary-dominated (i.e. late-time) model coupled to an early-time hydraulic fracture model. Based on the results thus far, Fetkovich style analysis does not yield much additional information because the simulated data does not fall onto the decline portion of the type curves.

First, the match using q_d vs. t_d can be seen in Figure 69. The dashed line is the analytic model for early-time fracture flow. The solid line is the analytic model for pseudoradial and boundary dominated flow. As before, the data does not yet reach the decline-curve stem of the type curve. Therefore, there is a high degree of uncertainty in the match. It should also be noted that that this data displays no evidence of the early-time hydraulic fracture behavior. Said another way, this data does not exhibit anywhere near the correct value for C_{df} as is indicated by its failure to follow the early-time hydraulic fracture curve in Figure 69. The results from this match can be seen in Table 14.

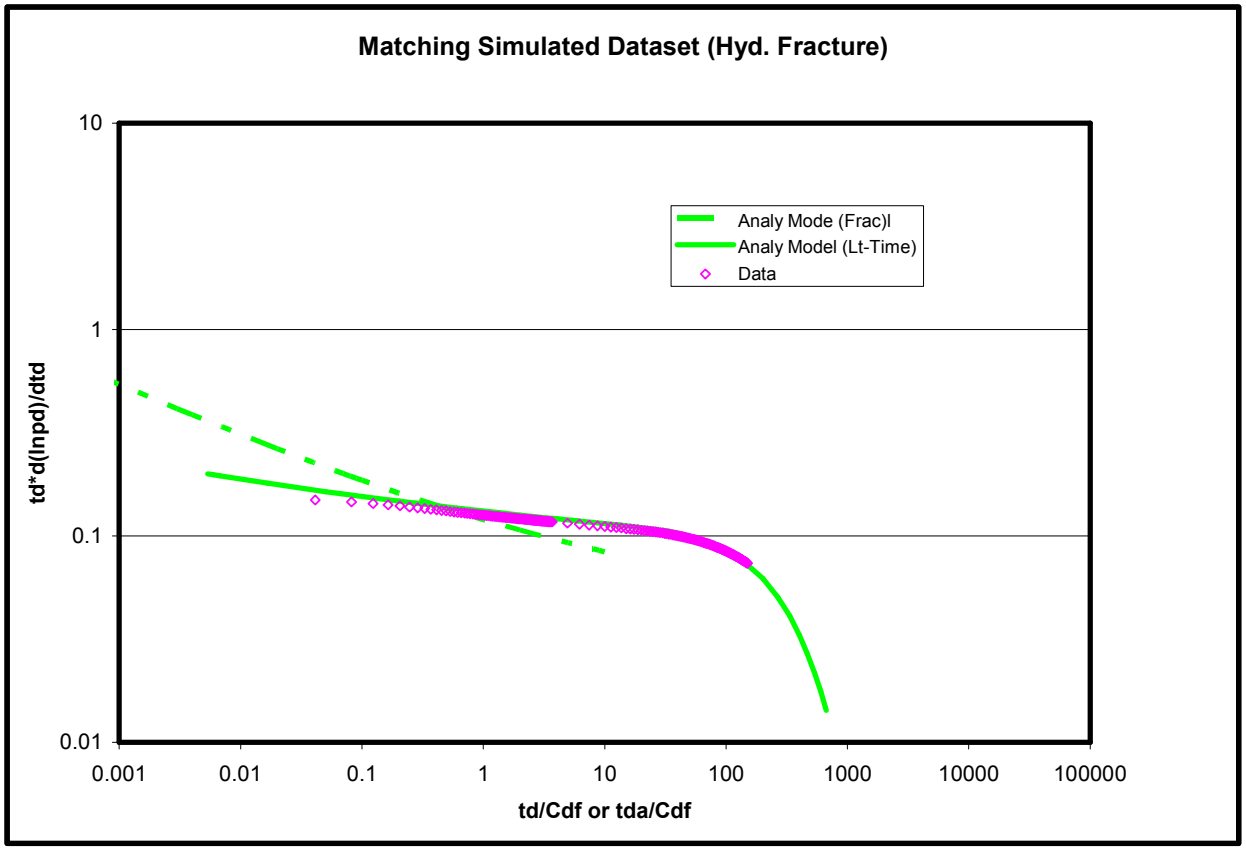

Figure 69 – match using q_d vs t_d for a hydraulically fractured system with adsorbed gas

Lastly, GPA was used to analyze the data, and the results can be seen in Figure 70. The data still reaches the boundary-dominated portion of the type curve. The match resulting from using a hydraulic fracture model offers the same visual quality as that of a single porosity or dual porosity model. In this case, there are a few data points that fall on the early-time hydraulic fracture curve with the majority falling on the pseudo-radial and late-time portions of the solution. The results from this match can be seen in Table 14.

Table 14 – Summary of matching data for hydraulically fractured systems with adsorbed gas.

	Drainage radius, r_e (ft)	Porosity (φ_m)	Matrix Perm. (md)	C_{df}	G/A*	Match Term $(kG/\phi A)$ *
q_d vs t_d	3000	0.1	1.1	n/a	0.33	n/a
GPA (p_{wd} vs t_{da_new})	2640	0.1	1.1	0.4	0.32	3.52
Actual (from model)	2640	0.1	1.8 (k_f) 0.01 (k_m)	0.3	0.32	5.76**

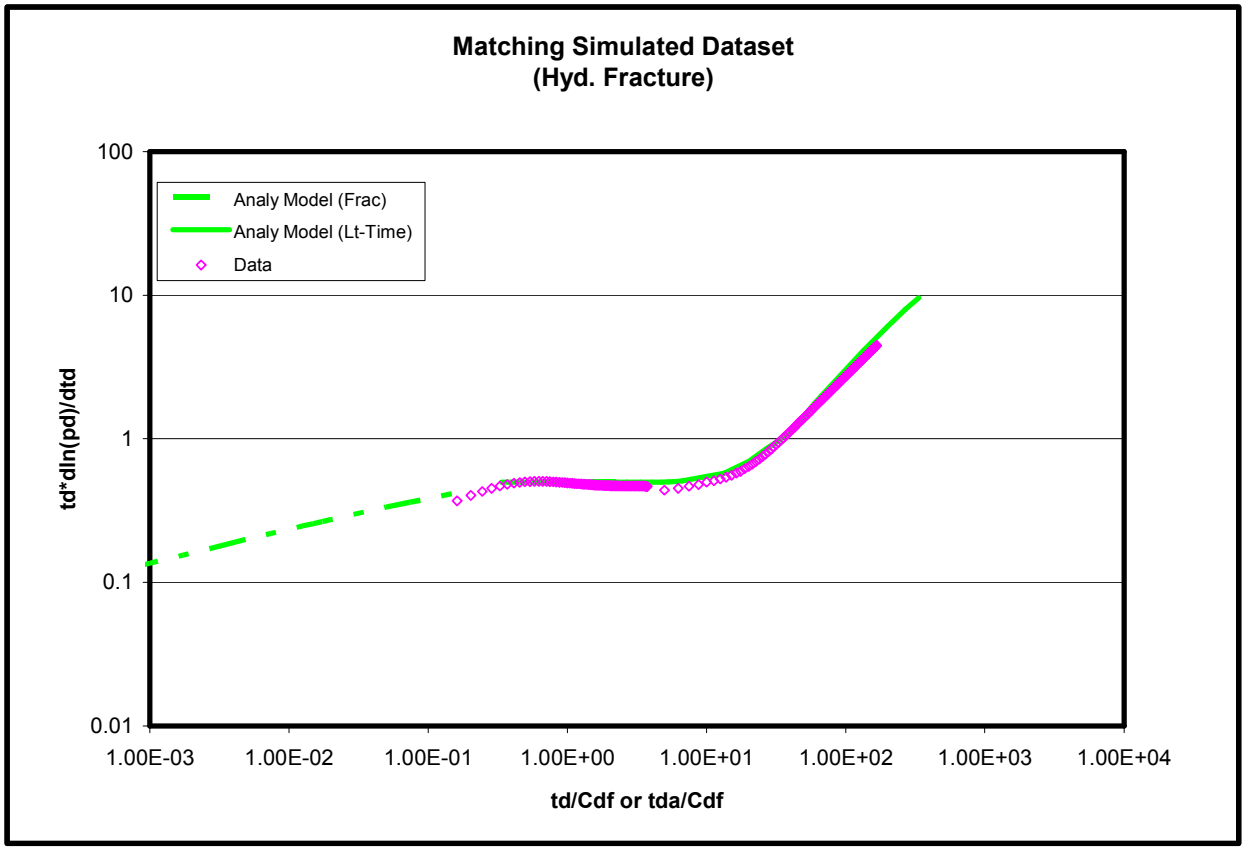

Figure 70 – match using GPA for hydraulically fractured system with adsorbed gas

Figure 70 gives some indication of what the value of C_{df} might be with this hydraulic fracture model. But, the data does not go far enough back in time to allow for an accurate determination of C_{df}. It appears that $C_{df} \approx 0.4$ which is appropriate considering the actual value for C_{df} is 0.3. Interestingly, GPA does give some indication of C_{df} where as q_d vs t_d gives none at all. This may be due to the fact that GPA uses a diagnostic (i.e. derivative) plotting method to help identify flow regimes. Also, very early-time data is notoriously inaccurate, even from a simulator (there were time-step cuts in the simulated data at early-time). On another note, GPA and q_d vs t_d both give reasonable estimates of other reservoir parameters including matrix permeability and drainage radius. The q_d vs t_d analysis yields a slightly erroneous drainage radius most likely because the data does not entirely proceed down the decline curve stem.

6.1.5 Analysis as a Dual Porosity Hydraulically Fractured System with Adsorbed Gas

Here, the simulated data will be analyzed as a dual porosity, hydraulically fractured system with adsorbed gas. The adsorbed gas will be accounted for using the new material balance time method with the correction for compressibility put forth by Bumb and McKee (1988).

First, the match using q_d vs. t_d can be seen in Figure 66. As before, the data does not yet reach the decline-curve stem of the type curve. Therefore, there is a high degree of uncertainty in the match.

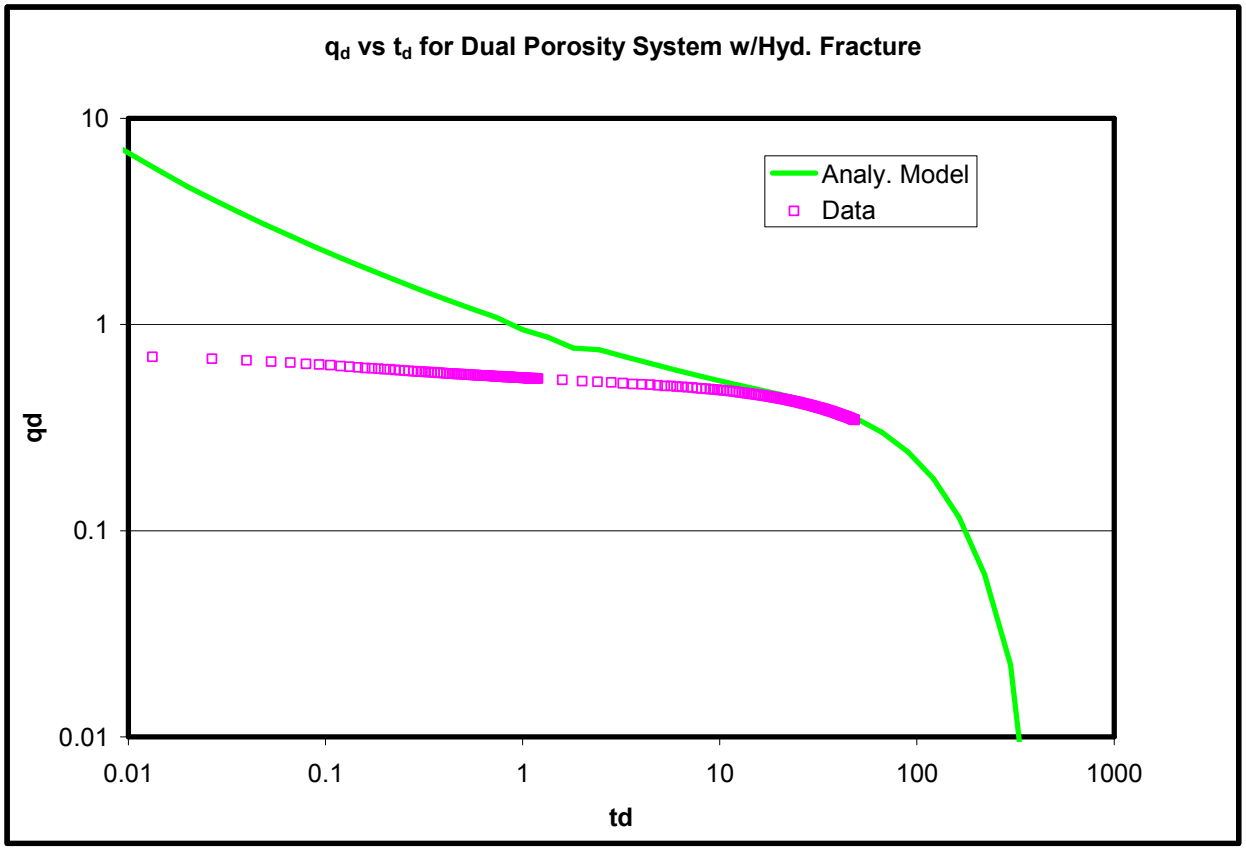

Figure 71 – match using q_d vs t_d for a dual porosity hydraulically fractures system with adsorbed gas.

Figure 71 is not a good match. No attempt was made to match the early time portion of the data to the analytical model. It was shown earlier that the analytical solution published in literature for a dual porosity hydraulically fractured system does not correlate well to simulated results. Figure 71 does show a reasonable late-time match, and this is similar to the results shown earlier when comparing simulated data to this analytical model.

Lastly, GPA was used to analyze the data, and the results can be seen in Figure 72. The data still reaches the boundary-dominated portion of the type curve. The match resulting from using a hydraulic fracture model offers the same visual quality as that of a single porosity or dual porosity model.

Figure 72 is a good match, but it is not as good as the dual porosity or the hydraulic fracture results. It was shown earlier that this analytical model does not replicate the early time results of a similar simulated model. The dimensionless fracture half-length obtained from this analysis does not at all match that of the model. This will be discussed later. A summary the parameters used to achieve this match can be seen in Table 15.

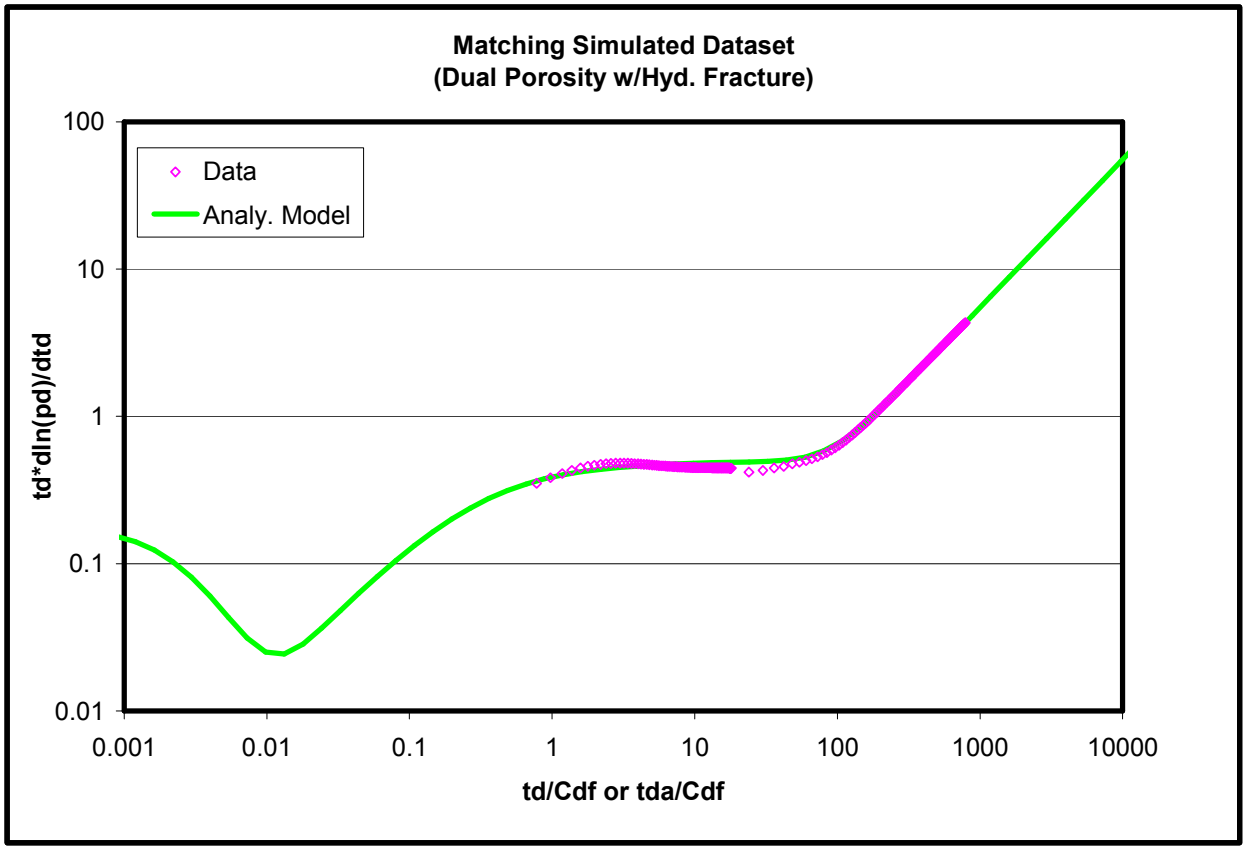

Figure 72 – match using GPA for dual porosity hydraulically fractured system with adsorbed gas.

It should be made very clear that the match obtained using a dual porosity hydraulically fractured analytical model can be very misleading for two reasons. First, it was shown in section 4.1 that the analytical model does not replicate simulated results. While this does not mean the analytical model is incorrect, it does cast serious doubt on it. Second, early-time data was not matched at all in the q_d vs t_d analysis. That implies that the fracture parameters from the match are more or less meaningless. The match from GPA used a fracture half-length of 75 ft instead of the real half-length (from the simulator model dataset) of 480 ft. This is somewhat understandable since it was shown previously that this analytical solution could not replicate early-time data from the simulation models used in this study. So, this makes the parameters obtained from these matches highly suspect.

One thing should be clear, there is a lot of uncertainty in production data analysis. Even with clean, simulated data, the analyses could not reproduce in all cases exactly the parameters that were used in the simulated model. This is especially true for production data when none of the entry parameters are known with a high degree of certainty, even the rate data itself. Normally, things such as dual porosity parameters require precise and accurate data to determine reliable estimates for their values. In addition, dual porosity and hydraulic fracture parameters are

Table 15 – Summary of matching parameters for dual porosity hydraulically fractured systems with adsorbed gas

	Drainage radius, r_e (ft)	Porosity (ϕ_m)	Matrix Perm. (md)	x_e/x_f	C_{df}	G/A*	Match Term ($kG/\phi A$) *
q_d vs t_d	3000	0.1	0.3	5.5	0.4	0.33	n/a
GPA (p_{wd} vs t_{da_new})	2640	0.05	1.1	35	0.6	0.32	3.52
Actual (from model)	2640	0.1	1.8 (k_f) 0.01 (k_m)	5.5	0.3	0.32	5.76**

obtained from early time data. This is when a well is just brought on production; the data is at its least reliable at this time especially if the well is cleaning up. If one jumps at the opportunity to use a more complicated model without any knowledge of the region, reservoir, or well characteristics, substantial amounts of time may be used for little to no additional information obtained. Also, assuming that this simulated dataset is representative of shale gas reservoir performance suggests these reservoirs do not exhibit substantial effects of hydraulic fracturing. They behave more like dual porosity reservoirs without hydraulic fractures.

Lastly, GPA can provide valuable insight were other analysis methodologies fail to provide any definitive insight. In every case presented here, GPA has shown the production data reaches boundary-dominated flow much earlier than the other analysis methods do. This is extremely important for the both the accuracy and usefulness of the analysis performed. For example, it is perfectly reasonable to assume a case where less than 10 years of production data is available. This could mean that the production data reaches boundary-dominated flow on a GPA plot, but does not reach it on a Fetkovich plot. On a cautionary note, GPA relies on a diagnostic plot (i.e. derivative plot) to identify flow regimes and provide a good, sometimes better, match. However, this approach may fail in the presence of very noisy production data. To some degree, smoothing production can address this problem. It is also a fairly reasonable approach given that the shape and length of the production rate and pressure curves are what are really important when doing GPA. It is common practice when doing production data analysis to disregard entire groups of data points that are considered unreliable or just simply wrong. In addition, data smoothing is much less time consuming than re-initialization which is virtually always required to perform a proper Fetkovich analysis.

6.2 Barnett Shale Example Well #1

Now, the insights gained from the simulation example cases detailed previously will be applied to a field case. In particular, it was shown that adsorption does not have a large impact on the analysis when v_L is small and p_L is large which is the case for this field case. It was also shown that an analysis based on a complicated reservoir model does not always increase the amount of information obtained from the analysis, but it does not hurt the analysis results (i.e. nothing is lost).

6.2.1 Data and Data Handling

Production data for 32 months of what will be called Barnett Shale Example Well #1 were obtained from a database provided by Devon Energy Corporation. Daily gas rate, oil rate, water

rate, flowing tubing pressure, and casing pressure have been recorded for the first two months. After that, all rates are recorded daily, but flowing tubing pressure and casing pressure are only recorded weekly. It is not known how the rates were obtained (i.e. are they allocated or are they actual wellhead rates). For the purposes of this work, it is assumed that they are actual wellhead rates. Table 16 is an initial set of properties that was used when matching to the analytical models.

Table 16 – Initial Properties for Barnett Shale Example Well #1

γ_g =	0.6	
r_e =	625	Ft
r_w =	0.33	Ft
A =	28.2	Acres
h =	433	Ft
v_b =	5.31E+08	ft^3
S_w =	0.3	Fraction
ϕ =	0.06255	Fraction
T_{res} =	180	^oF
p_i =	4000	Psia
p_L =	635	psia
v_L =	89	scf/ton

The most important aspect to note about this well is that it is reported to have some interference from neighboring wells. Also, the shift to weekly tubing head pressures will definitely pose a problem if this shift turns out to coincide with any important flow regime changes.

The first step in analyzing this data was to remove any production data entries that did not have an associated tubing head pressure. This resulted in 165 data points that had complete data (i.e. rates and pressures). Next, bottomhole pressure was estimated using the Cullender and Smith flow correlation (Brill and Beggs, 1988). Then, both the rate and pressure data were smoothed using an exponential smoothing algorithm. The algorithm uses a dampening factor (α) to smooth the data. The equation used in the smoothing was

$$x_{smth}(t) = \alpha x(t) + (1-\alpha)x_{smth}(t-1) \qquad \text{Eq 128}$$

For both the rate and pressure streams for Barnett Shale Example Well #1, the value of α was 0.25. The smoothed rate and pressure profiles can be seen in Figure 74 and Figure 75.

6.2.2 Analysis as a Single Porosity System

The smoothed rate and pressure profiles were used in the analysis with no further modification. The smoothed rate profile has 103% of the cumulative production of the original rate profile. Since GPA was consistently shown to be a good analysis methodology, it was used to analyze the first field case. First, it was assumed that this was a single porosity reservoir with adsorbed gas. This minimizes the complexity of the analysis and allows for a solid set of base parameters

with which to do more complicated analysis. The correction for compressibility proposed by Bumb and McKee (1988) was applied. To test the robustness of the match, 3 values of initial pressure were used (4000 psi, 5000 psi, and 6000 psi). This parameter is perhaps the most difficult parameter to obtain in a low permeability shale-gas system, and it is the most critical parameter in the material balance time approach to production data analysis. In addition, the values of the adsorption parameters will be increased in one trial to show the effect of using different adsorption parameters. The individual match plots for each pressure are not shown here, but the visual result was the same in all three cases and can be seen in Figure 76. The match plots for the initial pressures of 5000 psi and 6000 psi can be seen in the Appendix A.

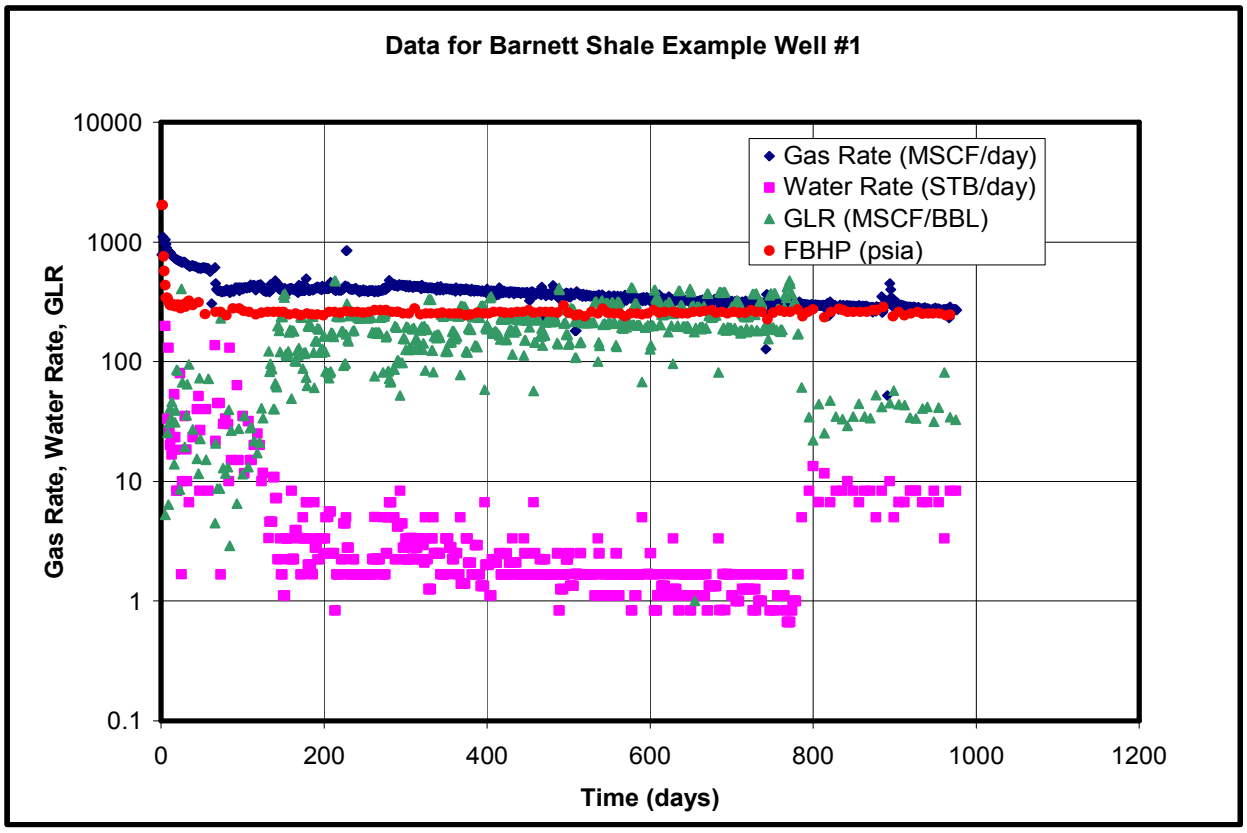

Figure 73 – Combined data plot for Barnett Shale Example Well #1

Figure 76 shows the match of Barnett Shale Example Well #1. The first thing that should be noted is the lack of any early-time or radial flow match to the analytical solution. What could be considered a radial flow section appears to be 2 to 3 times the typical value for radial flow of 0.5. This seems to indicate that there are multiple (2 or 3) boundaries of some sort affecting this system. In this case, both the dimensionless pressure and the dimensionless pressure derivative were used to constrain the match. At late-time, both p_{wd} and p_{wd}' overlay the type curve. If an attempt is made to match the early-time portion of the data, it is not possible to get both p_{wd} and p_{wd}' to simultaneously overlay the type curve. This was evidence that the early-time data will not fit a single porosity type curve. This could be because the data does not come from a single porosity system or the data are inaccurate. A summary of the results for this match can be seen in Table 17.

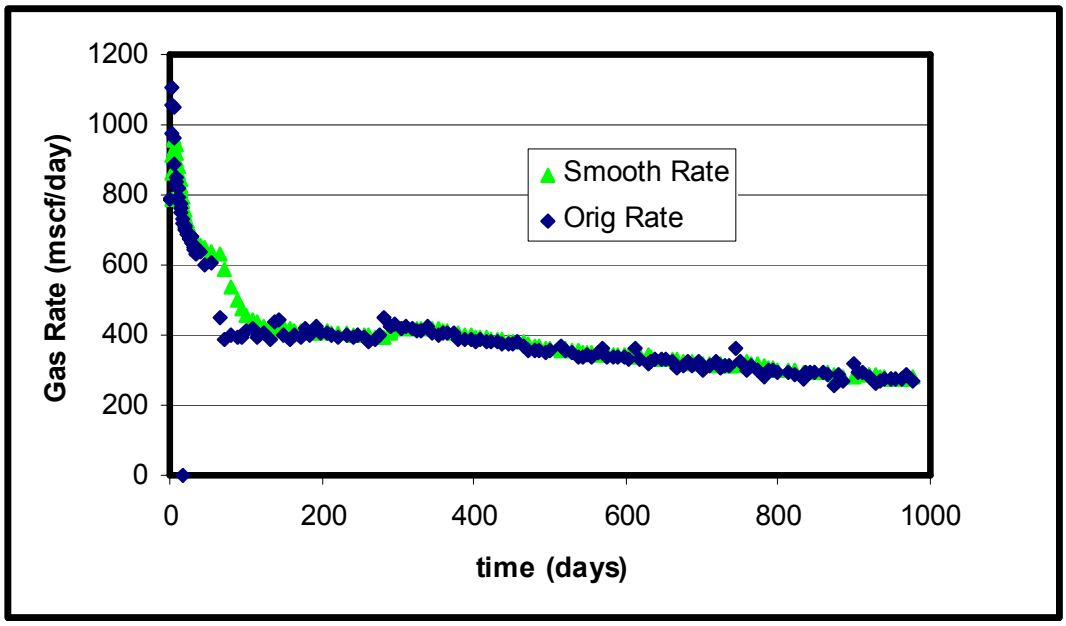

Figure 74 – Smoothed rate profile for Barnett Shale Example Well #1

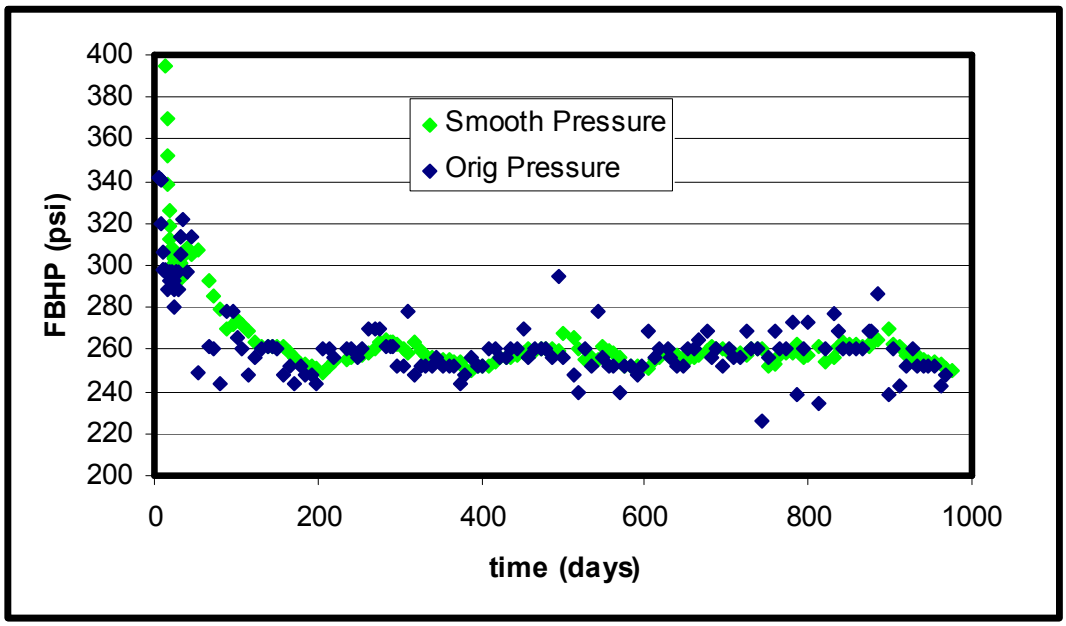

Figure 75 – Smoothed pressure profile for Barnett Shale Example Well #1

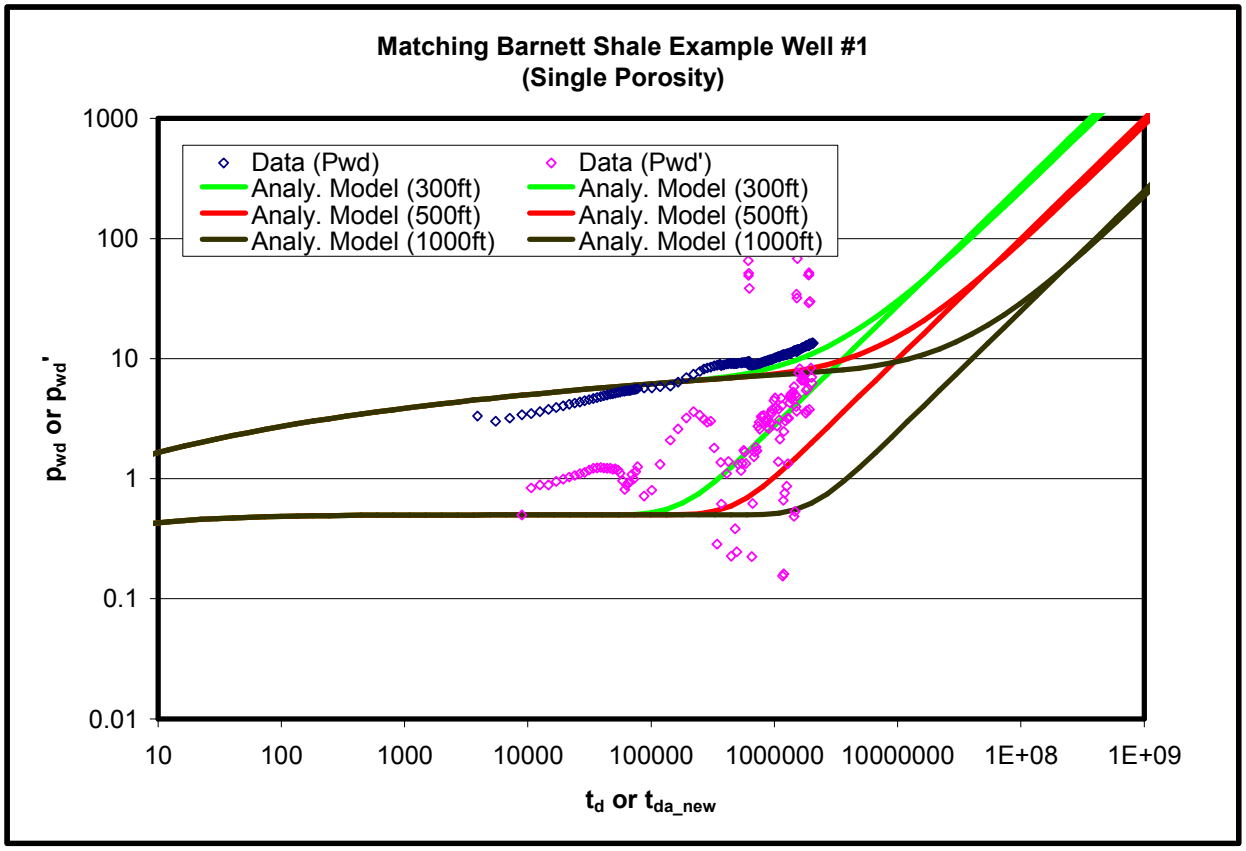

Figure 76 – match using GPA for Barnett Shale Example Well #1 assumed to be a single porosity system with initial pressure of 4000 psi.

6.2.3 Analysis as Dual Porosity System

Next, the data from this well was analyzed as a dual porosity system to see if any additional information can be obtained. The correction for compressibility proposed by Bumb and McKee (1988) was applied.

Figure 77 shows the match of Barnett Shale Example Well #1 assuming it is a dual porosity system. In this case, both the dimensionless pressure and the dimensionless pressure derivative were used to constrain the match. Figure 77 shows a better overall match to the entire dataset rather than just late-time, especially for p_{wd}'. There are what appear to be two flat portions on the derivative curve of the analytic model. These flat portions are separated by sections of unit-slope. These flat portions can be interpreted as two distinct radial flow periods separated by boundary dominated flow. The first representing radial flow through a fracture system, and the second representing radial flow through the matrix. The first section of boundary dominated flow occurs when the boundary is seen through the fracture system. The second section occurs when a boundary is seen through the matrix. While the second radial-flow portion of this dataset does not perfectly overlay the type curve, the trend is clearly seen. An alternative interpretation is that this data comes from a multilayered reservoir. However, information to substantiate this interpretation was not provided. A summary of the results from this match can be seen in Table 17.

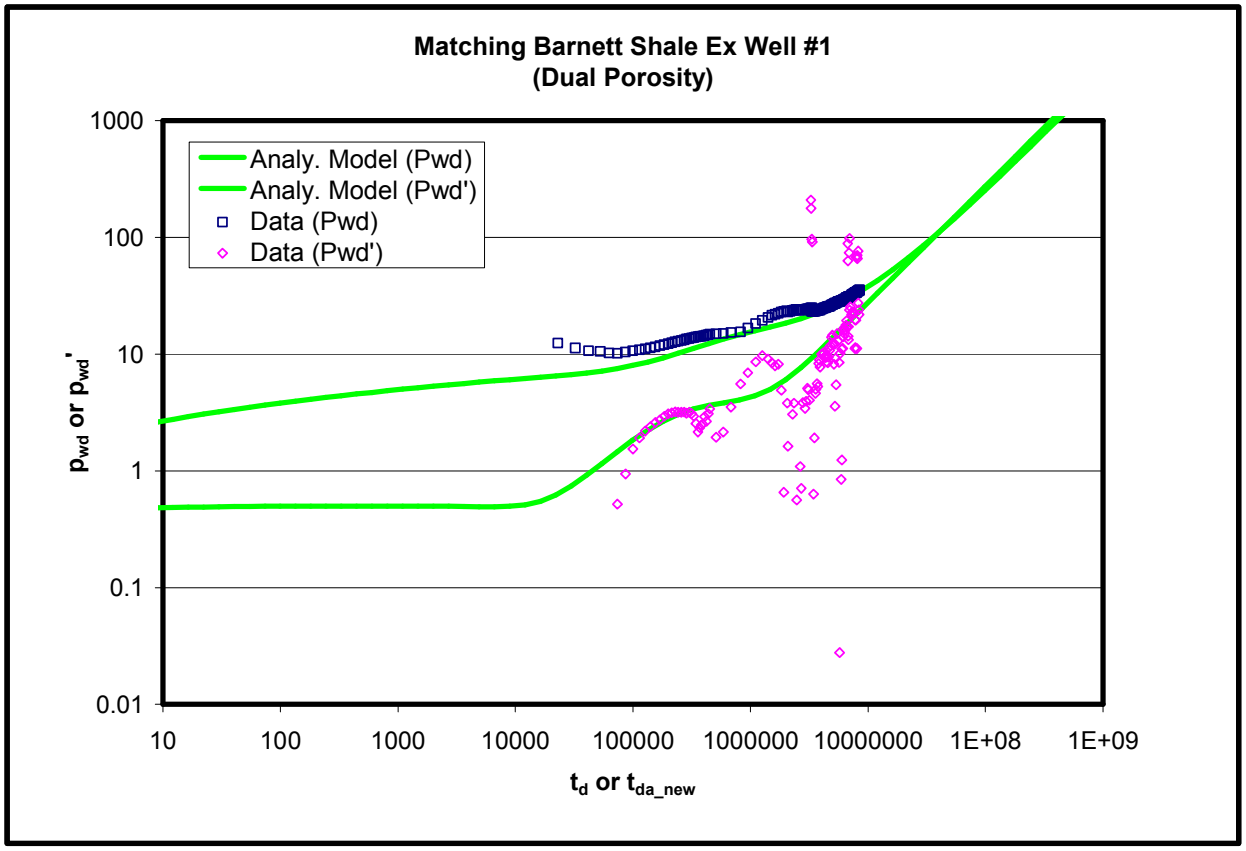

Figure 77 – match using GPA for Barnett Shale Example Well #1 assumed to be a dual porosity system with initial pressure of 4000 psi.

Table 17 shows a summary of the matching results for the Barnett Shale Example Well #1. The matrix permeability is much higher than initially expected. However, it has been noted before that the permeability returned by these type curves is effective system permeability. This system

Table 17 – Summary of Matching Results for Barnett Shale Example Well #1

Model Type	Drainage radius, r_e (ft)	Porosity (ϕ) or ω	Matrix Perm. (nd) or λ	G/A*	Match Term ($kG/\phi A$) *
Single Poro. (4000psi)	300	0.05	8000**	3.55	0.57
Single Poro. (5000psi)	300	0.05	5000**	4.16	0.42
Single Poro. (6000psi)	300	0.05	3000**	4.66	0.28
Lrg. Adsorption	200	0.05	8000**	3.55	0.57
Dual Porosity	300	0.1	2.5×10^{-7}	0.82	2.44***

Using free gas
Represents total effective system permeability
Using fracture permeability

is most likely a dual porosity system, and the well is hydraulically fractured. Therefore, it is reasonable to assume that it would behave as if it had a larger effective system permeability. The drainage radius obtained is smaller than the initial dataset indicated. This could be due to the interference that is known to affect the performance of this well. It could also be reality. A reasonable scenario in this situation is for the drainage area to represent the stimulated region. Shale gas reservoirs have very low permeability; it is not unreasonable to assume that little or no production or pressure support is coming from areas not directly connected to the hydraulic fracture system. This is somewhat supported by the fact that the analysis indicates that the average reservoir pressure has dropped from 4000 psi down to 2200 psi.

Changing the adsorption parameters does have an effect on the results of the analysis because the correction for adsorption put forth by Bumb and McKee (1988) was used. However, to obtain a noticeable shift in the position of the data on the type curve plot that could not be confused for natural data scatter, a value for v_L that was 8 times larger than the original value assumed was required. As can be seen in Table 17, the effect is to have a larger match term ($kG/\phi A$). This is attributed to the smaller drainage area that is required to match the data since a larger value for v_L shifts the data to the left on the type curve plot. Recall that adsorption effects system compressibility in this type of analysis. With a larger system compressibility due to adsorption, this causes t_{da_new} to be smaller at any given point (recall the definition of t_{da_new} in Eq 124). This requires using either a smaller drainage radius in the analytical solution or a smaller porosity in the calculation of the dimensionless plotting functions for the production data. A schematic of this can be seen in Figure 78.

The varying of initial pressure does not have a large effect on the outcome of the matching process. While the match term does decrease in value, a change in initial pressure does not truly affect t_{da_new} because any increase in initial pressure is offset by an increase in gas in place. Thus, an increase in the initial pressure results in a positive vertical shift of the data on the type curve plot because it effects dimensionless pressure, not t_{da_new}. This vertical shift is best counteracted by decreasing the permeability or the reservoir thickness. This is reflected in the changes to the match term $kG/\phi A$. Permeability is in t_{da_new}, so there will be a slight horizontal shift in the end. It is conceivable that a very large change in initial pressure could cause a significant increase in estimated permeability that would have to be offset by changing other match parameters. But, that was not the case here. However, do not underestimate the importance of knowing initial pressure accurately. Any uncertainty in this parameter effects every parameter returned from the analysis.

An important thing to note about the data from Table 17 is the true nature of the matching/output parameters obtained from production data analysis. For example, the match for the dual porosity system will return a value of λ, ω, and dimensionless radius (r_d) used to generate the analytical type curve. The production data will return a value for the match term ($kG/\phi A$). If the value of any specific parameter is desired, an assumption will have to be made. If one wants fracture permeability from λ, values for matrix permeability, wellbore radius, fracture spacing, and fracture geometry must be provided. These values can in no way be determined from the match without additional information and/or assumptions.

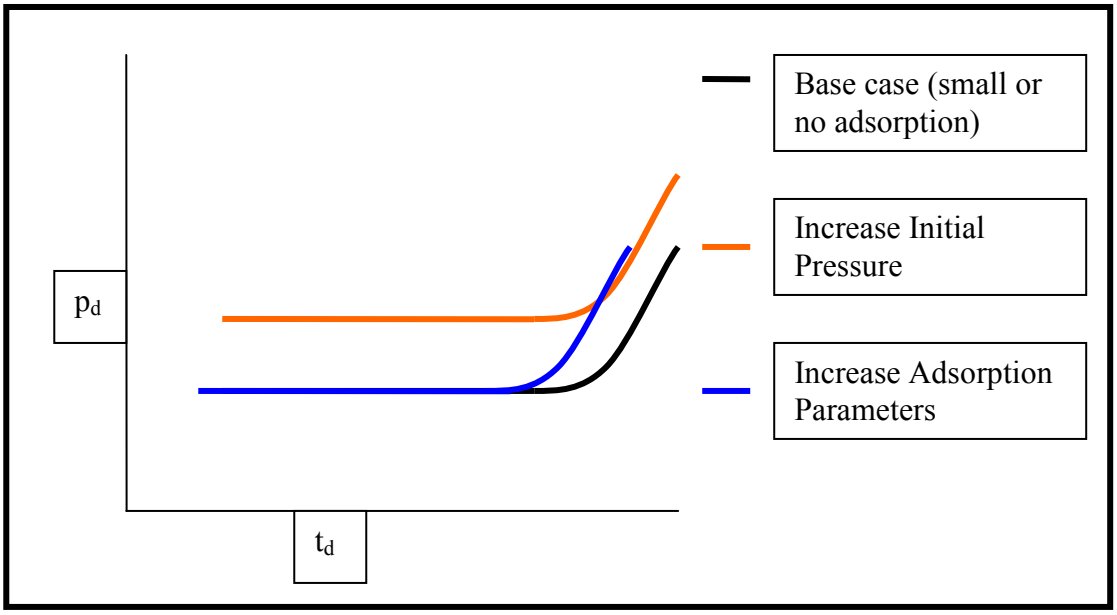

Figure 78 – Schematic showing the effects of initial pressure and adsorption parameters

6.3 Barnett Shale Example Well #2

Now, the insights gained from the simulation example cases detailed previously will be applied to another field case. In particular, it was shown that adsorption does not have a large impact on the analysis when v_L is small and p_L is large which is the case for this field case. It was also shown that an analysis based on a complicated reservoir model does not always increase the amount of information obtained from t
he analysis.

6.3.1 Data and Data Handling

17.5 years of production data for what will be called Barnett Shale Example Well #2 were obtained from a database provided by Devon Energy Corporation. Daily gas rate, oil rate, water rate, flowing tubing pressure, and casing pressure have been recorded for the first 4 months. After that, all rates are recorded daily, but flowing tubing pressure and casing pressure are only recorded weekly. It is not known how the rates were obtained (i.e. are they allocated or are they actual wellhead rates). For the purposes of this work, it is assumed that they are actual wellhead rates. No initial estimates for reservoir parameters were available for this well. This well comes from the same reservoir as the Barnett Shale Ex Well#1. Therefore, the initial set of reservoir parameters from the Barnett Shale Ex Well #1 was taken as a starting point for this analysis. Only the adsorption properties will be changed to reflect estimated average values for the reservoir. For this well, p_L was assumed to be 1400 psia and v_L was 89 scf/ton (6.8 scf/ft^3). The production data obtained can be seen in Figure 79.

The very good thing about the data from this second example well is the amount of it. There is no question that there will be some at least some depletion visible when the data is plotted. This should make for an excellent analysis. In addition, there appears to be 4 stimulations performed

on this well starting at about day 4000. These are most likely hydraulic fracture operations. However, only the first appears to have multiple points where both rate and pressure were recorded.

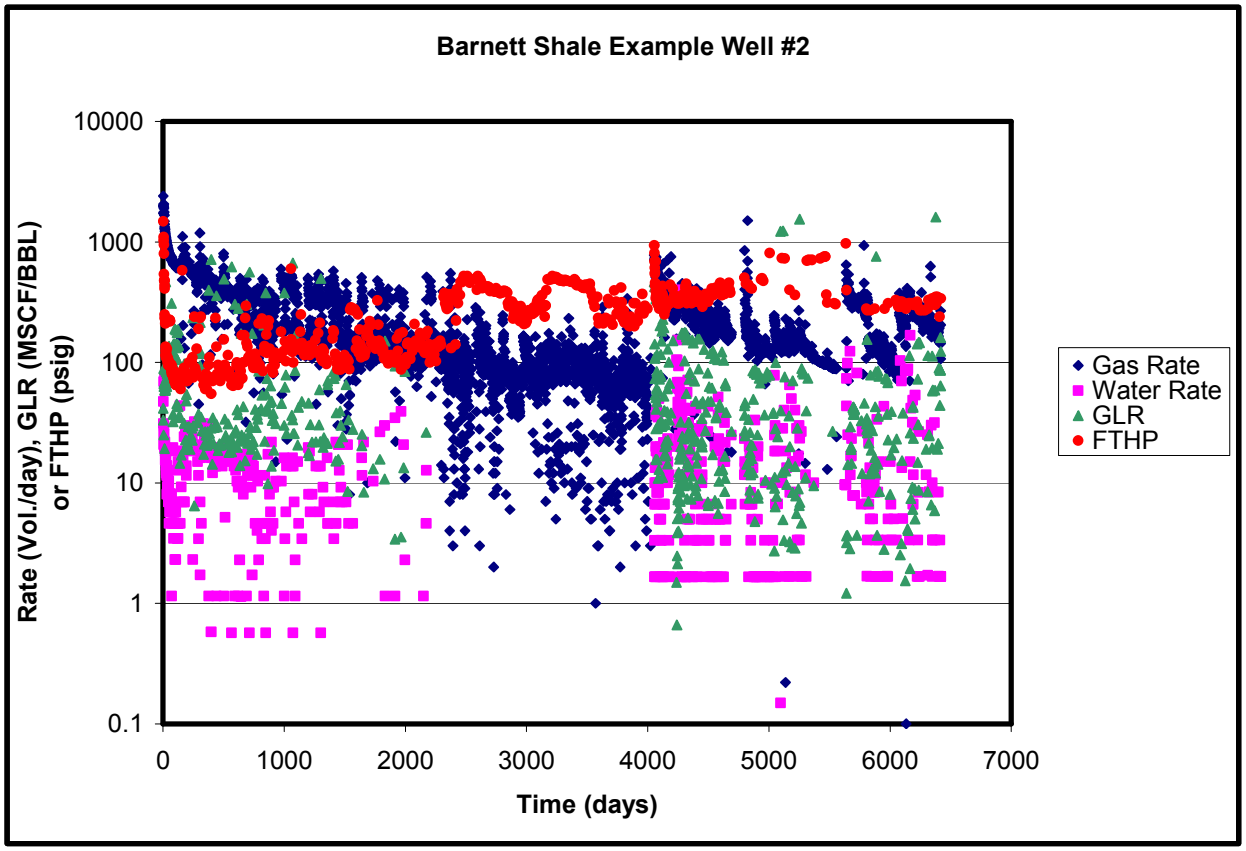

Figure 79 – Combined data plot for Barnett Shale Ex Well#2

The first step in analyzing this data was to remove any production data entries that did not have an associated tubing head pressure. This resulted in 732 data points that had complete data (i.e. rates and pressures). Next, bottomhole pressure was estimated using the Cullender and Smith flow correlation (Brill and Beggs, 1988). Then, both the rate and pressure data were smoothed using an exponential smoothing algorithm. The algorithm uses a dampening factor (α) to smooth the data. The equation is can be seen in Eq 128. For both the rate and pressure streams for Barnett Shale Example Well #2, the value of α was 0.15. The smoothed rate and pressure profiles can be seen in Figure 80 and Figure 81.

6.3.2. Analysis as a Single Porosity System

The smoothed rate and pressure profiles for the first 4050 days were used in this analysis with no further modification. The first of the stimulation jobs performed on this well will be analyzed in Section 6.3.4. The smoothed rate profile has 105% of the cumulative production of the original rate profile. First, it will be assumed that this is a single porosity reservoir with adsorbed gas. This minimizes the complexity of the analysis and allows for a solid set of base parameters with which to do more complicated analysis. While this data is noisy, GPA will be used due to its

ability to provide consistently accurate results without having to re-initialize the data. The correction for compressibility proposed by Bumb and McKee (1988) will be applied. The match achieved for this dataset can be seen in Figure 82.

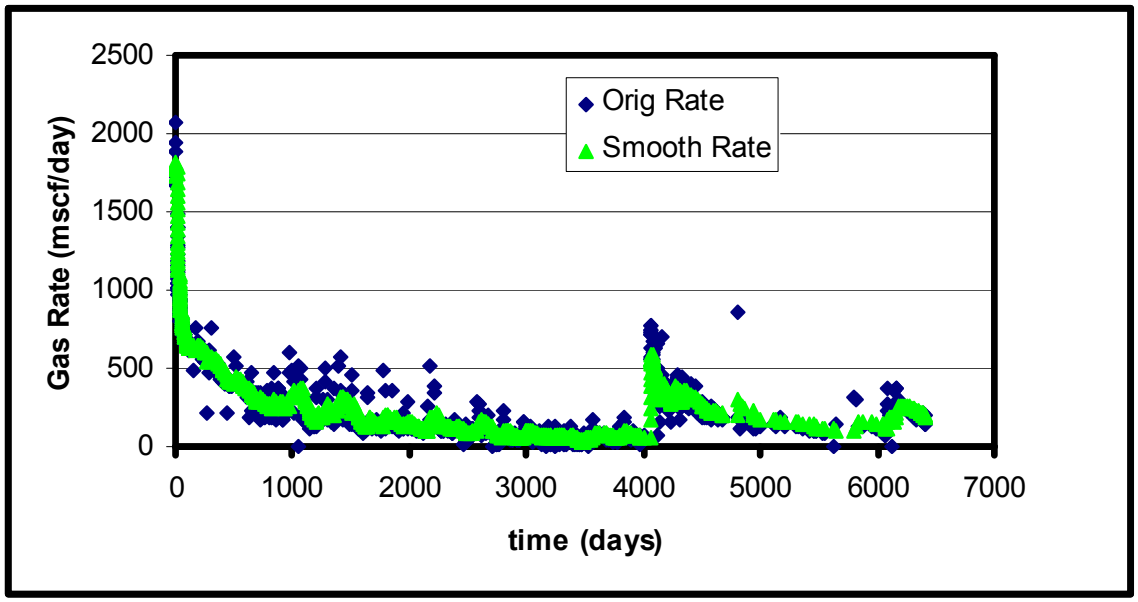

Figure 80 – Smoothed rate profile for Barnett Shale Ex Well #2

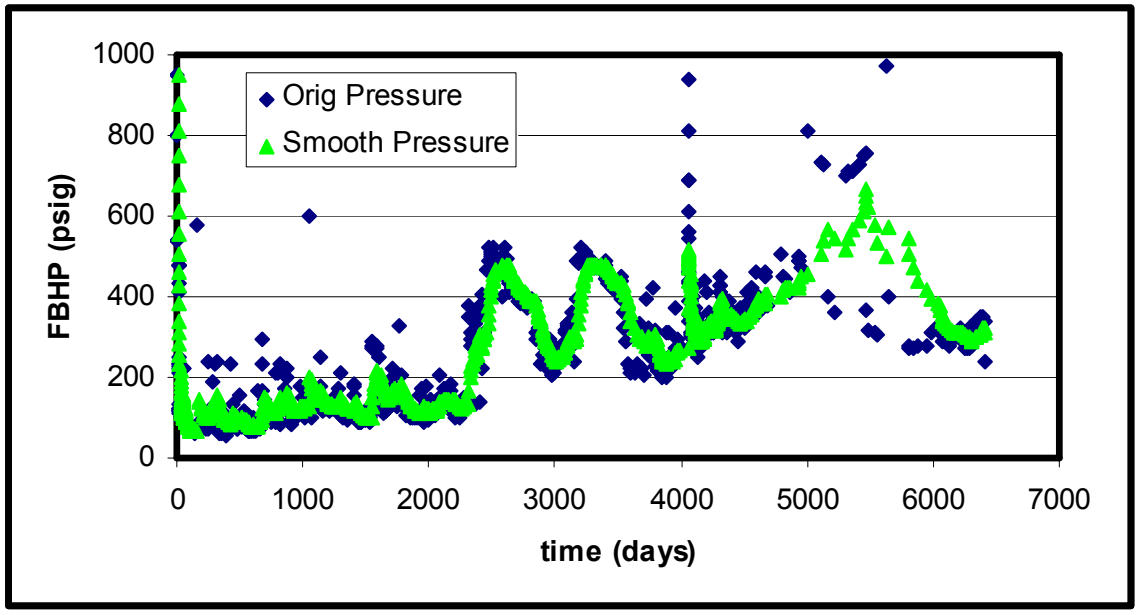

Figure 81 – Smoothed pressure profile for Barnett Shale Ex Well #2

The data in Figure 82 clearly exhibits boundary-dominated flow. However, the early-time data does exhibits the characteristics of a dual porosity system or perhaps a hydraulically fractured system. The quality of the early time data is excellent and looks as though it would fit very well

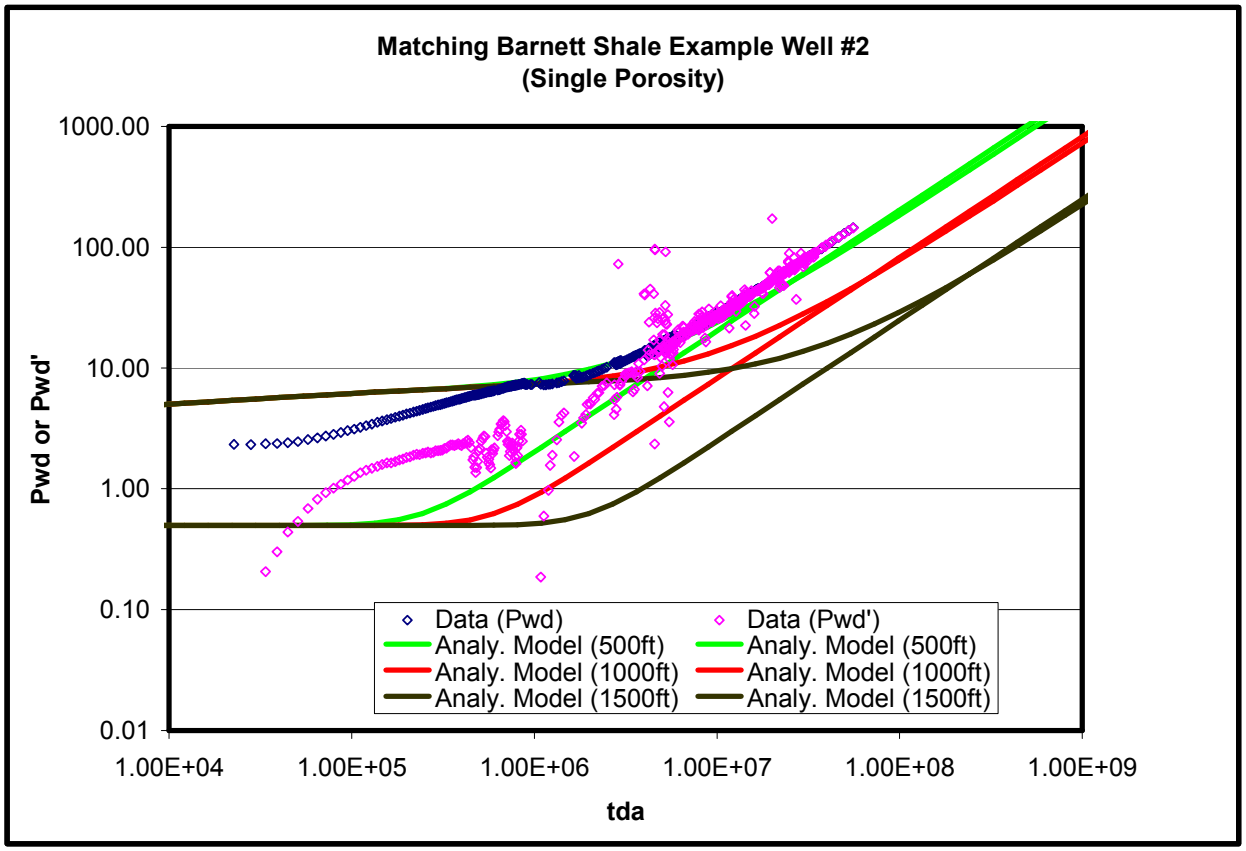

Figure 82 – match using GPA for Barnett Shale Ex Well #2 assumed to be a single porosity system with 4000 psi initial pressure.

over the type curve for a dual porosity system. The production data at late time is also of good quality, but there is little to no quality data in the radial flow period. Also note that while the late-time data does proceed up the boundary-dominated portion of the analytical solution, it does not perfectly overlay it at this initial pressure. A summary of the results of this analysis can be seen in Table 18.

6.3.3 Analysis as Dual Porosity System

Next, the data from this well will be analyzed as a dual porosity system to see if any additional information can be obtained. The correction for compressibility proposed by Bumb and McKee (1988) will be applied even though it was shown that it has no discernable impact with these quantities of adsorbed gas. It does not negatively impact the analysis in any way. To test the robustness of the match, 3 values of initial pressure were used (4000 psi, 5000psi, 6000 psi, and 7500psi). This parameter is perhaps the most difficult parameter to obtain in a low permeability shale-gas system. In addition, the values of the adsorption parameters will be increased in one trial to show the effect of using different adsorption parameters. The individual match plots for each pressure are not shown here, but the visual result were similar in all three cases and an

example can be seen in Figure 83. The match plots for the additional initial pressure used can be seen in the Appendix A.

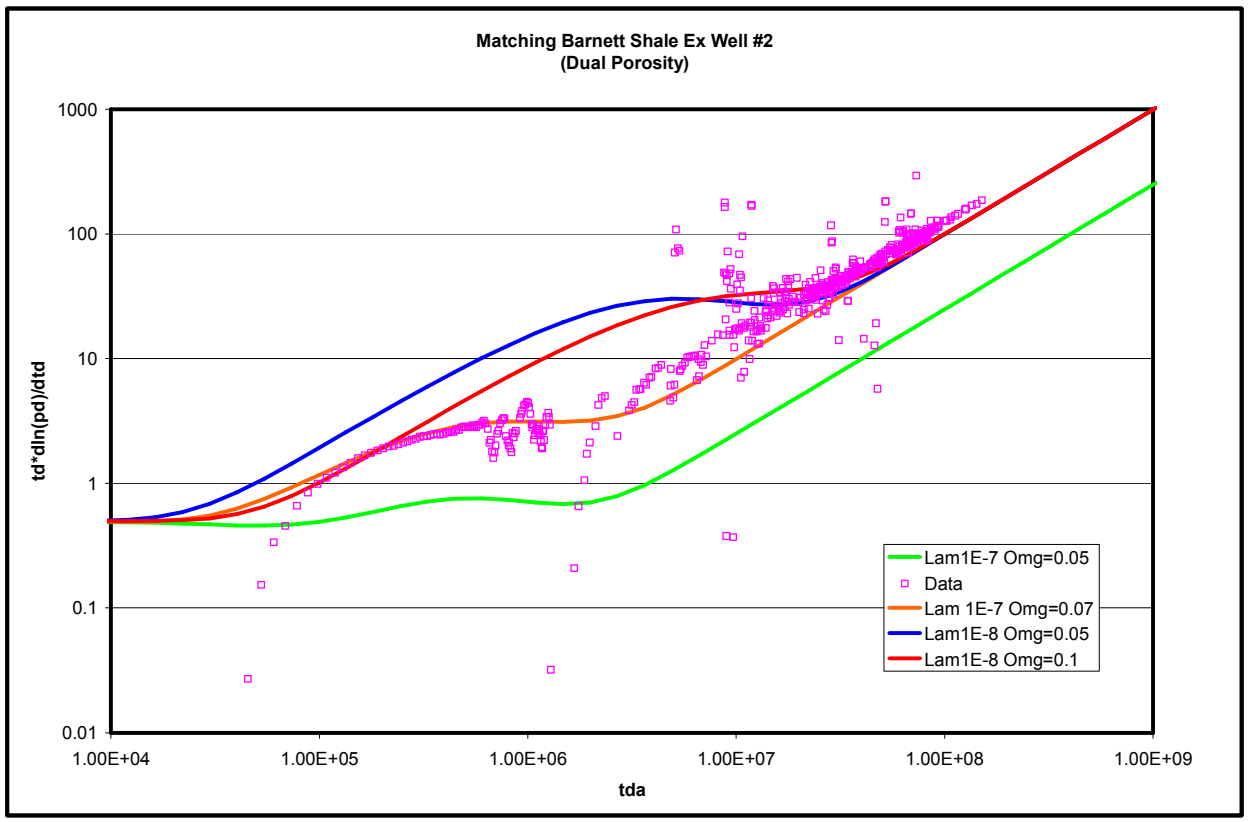

Figure 83 – match using GPA for Barnett Shale Example Well #2 assumed to be a dual porosity system

Figure 83 shows the match for the Barnett Shale Ex Well #2 assuming it is a dual porosity system. The match is of good quality especially at early-time. The smooth and distinct shape of the early-time data reduces the uncertainty of this match. Interestingly, this match has the characteristics of a dual permeability system. The first flat portion of the analytic solutions (solid lines) is a radial flow. Each of the analytic solutions also exhibits a second flat period of radial flow just after a unit-slope that could be interpreted as boundary-dominated flow. This is followed by an extended unit-slope indicating boundary-dominated flow. This could be interpreted as multiple layer behavior or as two different porosities, matrix and fracture, in a dual porosity system. Finally, as was seen in the single porosity scenario for this well, the late-time data does not quite overlay any of the type curves. The analysis results are provided in Table 18.

Table 18 shows a summary of the matching results for the Barnett Shale Example Well #2. The drainage radius obtained is smaller in the single porosity case than in the dual porosity case. This is not too troubling given the clear dual porosity behavior of the data. However, the production data bears out that this well was stimulated on numerous occasions, and these stimulations were probably hydraulic fracturing. A reasonable scenario in this situation is for the drainage area to represent the region contacted by the hydraulic fracture. Shale gas reservoirs

have very low permeability; it is not unreasonable to assume that no little or no production or pressure support is coming from areas not directly connected to the hydraulic fracture system. This very small drainage radius might very well be an effective drainage volume which is connected by the hydraulic fractures. This theory will be put to the test in Section 6.3.4.

Table 18 – Summary of matching results for Barnett Shale Ex Well #2

Model Type	Drainage radius, r_e (ft)	Porosity (ϕ_m) or ω	Matrix Perm. (nd) or λ	G/A*	Match Term ($kG/\phi A$) *
Single Porosity	350	0.0175	7000**	1.63	0.65
Dual Poro. (4000 psi)	500	0.085	1×10^{-7}	1.12	1.12
Dual Poro. (5000psi)	500	0.085	1×10^{-7}	1.07	1.0
Dual Poro. (6000psi)	500	0.085	1×10^{-7}	0.99	0.98
Dual Poro. (7500psi)	500	0.095	1×10^{-7}	0.36	0.95
Lrg. Adsorption	350	0.07	1×10^{-7}	0.97	3.28***

Using free gas. G/A with adsorbed gas is 2.65 for 7500 psi, 2.98 for 5000 psi, and 3.11 for 4000 psi.
Represents total effective system permeability
Using fracture permeability

The exercise to determine the sensitivity of the match to initial pressure was performed on the dual porosity cases because the data exhibits dual porosity behavior. The dual porosity parameters (λ and ω) did not initially change with pressure because initial pressure did not affect the shape of the data curve; it only affected its position on the type curve plot. The shape is what determines λ and ω. As initial pressure was increased, matrix porosity was decreased in an attempt to match the late-time portion of the analytic type curve. Fracture porosity was also changed to preserve the same value of ω. However, for the case of 7500 psi initial pressure, matrix porosity became small enough that a slightly larger ω was thought to be a better match. The match for 5000 psi and 6000 psi can be seen in the Appendix A.

Figure 84 is the match for Barnett Shale Ex Well #2 at 7500 psi. When performing log-log production data analysis, it is very important to achieve a very good match at late-time. It was necessary to increase the initial pressure to 7500 psi which is a higher pressure than expected for this field. This allowed a smaller porosity to be used without material balance indicating an unreasonably low reservoir pressure at the end of this production period. The reservoir pressure at the end of this production period was estimated to be about 600 psi. Flowing bottomhole pressures at the end of this production period are about 250 psi and gas production rates are about 100 MSCF/day.

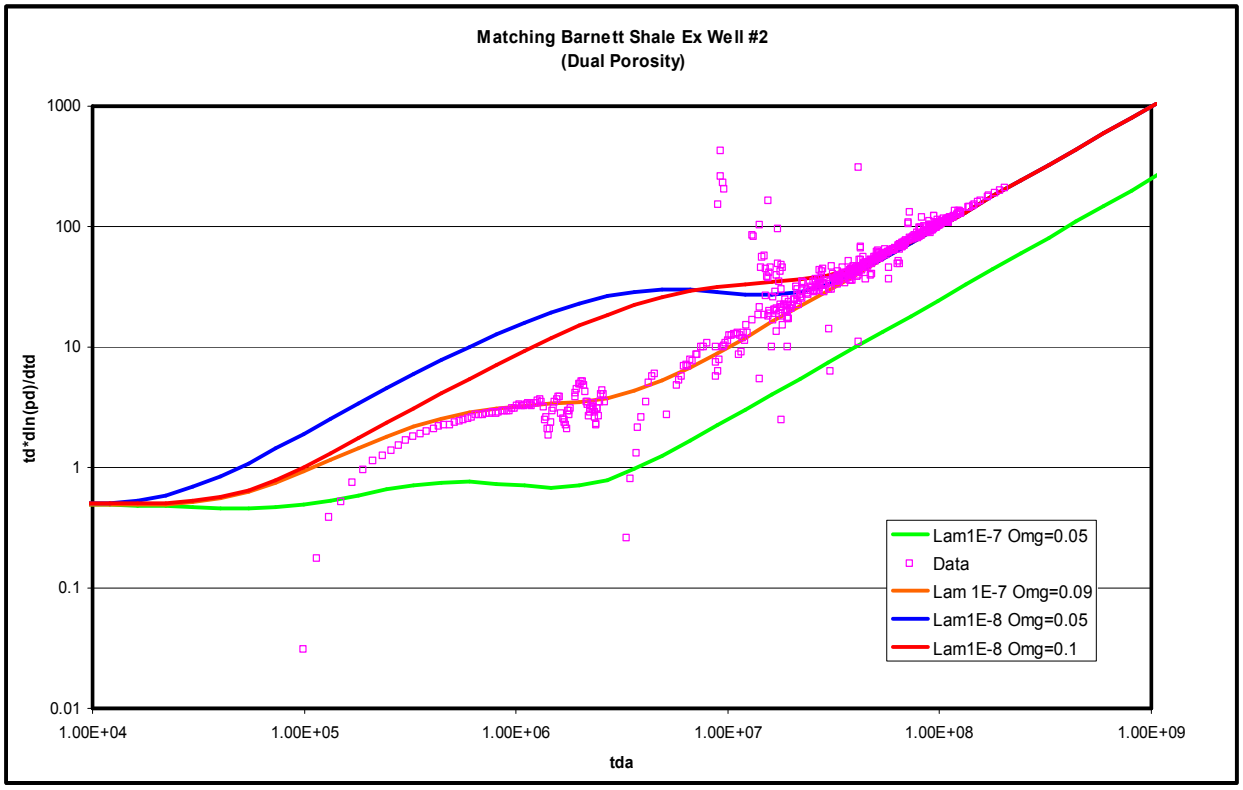

Figure 84 – Match using GPA for Barnett Shale Ex Well #2 with an initial pressure of 7500 psi.

Just as in the case of Barnett Shale Ex Well #1, the value of the adsorption parameters had to be increase dramatically to have any effect on the outcome of the analysis. Increasing these adsorption parameters causes an overcorrection for adsorption using the adjusted total system compressibility put forth by Bumb and McKee (1988). That results in the data being plotted too far to the left on the type curve plot. Therefore, porosity or drainage radius must be changed to bring the data back. In this case, the drainage radius is very small and λ is very small; this makes the two interconnected. Recall that λ represents the amount of connection or interaction between the natural fracture permeability and the matrix permeability. With this being small, dual porosity effects last until boundary-dominated flow. Therefore, drainage radius cannot be changed in this instance without changing λ and ω. It was chosen to lower porosity (therefore ω) slightly to bring the data back to its original position. This can be seen in the lower G/A for this scenario in Table 18.

6.3.4 Stimulation Analysis

Since this well had what appear to be multiple stimulation jobs performed on it after day 4000, an analysis was performed on the data from one of these operations. The same method of handling the production data that was used with the first two field cases was used again here. As can be seen in Figure 85 and Figure 86, only production data from the first stimulation job was used. This stimulation job was performed at around day 4050. All previous data was discarded, and only data from day 4050 up to the beginning of the next stimulation job was used. The value used for the dampening factor was 0.15.

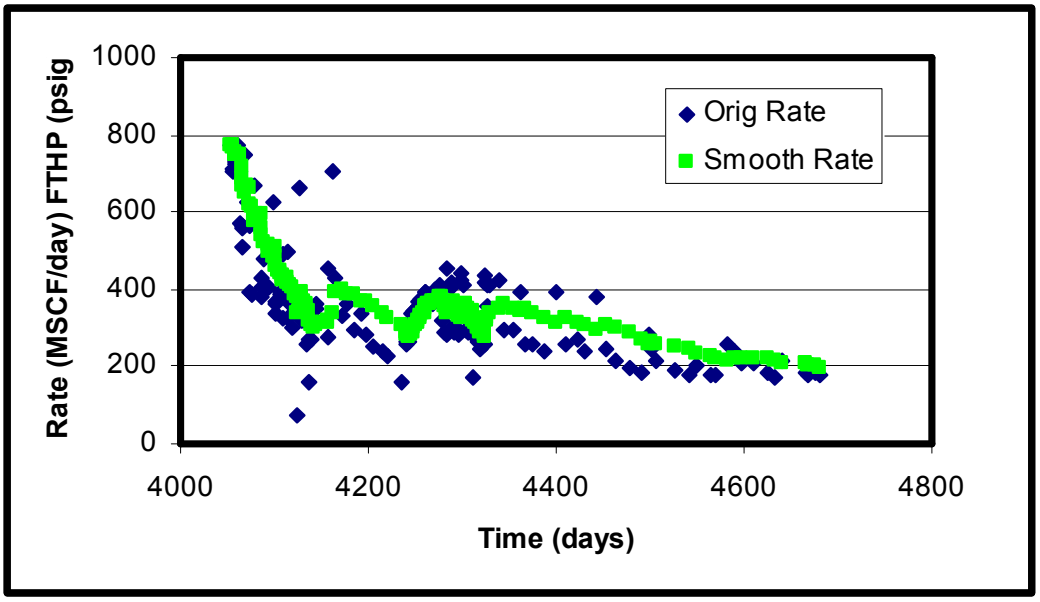

Figure 85 – Smoothed rate profile for the stimulation job at day 4050

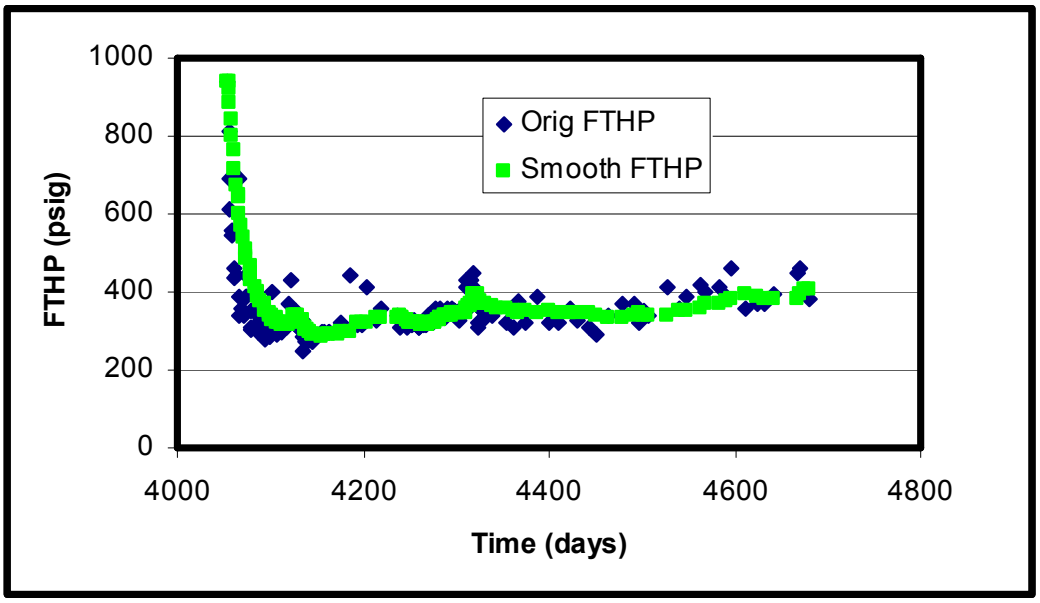

Figure 86 – Smoothed pressure profile for the stimulation job at day 4050

This data was assumed to come from a dual porosity system. No single porosity analysis will be performed as this system has already shown itself to behave more like a dual porosity system. The analysis can be seen in Figure 87.

This data does appear to have the same quality of a match as does the first set of data from this well. However, it does display similar dual permeability/dual porosity behavior that was seen in Figure 83. There was really no discernable boundary-dominated flow data for this stimulation job. So, it is really not possible to provide a definitive drainage radius. However, drainage

radius does slightly impact λ and ω if λ is small enough to cause dual-porosity effects to last until late-time. Therefore, this match is somewhat indicative of drainage radius. The dimensionless radius obtained from this match is less than what was obtained previously for this well. A summary of the results can be seen in Table 19.

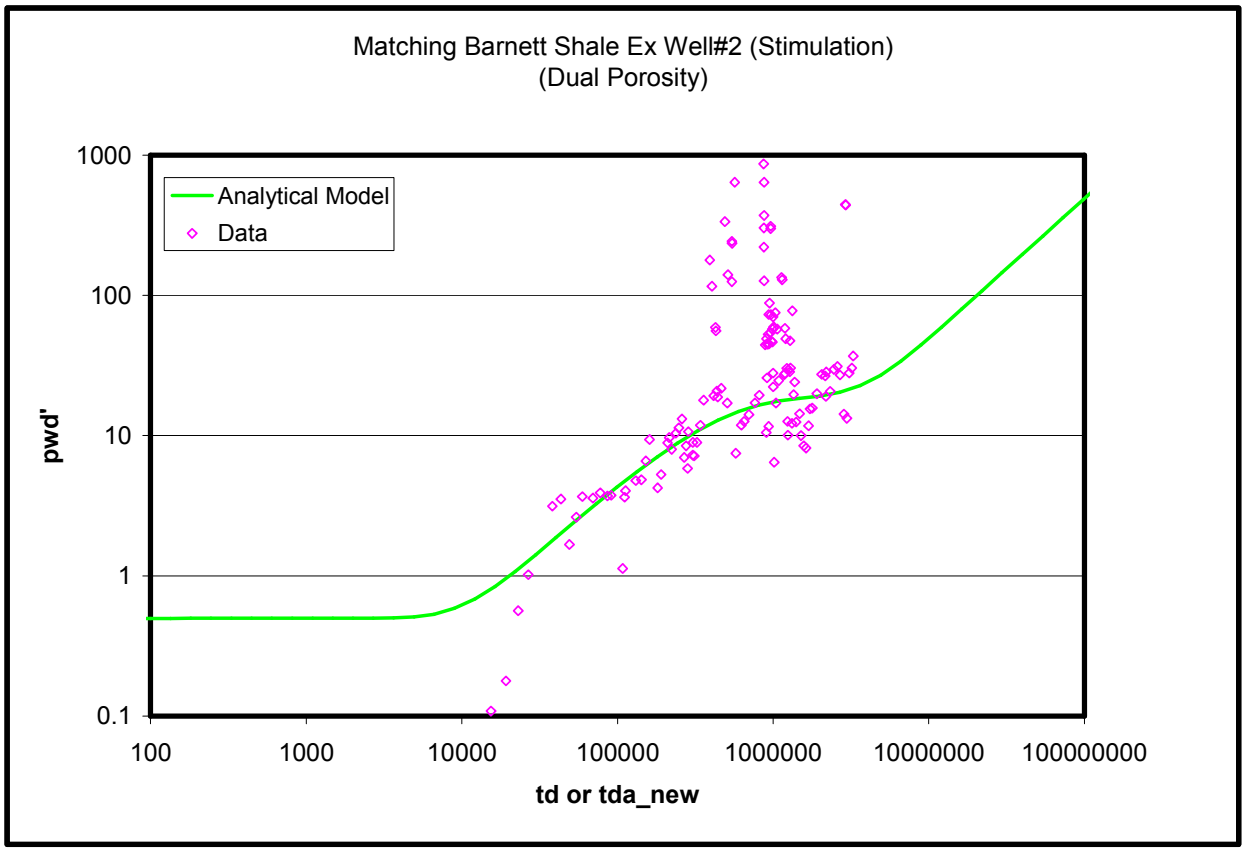

Figure 87 – match using GPA for the first stimulation job performed on Barnett Shale Ex Well #2

This match was achieved with the roughly the same dual porosity parameters and the same initial pressure as was used on the first section of data from this well. The small drainage radius is the most notable difference between the results of this match and the previous match. However, if one assumes that this well was hydraulically fractured before and then re-fractured at day 4050, this can make sense. Let us assume that the only producing portions of the reservoir are those

Table 19 – Summary of matching results for the first stimulation job performed on Barnett Shale Ex Well #2

Model Type	Drainage radius, r_e (ft)	ω	Λ	G/A*	Match Term $(kG/\phi A)$ *
Dual Porosity	225	0.075	9E-8	3.52	2.49

directly connected to the hydraulic fracture by the natural fracture matrix. This assumption is reasonable if one also assumes that any hydraulic fracture in the shale reservoir merely props open the natural fracture matrix (Gale, et al. 2007). This area that is connected to the hydraulic fracture is very small and is drained rapidly. This is evident when matching the first data section of this well; the average reservoir pressure estimated at for the last data point was 700 psi. This is more than a 3000 psi drop in reservoir pressure from the initial reservoir pressure of 4000 psi. As production declines, it becomes necessary to contact new reservoir. Another fracture operation is performed and the well resumes producing at its original high rate. According to the analysis here, reservoir pressures seen after the fracturing are at or near original reservoir pressure. Each time the well is fractured additional, apparently new reservoir area is contacted. This can be seen by comparing the initial rates of the all of the stimulation jobs that can be seen in Figure 79 and the fact that both the first data section on the stimulated data section can be matched using the same initial pressure and the same dual porosity parameters.

7. SUMMARY, CONCLUSIONS, AND RECOMMENDATIONS

7.1 Summary

It was shown from the beginning of this work that there was a gap in the understanding of how adsorption affects the analysis of production data. With the exception of a work by Bumb and McKee (1988) that was expanded upon by Spivey and Semmelbeck (1996), all efforts pertaining to understanding this phenomenon were focused on empirical relationships like those proposed by Lane, et al. (1989).

This work has shown that production data from reservoirs that contain adsorbed gas can be analyzed in dimensionless space. Using a combination of a semi-analytic time function (a slightly modified version of material balance time from Palacio and Blasingame (1993)) and analytical constant-rate solutions, production data from many of the common reservoir systems are capable of being accurately analyzed regardless of whether or not they contain adsorbed gas.

This work has documented the effects of adsorption on four common reservoir systems: single porosity, dual porosity, finite conductivity vertical fracture, and dual porosity with a finite conductivity vertical fracture. Furthermore, it has been shown that a consistent analysis method can be applied to these various systems to obtain an accurate analysis of production data from reservoirs that contain adsorbed gas.

Also, three common analysis methods were examined to determine which, if any, yields superior results in analyzing a simulated production dataset. The results from these various analysis methods were compared against one another. Lastly, the insights gained from this work were applied to two field datasets from the Barnett Shale provided by Devon Energy Corporation.

7.2 Conclusions

Agarwal (1999) confirmed that material balance time (Palacio and Blasingame, 1993) could be used to convert a constant-pressure system to an equivalent constant-rate system. This was reconfirmed in this work, and it was shown to work for the four types of reservoir systems shown in this work. This was completely expected and very necessary since the application of GPA (Cox, et al., 2002) depends on applying this methodology. In addition, the analytical solutions to three of these four reservoir systems were shown to be identical to simulated results. The dual porosity system with a finite conductivity vertical fracture was the only system in which the simulated results did not match the analytical solution. This is most likely due to an inaccurate analytical solution as only one example of a closed form solution for this type of system could be found in the literature.

While adsorption is a complicated mechanism, its effects on production data and production data analysis seem to be consistent and relatively simple. For systems produced at constant rate or constant pressure, adsorbed gas causes a given rate or flowing bottom-hole pressure to be sustained for a longer period of time compared to a system without adsorbed gas. Mechanistically, this is logical in that adsorption acts to replenish free gas in the pore spaces that has been produced as reservoir pressure is lowered. This effect can be, and usually is, greater at late-time depending on the shape of the Langmuir isotherm.

In dimensionless space, adsorption is seen as an increase in system compressibility. This can be calculated for any type of system using the equation provided by Bumb and McKee (1988). Production data plotted without using this equation for compressibility in calculating the plotting functions will plot too far to the right on the graph. This could result in several analysis errors, but the most common would be a porosity that is too large or a dimensionless radius that is too large. However, the effect of adsorption on dimensionless type curves can be very subtle depending on the amount of adsorbed gas in relation to the amount of free gas. In many cases, the effects of adsorption will not be noticeable, or it would be permissible to discount them given the normal scatter and uncertainty that surrounds production data. It is foreseeable that coalbed methane systems may have enough adsorbed gas relative to free gas that the effects of adsorption would be noticeable and significant.

When using material balance time to convert a constant-pressure system to an equivalent constant-rate system, two extra cautions must be taken. The use of material balance time makes for a more complicated plotting function. Since it includes original gas in place, adsorption can greatly affect where production falls on a dimensionless plot that uses material balance time to calculate dimensionless time. Recall that none of the analytical solutions used in this work account for adsorbed gas. It was shown that it is necessary to use free gas in the equation for material balance time so that production data from a system with adsorbed gas will overlay an analytical solution for the same system without adsorbed gas.

Secondly, the use of material balance time in dimensionless time eliminates compressibility from the equation for the plotting function. Therefore, it was necessary to slightly modify the equation for material balance time to allow compressibility to remain in the plotting function. It is recommended to use this definition of material balance time when analyzing systems with significant amounts of adsorbed gas.

Three common methods of analyzing production data analysis were compared using a simulated dataset. In this particular case, GPA seemed to be the more effective method consistently generating slightly more accurate results. More importantly, its use of a diagnostic (derivative) curve enabled it to recognize late-time boundary dominated flow earlier than the other methods. However, as with all material balance time methods its plotting functions require more inputs as compared to the other analysis methods. Most importantly, they hinge on an accurate estimate of initial pressure which is very hard to obtain in low permeability systems such as shale gas reservoirs.

The analysis of the two field datasets yields two very important pieces of information. First, it showed exactly what type of data can be returned from such an analysis. For the case of GPA, an analyst can provide the values for the parameters that were used to calculate the matched analytical model and a value for the term $kG/\phi A$. To obtain additional information, the value of some other parameter must be assumed. But, the analysis has constrained the value of 4 very important parameters.

In addition, it showed that GPA could be a valuable diagnostic tool for shale gas reservoirs. If the analysis of the Barnett Shale Ex Well #2 is reasonably correct, analyzing the data from any new fracture job performed on a well and comparing it to the original analysis will allow an

analyst to discern whether or not a re-frac is necessary at that time. If the well has not returned to boundary-dominated flow that would indicate that there is more virgin reservoir that can be contacted by the current hydraulic fracture. If this is not the case, then it is time to re-frac. Finally, it seems that the initial pressure of the reservoir drained by Barnett Shale Ex Well #2 may be significantly higher than was expected. The analysis performed in this work suggests that it could be has high as 7500 psi.

7.3 Recommendations

While this work did examine the effects of adsorption on various type curves and its impacts on the analysis of production data, a wide range of adsorption properties was not used in this work. To fully understand when the effect of adsorbed gas is significant, a comprehensive range of adsorption properties should be used. In particular, how does the magnitude of p_L effect the time at which adsorption becomes noticeable? Specifically, at what magnitude does this effect become noticeable? Also, what combinations of p_L and v_L seen in the field are the most likely to cause a noticeable change in the outcome of the analysis?

Further investigation of the dual porosity with a finite conductivity vertical fracture system is necessary. Since this solution did not replicate the results of the simulation models, it was not possible to use this solution to analyze the field datasets. As was seen in the Barnett Shale Ex Well #2, an analytical solution that can handle both dual porosity effects and hydraulic fracture effects would have been very useful in ascertaining the fracture half-length for the multiple stimulation jobs performed on this well.

All of the dual porosity analytic solutions in this study used pseudosteady state interporosity flow to describe the pressure behavior of the matrix blocks. This is valid if the matrix blocks are relatively small and their permeability is relatively large. The values for lambda obtained from the field case matches result in very large matrix blocks. In addition, shale gas systems have very small matrix permeability. Using analytic solutions that incorporate transient interporosity flow may be required to more accurately model shale gas systems. Appendix B shows preliminary matches for the Barnett Shale Ex Well #2 using transient interporosity flow. The importance of using transient interporosity flow needs to be addressed in future work.

Lastly, the importance of an accurate initial pressure estimate cannot be stressed enough if one plans to use GPA. Nearly every output parameter either directly or indirectly depends on the accuracy of the initial pressure used. Note that this is a weakness of all production data analysis methods that rely on material balance time. In addition, matching a given flowrate to the correct p_{wf} is also extremely important. This acts as a quality control for the data. While initial pressure is difficult to measure accurately in low permeability formations, the value of information gained from this sometimes costly measurement may very well outweigh the expenditure. A simple probability, or decision tree, analysis would bear this out.

REFERENCES

Agarwal, Ram G., David C. Gardner, Stanley W. Kleinsteiber, and Del. D Fussell: "Analyzing Well Production Data Using Combined-Type-Curve and Decline-Curve Analysis Concepts," SPE 57916 presented at the SPE Annual Technical Conference and Exhibition, New Orleans, September 27-30, 1999.

Aguilera, R.: "Well Test Analysis of Dual-Porosity Systems Intercpeted by Hydraulic Vertical Fractures of Finite Conductivity," SPE 18948 presented at the SPE Rocky Mountain Regional/Low-Permeability Reservoirs Symposium, Denver, March 6-8, 1989.

Arps, J. J.: "Analysis of Decline Curves," Published in Petroleum Transactions, AIME, 160 (1945): 228-247.

Blasingame, T. A. and W. J. Lee: "The Variable-Rate Reservoir Limits Testing of Gas Wells," SPE 17708 presented at the SPE Gas Technology Symposium, Dallas, June 13-15, 1988.

Brill, James P. and H. Dale Beggs: Two-Phase Flow in Pipes, 6th Ed, (1988).

Bumb, A. C. and C. R. McKee: "Gas Well Testing in the Presence of Desorption for Coalbed Methane and Devonian Shale," SPE Formation Evaluation, Vol. 3, No. 1 (1988, March): 179-185.

Carter, Robert D.: "Characteristic Behavior of Finite Radial and Linear Gas Flow Systems-Constant Terminal Pressure Case," SPE/DOE 09887 presented at the SPE/DOE Low Permeability Symposium, Denver, May 27-29, 1981.

Cinco-Ley, H. and H.-Z. Meng: "Pressure Transient Analysis of Wells with Finite Conductivity Vertical Fractures in Double Porosity Reservoirs," SPE 18172 presented at the SPE Annual Technical Conference and Exhibition, Houston, October 2-5, 1988.

Cox, Stuart A., John V. Gilbert, Robert P. Sutton, and Ronald P. Stoltz: "Reserve Analysis for Tight Gas," SPE 78695 presented at the SPE Eastern Regional Meeting, Lexington, October 23-25, 2002.

Ehlig-Economides, Christine A. and Jeffery Joseph: Well Test Analysis for Wells Produced at a Constant Pressure, A Ph.D dissertation, Standford University, June, 1979.

Fetkovich, M. J.: "Decline Curve Analysis Using Type Curves," Journal of Petroleum Technology, Vol. 32, No. 6 (1980, June): 1065-77.

Fetkovich, M. J., M. E. Vienot, M. D. Bradley, and U. G. Kiesow: "Decline-Curve Analysis Using Type Curves – Case Histories," SPE 13169 presented at the SPE Annual Technical Conference and Exhibition, Houston, Sept 16-19, 1987.

Fetkovich, M. J., E. J. Fetkovich, and M. D. Fetkovich: "Useful Concepts for Decline Curve Forecasting, Reserve Estimation, and Analysis," SPE 28628 presented at the SPE Annual Technical Conference & Exhibition, New Orleans, September 25-28, 1994.

Fraim, M. L. and R. A. Wattenbarger: "Gas Reservoir Decline-Curve Analysis Using Type Curves with Real Gas Pseudopressure and Normalized Time," SPE Formation Evaluation, Vol. 2, No. 6 (1987, December): 671-682.

Gale, Julia F. W., Robert M. Reed, and Jon Holder: "Natural Fractures in the Barnett Shale and their Importance for Hydraulic Fracture Treatments," AAPG Bulletin, Vol. 91, No. 4 (2007, April): 603-622.

Gringarten, Alain C.: "Interpretation of Tests in Fissured and Multilayered Reservoirs with Double-Porosity Behavior: Theory and Practice," Journal of Petroleum Technology, Vol. 36, No. 4 (1984, April): 549-564.

Hazlett, W.G., W. J. Lee, G. M. Nahara, and J. M. Gatens III: "Production Data Analysis Type Curves for the Devonian Shales," SPE 15934 presented at the SPE Eastern Regional Meeting, Columbus, November 12-14, 1986.

Hill, David G., John B. Curtis, and Paul G. Lillis: "An Overview of Shale Gas Exploration and Current Plays," Proceedings of the 26th Annual International Conference on Offshore Mechanics and Arctic Engineering, San Diego, June 10-15, 2007.

Hurst, W.: "Water Influx into a Reservoir and its Application to the Equation of Volumetric Balance," Published in Petroleum Transactions, AIME, 151 (1943): 57-72.

Lane, H. S., A. T. Watson, S. A. Holditch & Assocs. Inc., and D. E. Lancaster: "Identifying and Estimating Desorption from Devonian Shale Gas Production Data," SPE 19794 presented at the 64th Annual Technical Conference and Exhibition of the Society of Petroleum Engineers, San Antonio, October 8-11, 1989.

Lane, H. S., D. E. Lancaster, S. A. Holditch & Assocs. Inc., and A. T. Watson: "Estimating Gas Desorption Parameters from Devonian Shale Well Test Data," SPE 21272 presented at the SPE Eastern Regional Meeting, Columbus, November 1-2, 1990.

Lee, W. J. and R. A. Wattenbarger: Gas Reservoir Engineering. SPE Textbook Series Vol. 5 (1996).

Montgomery, Scott L., Daniel M. Jarvie, Kent A. Bowker, and Richard M. Pollastro: "Mississippian Barnett Shale, Fort Worth Basin, North-Central Texas: Gas-Shale Play with Multi-Trillion Cubic Foot Potential," AAPG Bulletin, Vol. 89, No. 2 (2005, February): 155-175.

Olarewaju, J. S. and W. J. Lee: "New Pressure-Transient Analysis Model for Dual-Porosity Reservoirs," SPE Formation Evaluation, Vol. 38, No. 3 (1989, September): 384-390.

Palacio, J. C. and T. A. Blasingame: "Decline-Curve Analysis Using Type Curves-Analysis of Gas Well Production Data," SPE 25909 presented at the SPE Joint Rocky Mountain Regional Low Permeability Reservoirs Symposium, Denver, April 26-28, 1993.

Schenk, Christopher J.: "Geologic Definition and Resource Assessment of Continuous (Unconventional) Gas Accumulations - the U.S. Experience," AAPG 66086 presented at the Ancient Oil-New Energy Conference, Cairo, October 27-30, 2002.

Schlumberger: Modern Reservoir Testing, Schlumberger, 1994.

Serra, K., A. C. Reynolds, R. Raghavan: "New Pressure Transient Analysis Methods for Naturally Fractured Reservoirs," Journal of Petroleum Technology, Vol. 35, No. 12 (1983, September): 2271-2283.

Spivey, J. P. and M. E. Semmelbeck: "Forecasting Long-Term Gas Production of Dewatered Coal Seams and Fractured Gas Shales," SPE 29580 presented at the SPE Rocky Mountain Regional/Low-Permeability Reservoirs Symposium, Denver, March 20-22, 1995.

Stehfest, H.: "Algorithm 368, Numerical Inversion of Laplace Transforms", D-5 Communications of the ACM, Vol. 13, No. 1 (1970, January): 47-49.

Van Everdingen, A. F. and W. Hurst: "The Application of the Laplace Transformation to Flow Problems in Reservoirs," T.P. 2732 presented at the AIME Annual Meeting, San Francisco, February 13-17, 1949.

Warren, J. E. and P. J. Root: "The Behavior of Naturally Fractured Reservoirs," SPE 00426 presented at the Fall Meeting of the Society of Petroleum Engineers, Los Angeles, October 7-10, 1962.

NOMENCLATURE

A	area
B	formation volume factor
c	compressibility
C	wellbore storage coefficient
C_A	shape factor
C_{df}	dimesionless fracture conductivity
D	decline rate
G	free gas in place
G_{tot}	free gas + adsorbed gas
h	height
I	Bessel function of second kind
J	productivity index
k	permeability
K	Bessel function of first kind
L	length of block
M	molecular weight
m(p)	pseudopressure
n	number of fracture planes
N	Stefhest number
N_{pi}	ultimate production for reservoir pressure = 0
p	pressure
$\overline{P}$	Laplace space pressure
q	flow rate
r	radius
R	gas constant
s	Laplace variable
S	saturation
T	temperature
t	time
t_a	material balance time
t_{da}	dimensionless material balance time
t_{da_new}	dimensionless material balance time with ct modification
t_{dxf}	dimensionless time base on x_f
V	Stefhest inversion term
v_{ads}	adsorbed gas concentration
w	fracture width
x	half-length
z	real gas deviation factor
α	fracture geometry term
λ_{cart}	gas correction factor
λ	fracture connectivity factor
μ	viscosity
ν	velocity
ρ	density

ϕ	porosity
Φ	potential
ω	storativity ratio

Subscripts

0	order 0 of Bessel function
1	order 1 of Bessel function
d	dimensionless
e	external or drainage
f	fracture
f+m	matrix + fracture
fh	hydraulic fracture
g	gas
i	initial
L	Langmuir
m	matrix
o	oil
p	produced
sc	standard conditions
t	total
w	water
wd	dimensionless wellbore flowing
wf	wellbore flowing

APPENDIX A

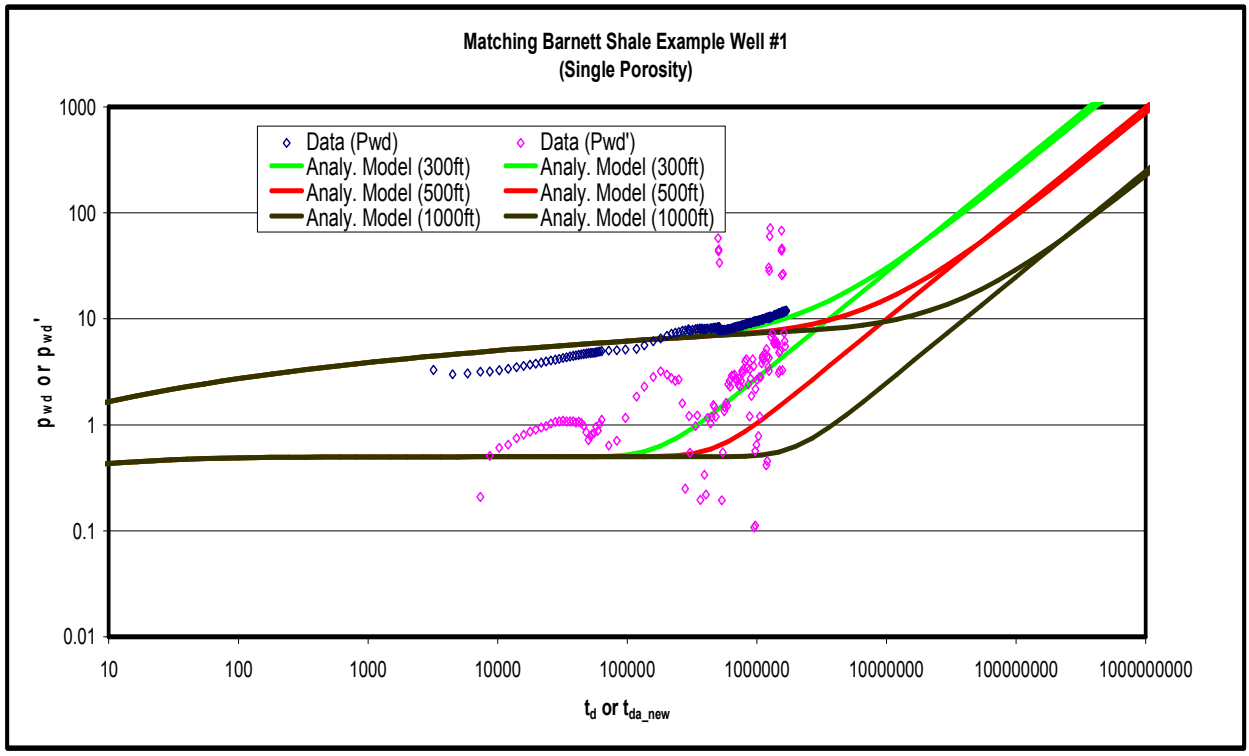

Match for Barnett Shale Ex Well #1 at 5000 psi.

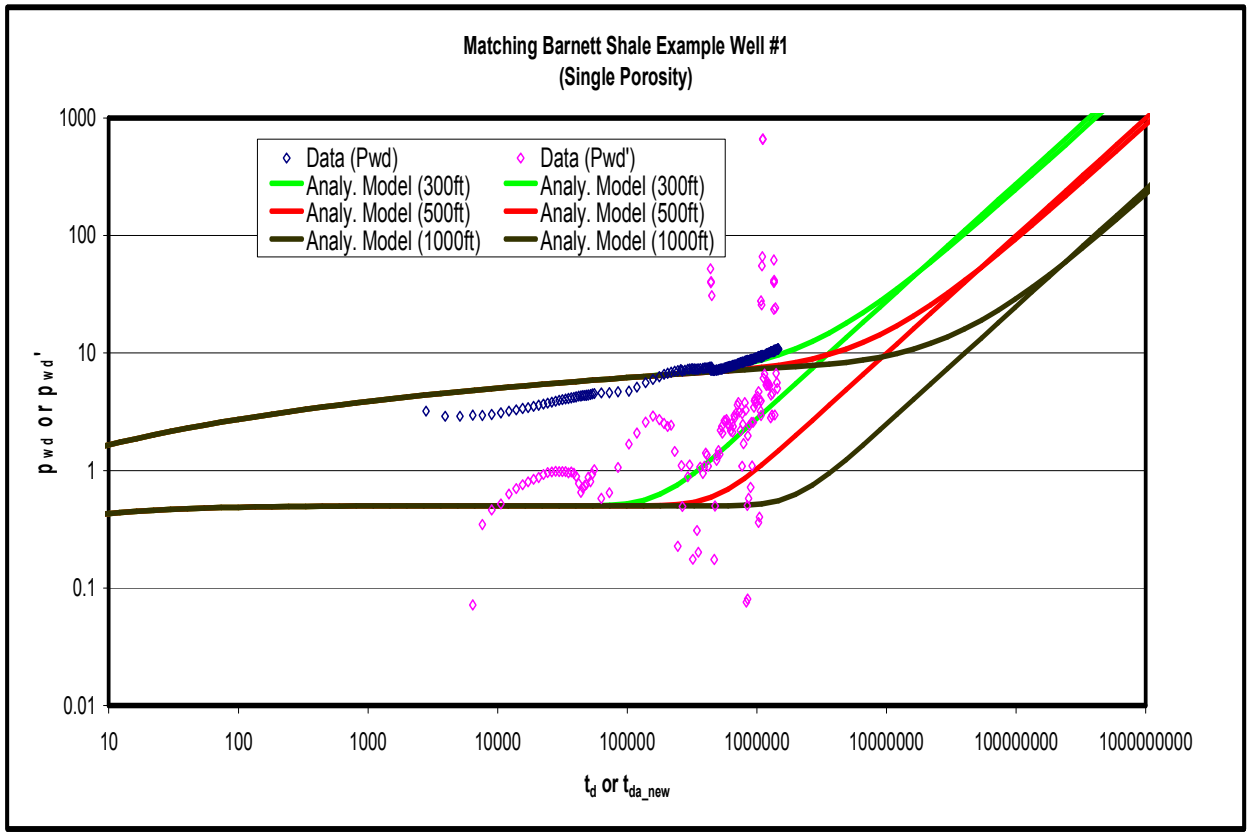

Match for Barnett Shale Ex Well #1 at 6000 psi.

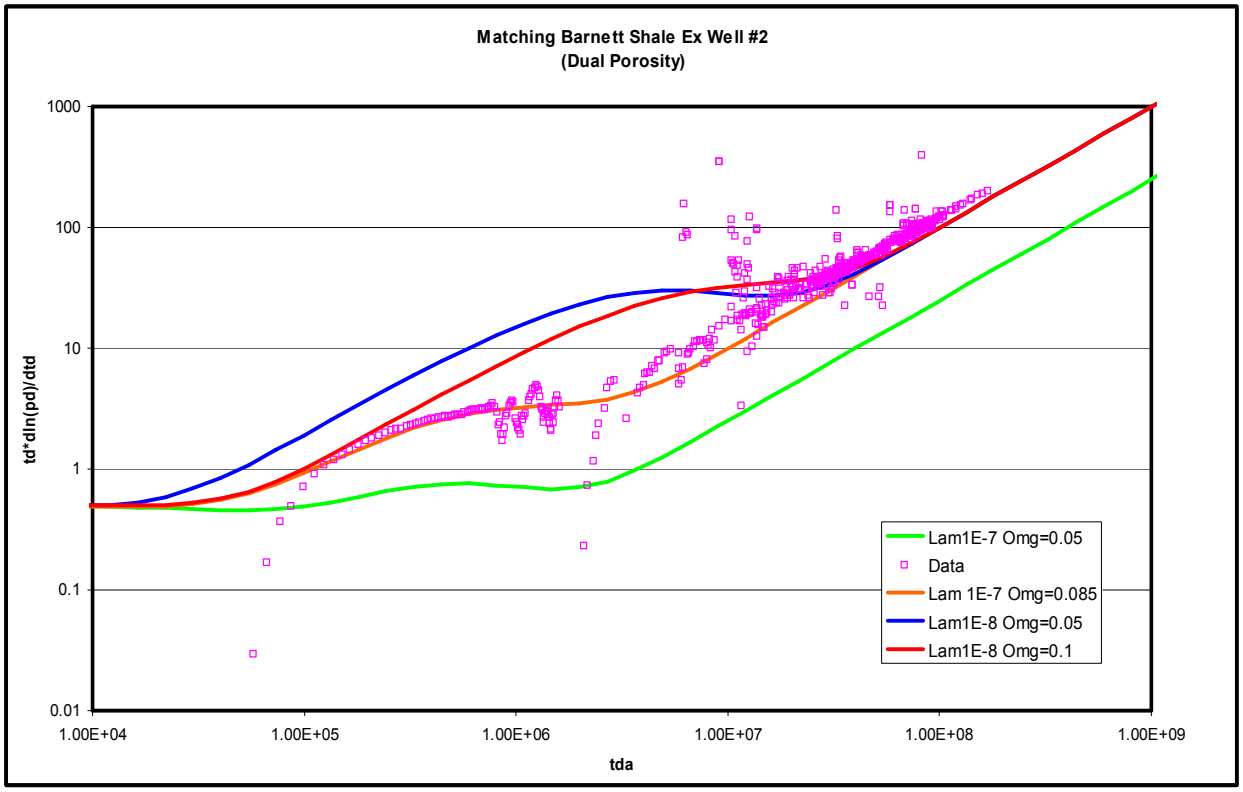

Match for Barnett Shale Ex Well #2 at 5000 psi.

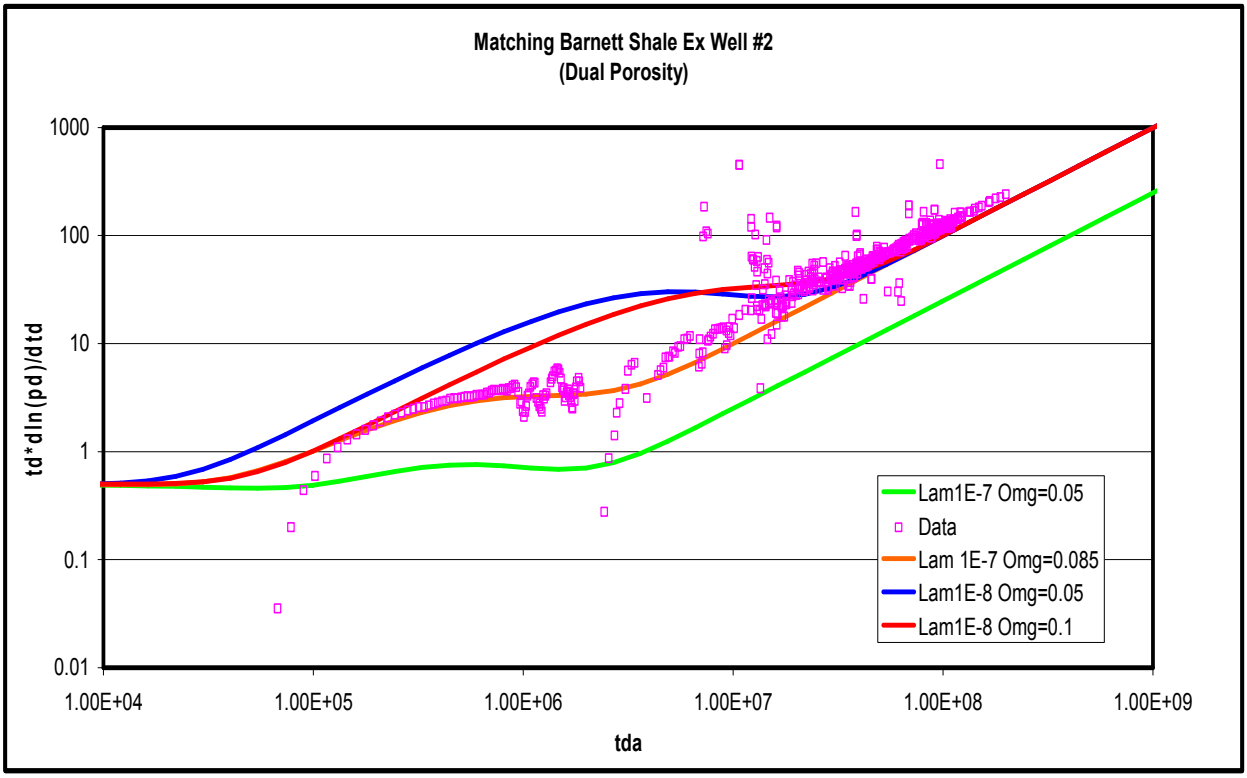

Match for Barnett Shale Ex Well #2 at 6000 psi

APPENDIX B

The dual porosity analytic models used in this work contained a pseudosteady state interporosity flow relationship. This is a concern for the analysis of field cases. It is necessary to use a transient interporosity flow relationship when the matrix block size becomes relatively large compared to the drainage radius.

Assuming a cube fracture geometry, the matrix block size for the Barnett Shale Ex Well #2 was found to be larger than the drainage radius. Therefore, a dual porosity analytic model with transient interporosity flow was used in addition to the pseudosteady state interporosity flow for the Barnett Shale Ex Well #2. The match for Barnett Shale Ex Well #2 can be seen below.

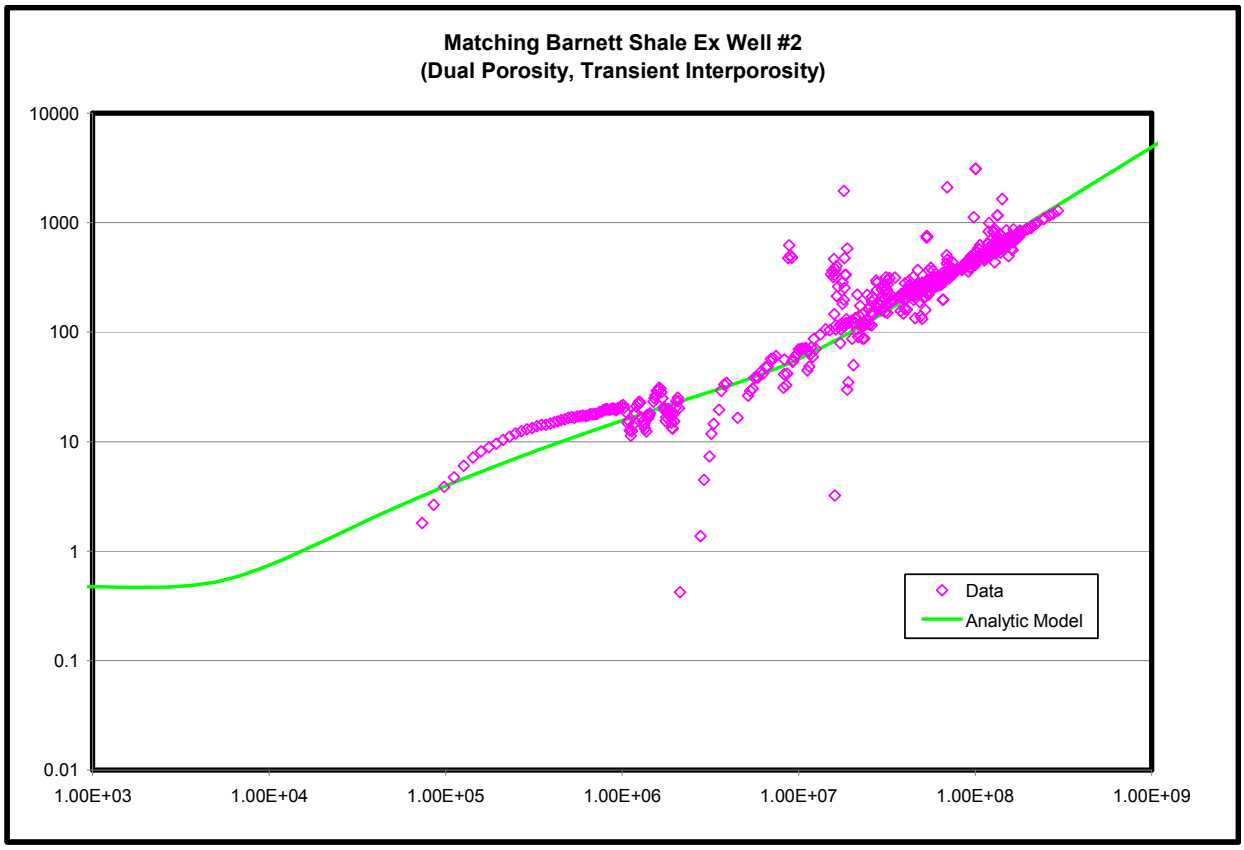

This is not as good a visual match at early time as the pseudosteady state interporosity flow model is. However, this match was achieved using 4000 psi and similar values of λ and ω that were obtained using pseudosteady state interporosity flow.

Model Type	Drainage radius, r_e (ft)	ω	λ	G/A*	Match Term $(kG/\phi A)$ *
Dual Porosity	500	0.05	1E-7	5.37	6.77

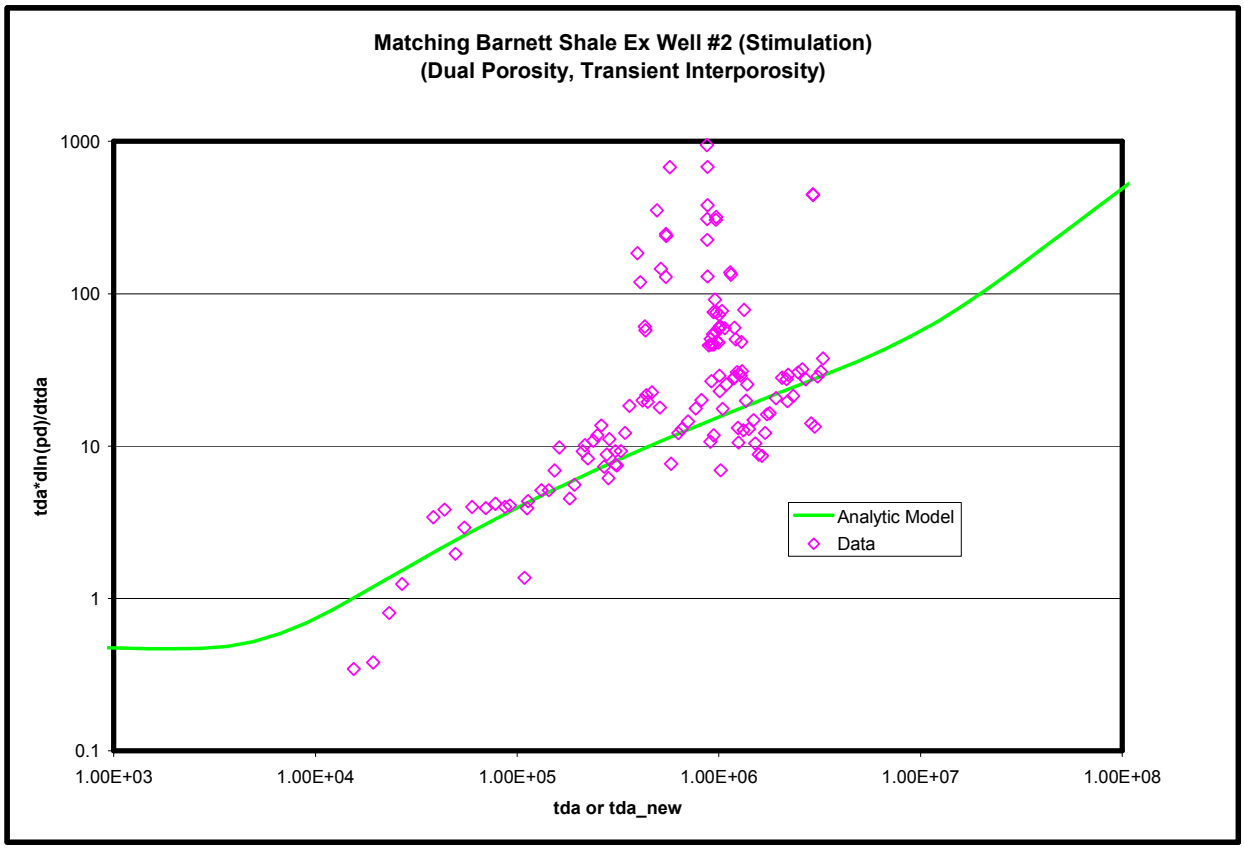

Here is the match for the stimulation performed on Barnett Shale Ex Well #2. The analytic model used in this match has transient interporosity flow. This match was achieved with an initial pressure of 4000 psi and similar values of λ and ω that were obtained from using pseudosteady state interporosity flow.

Model Type	Drainage radius, r_e (ft)	ω	λ	G/A*	Match Term $(kG/\phi A)$ *
Dual Porosity	225	0.05	7.5E-8	3.39	2.34

VITA

Adam M. Lewis is a native of Baton Rouge, Louisiana. He began his collegiate education at Louisiana State University in 2001 and received his Bachelor of Science in Petroleum Engineering in 2005. He has worked in various industry positions and geographic locals as an intern. His technical interests include reservoir engineering, production engineering, and petroleum geology.